NOTE TO USERS

Particle Segregation in a Sheared Suspension with a Free Surface

by

Bo Jin

A Dissertation Submitted to the Graduate Faculty in Engineering in Partial Fulfillment of the Requirements for the Degree of Doctor of Philosophy

The City University of New York

2004

INFORMATION TO USERS

The quality of this reproduction is dependent upon the quality of the copy submitted. Broken or indistinct print, colored or poor quality illustrations and photographs, print bleed-through, substandard margins, and improper alignment can adversely affect reproduction.

In the unlikely event that the author did not send a complete manuscript and there are missing pages, these will be noted. Also, if unauthorized copyright material had to be removed, a note will indicate the deletion.

ProQuest Information and Learning Company
300 North Zeeb Road
P.O. Box 1346
Ann Arbor, MI 48106-1346

This manuscript has been read and accepted for the Graduate Faculty in Engineering in satisfaction of the dissertation requirement for the degree of Doctor of Philosophy.

November 12 '03 — Chairman of Examining Committee

Date

November 12, 2003 — Executive Officer

Date

Prof. Andreas Acrivos(Mentor)

Prof. Morton Denn

Prof. Joel Koplik

Prof. Charles Maldarelli

Prof. Boris Khusid

Supervisory Committee

THE CITY UNIVERSITY OF NEW YORK

Abstract

Particle Segregation in a Sheared Suspension with a Free Surface

by

Bo Jin

Advisor: Professor Andreas Acrivos

This thesis describes a further theoretical and experimental investigation of an unexplained phenomenon, in which, an initially uniform suspension of neutrally buoyant particles within a partially filled rotating cylinder is found to segregate into bands of particles separated by regions of low particle concentration or even particle-free liquid. First of all, we investigated in considerable detail coating flows of a viscous particle-free liquid in a partially filled rotating horizontal cylinder, often referred to as rimming flows, by means of an asymptotic analysis of the thin film lubrication equations and also examined the stability of their solutions. Secondly, a number of experiments were performed to probe further the whole process of the particle segregation phenomenon. One crucial experimental result was the observation that when the suspension contains a recirculating region (puddle), the particles first segregate radially by migrating out of the puddle into the unidirectional circumferential flow before segregating along the axis of the cylinder. Thirdly, an explanation for such a phenomenon was proposed on the basis of a model of rimming flows with an axially varying viscosity plus the experimental observation referred to above (i.e.

the radial particle segregation). A linear stability analysis for dilute suspensions with complete radial segregation showed that such a particle distribution is unstable to axial perturbations with the surface tension being responsible for the selection of the wavelength of the most rapidly amplified disturbance. The calculated and measured spacings between the bands were found to be in good agreement. Finally, particle segregation, as expected, was also found to occur in two new geometries (a cone and a sphere) and the location of the corresponding band(s) seen experimentally was predicted theoretically by solving numerically a general model equation for rimming flows within any axisymmetric horizontal rotating container and then taking into account the observed radial particle segregation similar to that in the case of the cylinder mentioned above.

Preface

This thesis describes a further theoretical and experimental investigation of a phenomenon discovered and studied by Tirumkudulu, Tripathi and Acrivos[1, 2] involving particle segregation in a sheared suspension with a free surface. This kind of segregation, which remained unexplained, can be observed in two different geometries: a partially filled horizontal Couette device and a partially filled horizontal single cylinder. Since the flow field in the latter geometry is easier to analyze than that in the Couette device, we focus our attention on the simpler of the two unexplained phenomena, in which, an initially uniform suspension of neutrally buoyant particles within a partially filled rotating cylinder is found to segregate into bands of particles separated by regions of low particle concentration or even particle-free liquid.

In chapter 1, we begin by investigating theoretically in considerable detail coating flows of a viscous pure liquid in a partially filled rotating horizontal cylinder, called rimming flows, on the basis of the modified lubrication equation proposed by Tirumkudulu and Acrivos[3], which was obtained by simply adding to the standard lubrication equation a term that accounts for the angular variation of the hydrostatic pressure. We first find that this equation can characterize the film profiles even when the fill fraction F is as large as 36%, where the film is far from thin. We show, using this modified lubrication equation, that the asymmetric solution of the standard lubrication equation does in fact represent the liquid film profiles everywhere except at the point of discontinuity but under extremely restrictive conditions which typically require that the value of the fill fraction be almost vanishingly small. Then, we examine the stability of these two-dimensional flows to two-dimensional disturbances as well as their stability to axial disturbances. We confirm the results

obtained earlier by Benjamin, Pritchard and Tavener [4] on the basis of the standard lubrication theory and show that the asymmetric profiles are asymptotically stable to small disturbances and that the symmetric profiles are only neutrally stable if surface tension effects are ignored. If the latter are included, however, the symmetric profiles are also shown to be asymptotically stable to small two-dimensional disturbances, but to be asymptotically unstable to axial disturbances.

In addition, we performed a number of experiments to probe further this whole process of particle segregation in a partially filled horizontal rotating cylinder. Interestingly, we found that bands did not form along the cylinder either in the absence of a recirculating flow at the bottom of the cylinder or when that recirculating flow region was relatively large. In the former case, no bands formed even after an axial variation of the suspension viscosity was imposed by placing a piece of ice along a section of the cylinder. An even more crucial result was the observation that, when the suspension contains a recirculating region (puddle), the particles first segregate radially by migrating out of the puddle into the unidirectional circumferential flow before segregating along the axis of the cylinder. Several additional interesting experiments are described in chapter 2.

In chapter 3, we first consider the structure of a class of three-dimensional flows of a pure liquid, again in a partially filled horizontal rotating cylinder, which are generated by an imposed axial variation of the fluid viscosity, and construct a simple model based on the modified lubrication equation for describing the free surface profiles. The profiles thereby computed are found to be in good agreement with those obtained by solving numerically the three-dimensional Stokes equations using the FIDAP software (Fluent.Inc). Moreover, by means of this model, we calculate the axial particle volumetric flow rate in very dilute suspensions, and find that although this flow rate vanishes at steady state if the concentration of the suspension at every cross section is kept uniform, there exists a net axial particle flow rate in

the direction of increasing viscosity if the particle volume fraction in the recirculating flow region near the bottom of the cylinder is lower than that in the region of the circumferential flow. On the basis of these theoretical results and experimental observations in chapter 2 (i.e. the radial particle segregation), we provide an explanation for the particle segregation phenomenon referred to above. A linear stability analysis for dilute suspensions with complete radial segregation shows that such a particle distribution is unstable to axial perturbations with the surface tension being responsible for the selection of the wavelength of the most rapidly amplified disturbance. The calculated and measured spacings between the bands are in good agreement.

Finally, in Appendix C, particle segregation, as expected, was also found to occur in two new geometries (a cone and a sphere) and the location of the corresponding band(s) seen experimentally was predicted theoretically by solving numerically a general model equation for rimming flows within any axisymmetric horizontal rotating container and then taking into account the observed radial particle segregation similar to that in the case of the cylinder mentioned above.

Acknowledgments

I wish to express my most sincere gratitude to my advisor, Professor Andreas Acrivos, for his patient guidance and continual encouragement throughout the course of my Ph.D.

I would like to thank my family for their love and support. This work is especially dedicated to my wife, Fang, who made it all worthwhile.

I would also like to thank Prof. Boris Khusid, Dr. Mahesh Tirumkudulu, Dr. Zhiyong Qiu, Dr. German Drazer for their valuable suggestions.

Many thanks to Andy Eng, Zhen Rong Xu, Mary Wright, Nikolai Markarian, Anil Kumar, Mike Yeksel.

This work was supported by the US Department of Energy under Grant Nos. DE-FG02-90ER14139 and DE-FG02-03ER46068.

Contents

List of Tables

List of Figures

Chapter 1

Study of rimming flows

1.1 Introduction

Coating flows within a rotating horizontal cylinder, often referred to as *rimming flows*, have received an increasing degree of attention in recent years on account of the fascinating variety of flow patterns that are encountered and the intriguing mathematical properties of the equations which have been developed to model the observed phenomena. To-date, most of the attention has been directed to the case of thin films for which the well-known lubrication approximation can be invoked to reduce the governing equations of viscous flow hydrodynamics to the particularly simple form,

$$\nu \frac{\partial^2 \hat{v}}{\partial y^2} = g \cos\theta \tag{1.1}$$

provided that inertial effects and surface-tension effects are negligible and that the pressure in the liquid is hydrostatic, being zero at the free surface. In Fig 1.1, $\hat{v}$ is the velocity component in the angular direction, θ is the angular coordinate, ν is

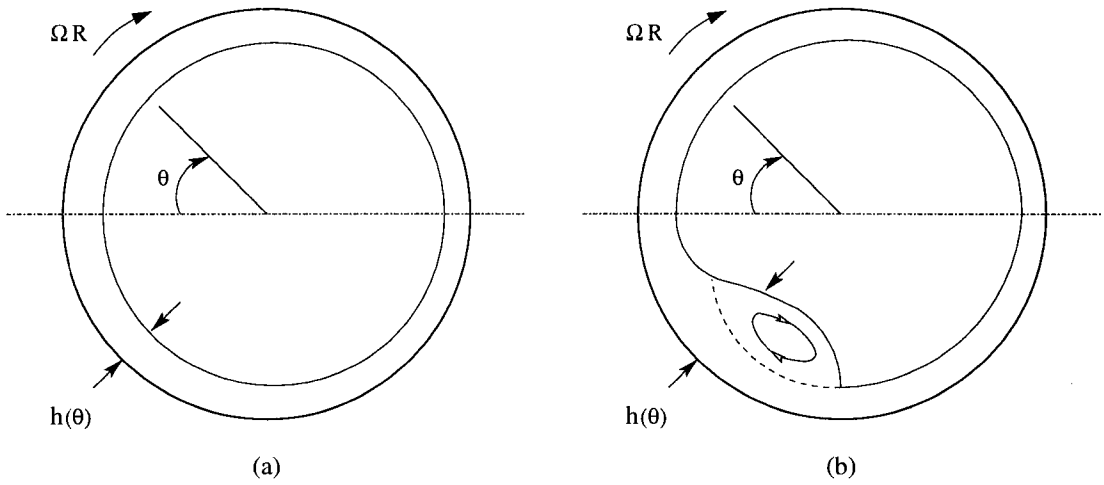

Figure 1.1: Sketch of the two families of liquid film profiles: (a) a homogeneous film, $\beta < \beta^*$; (b) an inhomogeneous film ($\beta > \beta^*$), where θ is the angular coordinate, Ω is the angular velocity of the cylinder, R is the inner radius of the cylinder and $h(\theta)$ is the film thickness.

the kinematic viscosity, g is the gravity constant, $y = R - r$ is the distance from

the rotating cylindrical boundary and r is the radial coordinate with R being the inner radius of the cylinder. There are two boundary conditions for this equation: the no-slip condition requires that $\hat{v} = \Omega R$ where Ω is the angular velocity of the cylinder; and $\hat{v}_y = 0$, the condition of vanishing shear stress at the free surface $y = h$ (*cf* Fig 1.1). Hence, the solution of equation (1.1) is

$$\hat{v} = \Omega R - \frac{g}{\nu}\cos\theta\left(hy - \frac{1}{2}y^2\right) \tag{1.2}$$

The approximations leading to equations (1.1) and (1.2) require that $h \ll R$ and $|\partial h/\partial\theta| \ll h$. On integrating of equation (1.2) with respect to y from 0 to h, we then obtain the total volumetric flow rate within the film per unit axial distance,

$$Q = \Omega R h - \frac{1}{3}\frac{g}{\nu}h^3\cos\theta \tag{1.3}$$

Now, let us define an important dimensionless parameter:

$$\alpha \equiv \sqrt{\frac{\Omega\nu}{gR}} \tag{1.4}$$

which, in fact, can be used to define a dimensionless thickness η and a dimensionless flow rate q by

$$\eta \equiv h/\alpha R \qquad \text{and} \qquad q \equiv Q/\alpha\Omega R^2$$

Therefore, equation (1.3) becomes

$$q = \eta - \frac{1}{3}\eta^3\cos\theta \tag{1.5}$$

which will be referred to as the standard lubrication equation. In addition, η is required to be periodic in 2π and to satisfy the integral conservation condition,

$$F = \frac{1}{\pi R}\int_{-\pi}^{\pi} h\mathrm{d}\theta = \frac{\alpha}{\pi}\int_{-\pi}^{\pi}\eta\mathrm{d}\theta \tag{1.6}$$

where F is the fill fraction (i.e. the fractional cross-sectional area occupied by the liquid).

Besides requiring that the liquid film be everywhere thin relative to R, the radius of the cylinder, equation (1.5) presupposes steady-state (hence q is independent of θ), as well as negligible inertia and surface tension effects, i.e. vanishingly small Reynolds number and inverse capillary number. Under these conditions, the remaining two independent dimensionless groups, F and α, can be combined into a single parameter β,

$$\beta \equiv F/\alpha = \frac{1}{\pi}\int_{-\pi}^{\pi} \eta \mathrm{d}\theta \tag{1.7}$$

the value of which determines the solution of equation (1.5) subject to equation (1.7) plus the periodicity condition $\eta(\theta + 2\pi) = \eta(\theta)$.

It is well-known that the solution to the cubic equation (1.5) depends critically on the value of β [3, 4, 5, 6, 7, 8]. Specifically, when $0 < \beta < \beta^* = 1.4142\ldots$ (corresponding to $0 < q < 2/3$), η is symmetric about $\theta = 0$ and everywhere continuous. This is referred to in the literature as a homogeneous film and a sketch of such a profile for $\beta = 1.30$ ($q = 0.628$) is shown in Fig 2 of ref[3]. When $\beta = \beta^*$, in which case q attains its maximum value $2/3$, the film is still continuous but has a discontinuous slope at $\theta = 0$ equal to $\pm 1/\sqrt{6}$. When $\beta^* < \beta < \beta^{**} = 2.21\ldots$ and $q = 2/3$, a physically acceptable solution to equation (1.5) can still be constructed with, however, a discontinuity at $\theta = \theta^* < 0$, the value of which is determined by β (*cf* Fig 2 in ref[3]). Moreover, $\theta = -\pi/2$ when $\beta = \beta^{**}$, and no physically acceptable solution exists to equation (1.5) subject to equation (1.7) when β exceeds that value. The discontinuity in the film thickness profile is disquieting of course, since its existence is incompatible with the assumptions underlying the lubrication analysis leading to equation (1.5). Equally troublesome, is the absence of solutions of (1.5) subject to (1.7) when $\beta > \beta^{**}$. This then raises the question as to whether and under what circumstances, the discontinuous solutions of equation (1.5) when $\beta > \beta^*$ can faithfully represent the dynamics of the film flow under consideration.

In order to answer this query, a model equation was recently proposed in ref[3]

which was obtained by simply adding to equation (1.5) a term that accounts for the angular variation of the hydrostatic pressure. Here, we briefly discuss the basis for this model:

First, from the lubrication analysis, it can be shown that the leading order term of the pressure in the thin film is still hydrostatic (*cf* ref[4]), hence,

$$p = \alpha(z - \eta)\sin\theta \tag{1.8}$$

where $p \equiv \hat{p}/\rho g R$ is the dimensionless pressure with $\hat{p}$ being the dimensional pressure and $z \equiv y/\alpha R$ is the dimensionless distance from the rotating cylindrical boundary. Then, inserting equation (1.8) into the θ-momentum equation leads to a new term containing the θ-component of ∇p on the right-hand of equation (1.1) in the dimensionless form, viz.

$$\frac{\partial^2 v}{\partial z^2} = \cos\theta + \frac{\alpha}{1 - \alpha z}\{(z - \eta)\cos\theta - \eta'\sin\theta\} \tag{1.9}$$

which can be rearranged into

$$\frac{\partial^2 v}{\partial z^2} = \{(1 - \alpha\eta)\cos\theta - \alpha\eta'\sin\theta\}$$

provided that $\alpha z \ll 1$, where $v \equiv \hat{v}/\Omega R$ is the dimensionless angular component of the velocity. Using the same boundary conditions as before ($v = 1$ at $z = 0$ and $\partial v/\partial z = 0$ at $z = \eta$), the solution of equation (1.9) is

$$v = 1 - \left(\eta z - \frac{z^2}{2}\right)\{(1 - \alpha\eta)\cos\theta - \alpha\eta'\sin\theta\} \tag{1.10}$$

Therefore, in lieu of equation (1.5), this extended lubrication analysis of ref[3] leads then to

$$q = \eta - \frac{1}{3}\eta^3\cos\theta + \frac{\alpha}{3}\{\eta^4\cos\theta + \eta^3\eta'\sin\theta\} \tag{1.11}$$

the solution of which must be periodic in 2π and must satisfy the exact integral conservation condition

$$F = \frac{\alpha}{\pi}\int_{-\pi}^{\pi}(1 - \frac{\alpha\eta}{2})\eta \mathrm{d}\theta \tag{1.12}$$

from which it follows that

$$\beta \equiv \frac{F}{\alpha} = \frac{1}{\pi}\int_{-\pi}^{\pi}(1 - \frac{\alpha\eta}{2})\eta \mathrm{d}\theta \tag{1.13}$$

As shown in ref[3] and also discussed further on p.16, equation (1.11) has the useful property that its solution, when the flow is turned off, i.e. when $\alpha \to 0$ with F fixed, gives the exact shape of the stagnant pool at the bottom of the cylinder. Thus, equation (1.11) subject to (1.13) has a continuous periodic solution for all α with F fixed (below some critical value as shown later), in contrast to equation (1.5) subject to (1.7) which does not have a solution if $\alpha < F/\beta^{**}$.

It is obvious that the solution of equation (1.11) subject to (1.13) now depends on the values of the two independent parameters F and α rather than merely on their ratio β as was the case with equation (1.5) subject to (1.7).

We now observe that equations (1.10) and (1.11), as well as equations (1.2), suitably non-dimensionalized, and (1.5) can be combined to yield

$$v = 1 - \left(\eta z - \frac{z^2}{2}\right)\frac{3(\eta - q)}{\eta^3} \tag{1.14}$$

Thus, depending on the sign of $(\eta - q)$, v is either increasing (for $\eta < q$) or decreasing (for $\eta > q$) monotonically with z and, in the latter case, reaches its minimum value on the free surface, i.e.

$$v_{min} = \frac{3q - \eta}{2\eta} \quad \text{at} \quad z = \eta \tag{1.15}$$

Hence, if $\eta < 3q$ for all θ, the angular component of the flow velocity is everywhere positive but, if $\eta > 3q$ within a certain range of θ, this implies the existence of a recirculating flow, or puddle, within that same range. Now according to the standard lubrication analysis, equations (1.5) and (1.7), v_{min} is everywhere positive when $\beta < 1.586\ldots \approx 1.6$ (where $q = 2/3$) but, when β reaches that value, v_{min} vanishes at $\theta = -\pi/3$ where $\eta = 3q = 2$. In turn, when β exceeds 1.6, a recirculating flow region is then created, the extent of which increases with β. The same conclusions

apply when η is computed from the solution of equation (1.11) subject to (1.13), although the critical value of β referred to above will now depend on α for any given F since, as was pointed out above, α and F are now independent parameters which can no longer be combined.

At this point, we also note for future use that, if the capillary contribution is included in the thin film approximation, then, according to ref[4], the expression for the hydrostatic pressure given previously ,i.e. (1.8), is modified into

$$p = \alpha(z - \eta)\sin\theta - \alpha^3 Ca^{-1}(\eta' + \eta''') \tag{1.16}$$

where $Ca^{-1} \equiv \sigma/R\Omega\mu$ is the inverse capillary number with σ being the surface tension and μ the liquid viscosity. We then arrive at

$$q = \eta - \frac{1}{3}\eta^3\cos\theta + \frac{\alpha}{3}\{\eta^4\cos\theta + \eta^3\eta'\sin\theta + Ca^{-1}\alpha^2\eta^3(\eta' + \eta''')\} \tag{1.17}$$

Of course, when η' and η''' are both $O(\eta)$ and

$$Ca \gg \alpha^2, \text{ implying a Bond number } Bo \equiv R^2 g\rho/\sigma \gg 1, \tag{1.18}$$

equation (1.17) reduces to equation (1.13) (this last condition was incorrectly stated as $Ca \gg \alpha^3$ in ref[3]). Some of the consequences of relaxing (1.18) have been examined in a recent study [9], but, in most of what follows, we shall suppose that surface tension effects are negligible to first order.

Off hand, it might appear that (1.5) and (1.7), the equations of the standard lubrication analysis, can be recovered from (1.11) and (1.13) by simply letting $\alpha = 0$ but, as will be seen presently, the issue is more complicated and, therefore, more interesting. This is because, as was pointed out earlier on several occasions, equations (1.11) and (1.13) involve two dimensionless parameters, F and α which, of course, are not independent, hence the limit $\alpha \to 0$ has to be taken with care. One reasonable choice, which actually corresponds to how an experiment is performed,

is to set the fill fraction F equal to some small value, say 0.1, and then vary α by varying Ω, the angular speed of the cylinder. As has been shown in ref[3], under these conditions (i. e. fixed F) equations (1.11) and (1.13) admit solutions which are periodic and continuous everywhere for all $0 < \alpha < \infty$ and which reduce to the exact film shapes in the limits $\alpha = \infty$ and $\alpha = 0$. The former gives a film of uniform thickness which can be obtained by solving $F = 2H - H^2$ with $H \equiv \alpha\eta$, while the latter gives a stagnant puddle symmetric about $\theta^* = -\pi/2$. The corresponding equation for the film thickness in this puddle is

$$H = 1 + \frac{\cos\varphi}{\sin\theta} \qquad \text{for} -\frac{\pi}{2} - \varphi < \theta < -\frac{\pi}{2} + \varphi \tag{1.19}$$

where $H \equiv \alpha\eta$ and φ is given implicitly by

$$F = \frac{1}{\pi}\int_{-\pi/2}^{-\pi/2+\varphi}\left\{1 - \frac{\cos^2\varphi}{\sin^2\theta}\right\}\mathrm{d}\theta = \frac{1}{\pi}\left\{\varphi - \frac{1}{2}\sin 2\varphi\right\} \tag{1.20}$$

provided that $\varphi < \pi/2$ or $F < 0.5$.

When $\alpha \to 0$ for fixed F, most of the liquid stays in the puddle at the bottom, but a small portion of it forms a thin film which coats the rest of the circumference. Therefore, the amount of the liquid in the puddle is less than the fill fraction F by the corresponding material in the thin film which, to $O(\alpha)$, equals

$$\frac{\alpha}{\pi}\left\{\int_{-\pi}^{-\frac{\pi}{2}-\varphi}\eta\mathrm{d}\theta + \int_{-\frac{\pi}{2}+\varphi}^{\pi}\eta\mathrm{d}\theta\right\} = \alpha\beta^{**} - \frac{\alpha}{\pi}\int_{-\frac{\pi}{2}-\varphi}^{-\frac{\pi}{2}+\varphi}\eta\mathrm{d}\theta \tag{1.21}$$

where η is given by the solution of the standard lubrication equation with $\beta = \beta^{**} \equiv 2.21\ldots$. Hence, given that $F < 0.5$, the fill fraction, to $O(\alpha)$, equals

$$F = \frac{1}{\pi}\left\{\varphi - \frac{1}{2}\sin 2\varphi\right\} + \alpha\beta^{**} - \frac{\alpha}{\pi}\int_{-\frac{\pi}{2}-\varphi}^{-\frac{\pi}{2}+\varphi}\eta\mathrm{d}\theta \tag{1.22}$$

By means of the above equation (1.22), we can determine φ and then substitute it into equation (1.19) to obtain the asymptotic form of the film thickness in the puddle.

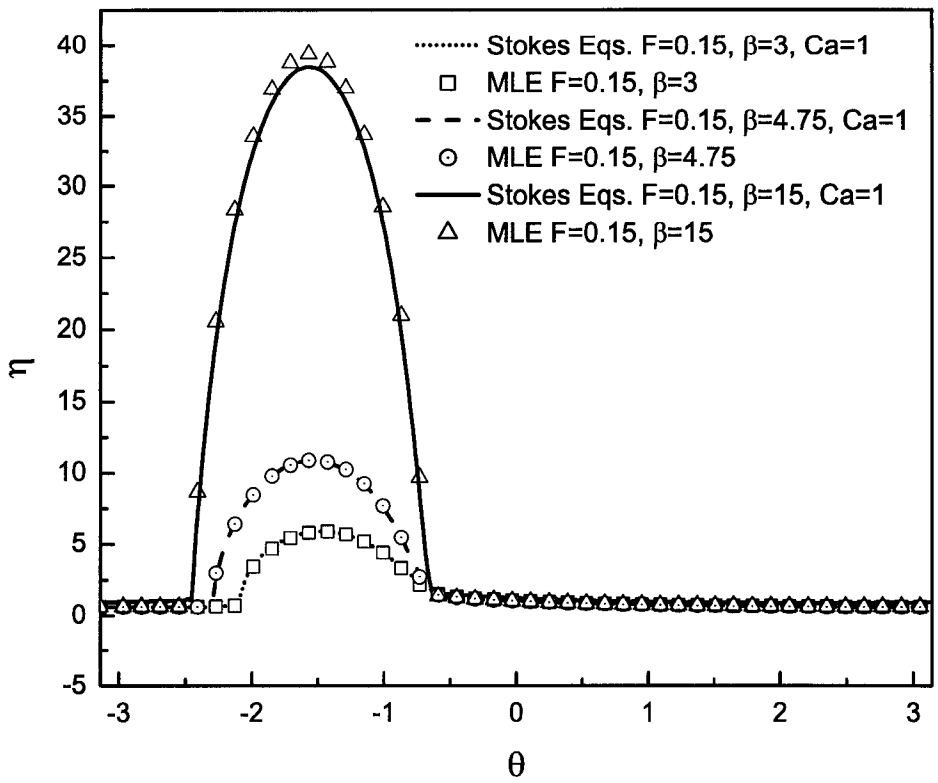

Figure 1.2: The film thickness profiles as obtained from the numerical solution of the modified lubrication equation (MLE) closely agree with those obtained by solving the two-dimensional Stokes equations for $F = 0.15 < 0.5$ for $\beta = 3,\ 4.75$ and 15.

As shown in Figs 1.2-1.3, there is good agreement for $F = 0.15$ between the numerical solution of (1.11) and (1.13), the solution of the full two-dimensional Stokes equations using the NEKTON software (Fluent. Inc), and the asymptotic solution developed above, equation (1.19), with φ being given by equation (1.22), as $\alpha \to 0$. Nevertheless, as we can see from Fig 1.3, there is a discrepancy between the location of the maximum value of H as given by equation (1.19) ($\theta = -\pi/2$) and that of the numerical solution of the modified lubrication equation even for α as low as 0.03157. In order to identify the origin of this discrepancy, we rescale the modified lubrication equation (1.11) with $H \equiv \alpha\eta$,

$$\alpha^3 q = \alpha^2 H - \frac{H^3}{3}\left\{(1-H)\cos\theta - \frac{\mathrm{d}H}{\mathrm{d}\theta}\sin\theta\right\} \tag{1.23}$$

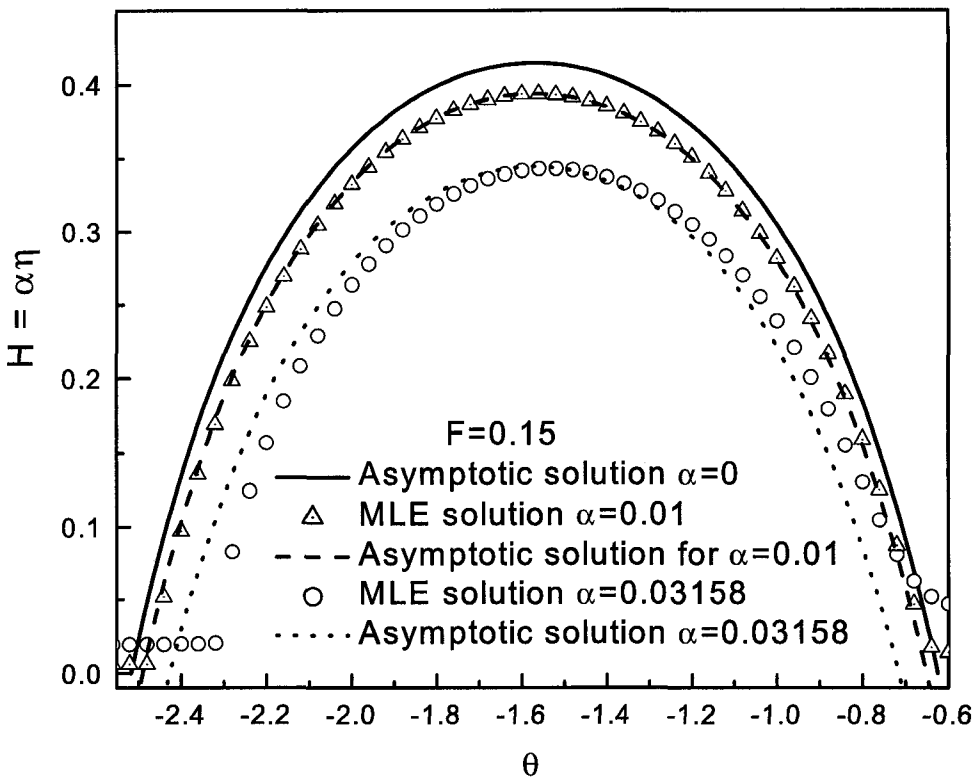

Figure 1.3: The film thickness profile as obtained from the asymptotic solution of equation (1.19), with φ being given by (1.22) is compared with those obtained from the numerical solution of the modified lubrication equation (MLE) for $F = 0.15 < 0.50$.

The leading order term, $O(1)$, gives,

$$(1 - H)\cos\theta - \frac{\mathrm{d}H}{\mathrm{d}\theta}\sin\theta = O(\alpha^2) \tag{1.24}$$

the solution to which subject to the boundary conditions $H = 0$ as $\theta = -\pi/2 \pm \varphi$, gives equation (1.19) with $H_{max} = 1 - \cos\varphi$ at $\theta = -\pi/2$. But since, by definition, $\mathrm{d}H/\mathrm{d}\theta = 0$ at $\theta = \theta^*$, we have, on account of equation (1.23),

$$\cos\theta^* = \frac{3}{H_{max}^2(1 - H_{max})}\alpha^2 + O(\alpha^3) \tag{1.25}$$

hence, expanding $\cos\theta^*$ about $\theta^* = -\pi/2$ and substituting $H_{max} = 1 - \cos\varphi$ into the above equation, we obtain the leading order correction to the location of H_{max},

$$\theta^* + \frac{\pi}{2} \approx \frac{3}{\cos\varphi(1 - \cos\varphi)^2}\alpha^2 \tag{1.26}$$

The coefficient of α^2 on the right-hand side of the above equation is, however, quite large, being equal, for example, to approximately 30 for $F = 0.15$, and therefore θ^* deviates significantly from $-\pi/2$ even if α is very small.

We can see therefore that since, as shown in Fig 1.2 (and also in Figs 3-6 of ref[3]), there is excellent agreement for $F \leq 0.15$ between the film profiles, as obtained from (1.11) and (1.13), and those computed by solving numerically the full two-dimensional Stokes equations using the NEKTON software (Fluent. Inc), the modified lubrication equation (1.11) subject to (1.13) can be used with confidence to represent the liquid film profiles for low fill fractions. In fact, as shown in Fig 1.4, this agreement extends to the case $F = 0.36$ where the film is far from thin. To be sure, owing to the presence of numerical instabilities, all the NEKTON software generated solutions referred to above were limited to maximum values of Ca of approximately unity, but in all cases involving an asymmetric film profile, the condition (1.18), $Ca \gg \alpha^2$, was met.

The case $F \sim 0.36$ merits special attention for the following reason:

Recall that, according to the standard lubrication approximation, equations (1.5) and (1.7), the liquid thickness profile will be symmetric only if β is below $\beta^* = 1.4142\ldots$ where q attains its maximum value $q_{max} = 2/3$. As first pointed out by Moffatt [5], the latter case can be obtained by setting $\theta = 0$ in equation (1.5) and then maximizing q with respect to $a_0 \equiv \eta(0)$. This leads to the condition that $a_0 = 1$, hence $q_{max} = 2/3$. Then, from the integral of the corresponding symmetric solution of equation (1.5) we find, on account of equation (1.7), the first critical value of $\beta = \beta^*$ quoted above. But when the process is repeated starting from equation (1.11), we find that

$$q = a_0 - \frac{1}{3}a_0^3 + \frac{\alpha}{3}a_0^4 \tag{1.27}$$

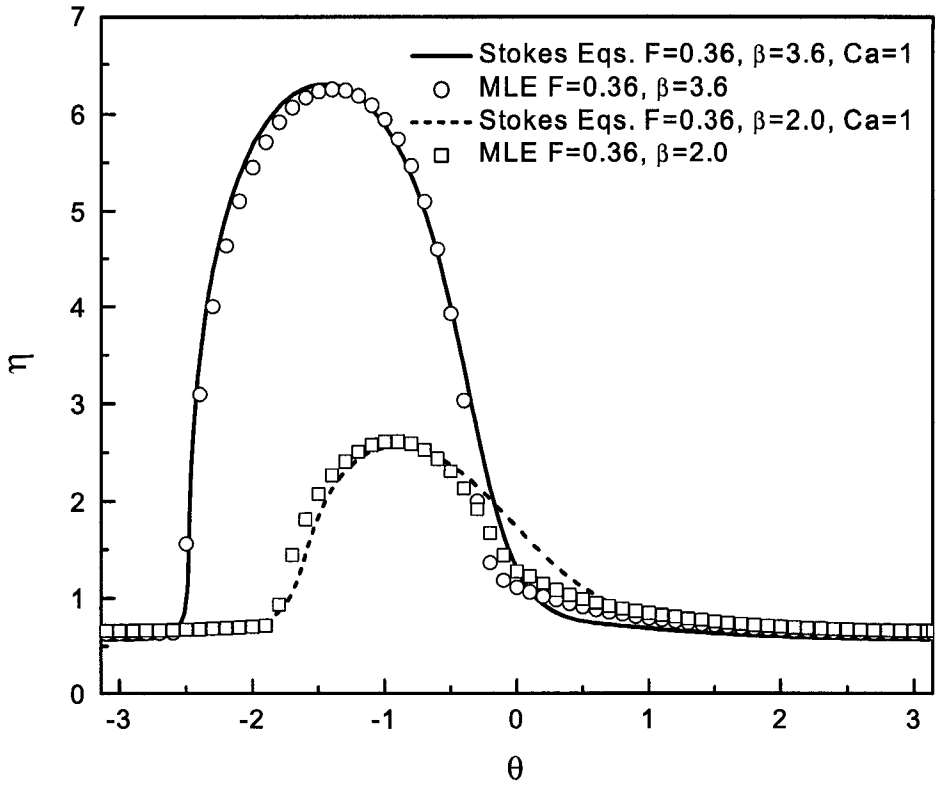

Figure 1.4: The solutions obtained from the two-dimensional Stokes equations and the modified lubrication equation (MLE) agree with each other for $\beta = 2.0 < \beta^{**}$ and $\beta = 3.6 > \beta^{**}$ when the fill fraction F is 36%.

and therefore,

$$\frac{\mathrm{d}q}{\mathrm{d}a_0} = 0 = 1 - a_0^2 + \frac{4\alpha}{3}a_0^3 \tag{1.28}$$

Clearly then, q_{max}, as obtained by solving equations (1.27) and (1.28), no longer equals 2/3 but in fact depends on the value of α. Similarly, β^*, as obtained from equation (1.13) using the symmetric solution of equation (1.11) with $q = q_{max}$, also becomes a function of α, albeit a weak one. This function, henceforth denoted as $\beta^*(\alpha)$, is seen plotted in Fig 1.5. But, interestingly, equation(1.28) has a positive real root for which q_{max} is positive, only if $\alpha \leq \sqrt{3}/6$. In fact, when $\alpha = \sqrt{3}/6$, $q_{max} = 0.866\ldots$ and from equations (1.11) and (1.13), $\beta^*(\sqrt{3}/6)$ is found to equal $1.788\ldots$ which is higher than the value $\beta^*(0) = 1.4142\ldots$ given by the standard lubrication analysis. The corresponding value of $F \cong 0.52$. But, when the film profile becomes

asymmetric, we have to solve another cubic equation (*cf* equation (17) in ref[3]),

$$1 - a_0^2 + \frac{5}{3}\alpha a_0^3 = 0 \tag{1.29}$$

for the value of a_0, which is substituted into equation (1.27) to obtain q. Therefore, there is another limitation to the maximum value of α which insures the existence of a real positive root of the cubic equation (1.29) for determining the flow rate q, that is, $\alpha \leq 2\sqrt{3}/15 \cong 0.231$.

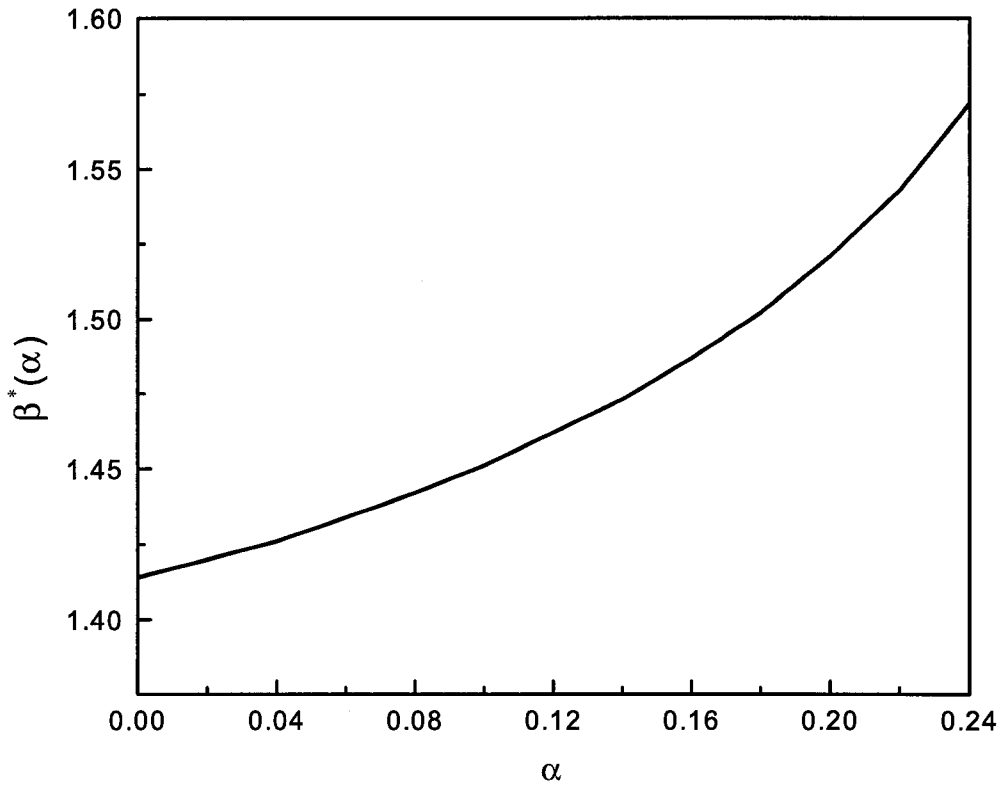

Figure 1.5: The parameter β^* given by the modified lubrication equation is increasing monotonically with α.

When $\alpha = 2\sqrt{3}/15 < \sqrt{3}/6$, we can use equation (1.28) to determine a_0 and, through equation (1.27), the maximum flow rate, viz. $q_{max} = 0.78\ldots$, and then from the numerical solutions of equation (1.11) subject to (1.13), $\beta^*(2\sqrt{3}/15) = 1.55\ldots$ which is only slightly higher than the value $\beta^*(0) = 1.4142\ldots$ given by the standard lubrication equation (1.5). The corresponding value of the fill fraction,

$F \equiv (2\sqrt{3}/15)\beta^*(2\sqrt{3}/15) \cong 0.36$ which is less than $F \cong 0.52$. Hence, as long as F does not exceed 0.36, the modified lubrication equation (1.11) has a periodic solution for all α.

First, let us discuss the case $F \leq 0.36$, for example, $F = 0.30$. Here, we find that equation (1.11) subject to (1.13) has: i) an asymmetric solution for $0 < \alpha < 0.197\ldots = 0.30/\beta^*(0.197\ldots)$ with the corresponding flow rate q increasing monotonically with α; ii) for $\alpha = 0.197\ldots$, either an asymmetric solution with $q = 0.750\ldots$, or a symmetric solution with $q = 0.760\ldots$, which, in fact, is the maximum flow rate for this value of F (these two solutions are shown in Fig 1.6); iii) a symmetric solution for $0.197\ldots < \alpha < \infty$, with the corresponding flow rate q decreasing monotonically with α starting with $q_{max} = 0.760\ldots$ at $\alpha = 0.197\ldots$. On the other hand, when $0.36 < F \leq 0.52$, equation (1.11) has a continuous, periodic solution but not over the whole range of $0 < \alpha < \infty$. For example, for $F = 0.4$, equation (1.11) subject to (1.13) has: i) an asymmetric solution for $0 < \alpha \leq 2\sqrt{3}/15$, with the corresponding flow rate q increasing monotonically with α; ii) no solution for $2\sqrt{3}/15 < \alpha < 0.250\ldots \equiv 0.40/\beta^*(0.250\ldots) < \sqrt{3}/6$; iii) a symmetric solution for $0.250\ldots \leq \alpha < \infty$ with the corresponding flow rate q decreasing monotonically with α from its maximum value $q_{max}(0.250\ldots) = 0.807\ldots$.

Shown in Fig 1.7 is a comparison between the film profiles as predicted from (1.11) and (1.13) and those from (1.5) and (1.7) for $F = 0.05$ and for a range of $\beta \equiv F/\alpha$. Clearly, the two sets are practically identical when the film is homogeneous ($\beta \leq \beta^*(0) \equiv 1.414\ldots \sim \beta^*(0.035)$, i.e. $\alpha \leq 0.0353\ldots$) but, when the film becomes asymmetric, the two sets obviously diverge, in fact catastrophically so when $\beta > \beta^{**} \equiv 2.21\ldots$ where a solution to (1.5) and (1.7) no longer exists over the whole range $-\pi \leq \theta \leq \pi$. Thus, one might be tempted to conclude that, for $\beta > \beta^*$, it is no longer possible to represent any liquid film profile by the discontinuous solutions of (1.5) and (1.7) even if the discontinuity were to be smoothed over by the solution

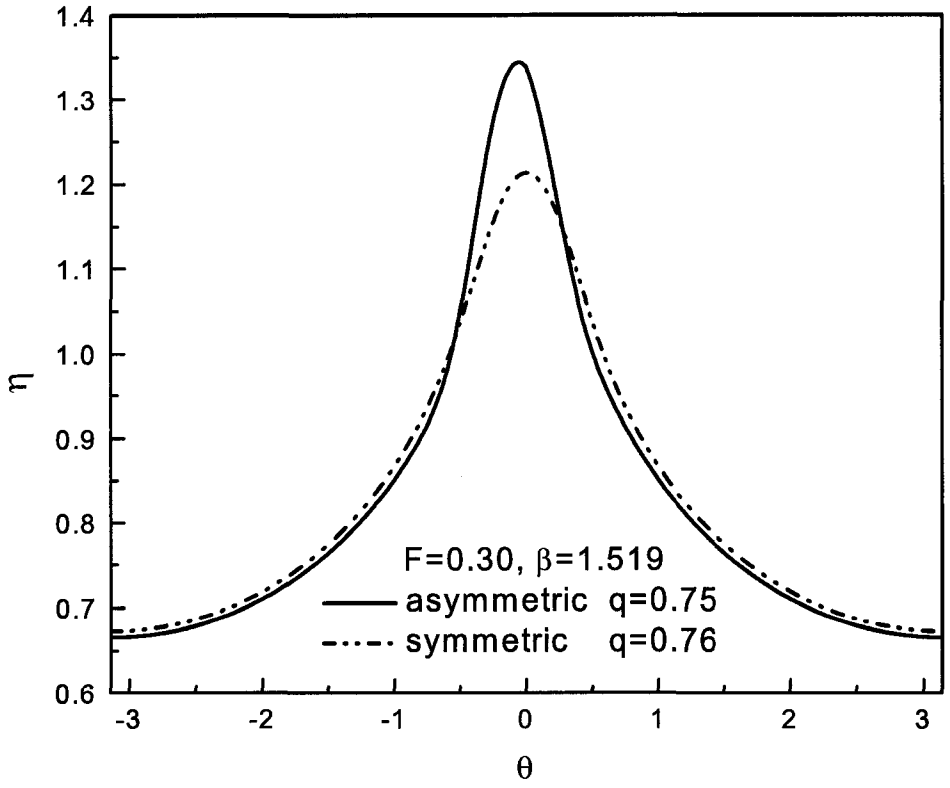

Figure 1.6: The asymmetric and symmetric solutions of the modified lubrication equation (MLE) for $F = 0.30$ and $\beta = 1.519$.

of an "inner" equation, for example (1.11) or possibly (1.17), which retain some of the terms that were left out in the standard lubrication analysis.

Nevertheless, in what follows, we shall first show, using (1.11) and (1.13), that the asymmetric solutions of (1.5) and (1.7) for $\beta > \beta^*$, do in fact represent the liquid film profile everywhere even when β exceeds β^{**}, except at the point of discontinuity but only for the case $F \to 0$, $\alpha \to 0$ with $\beta \equiv F/\alpha$ **fixed**. In general, however, this requires that the values of F be exceedingly small. We shall then examine the temporal stability on all these two-dimensional flows, as well as their stability to axial disturbances.

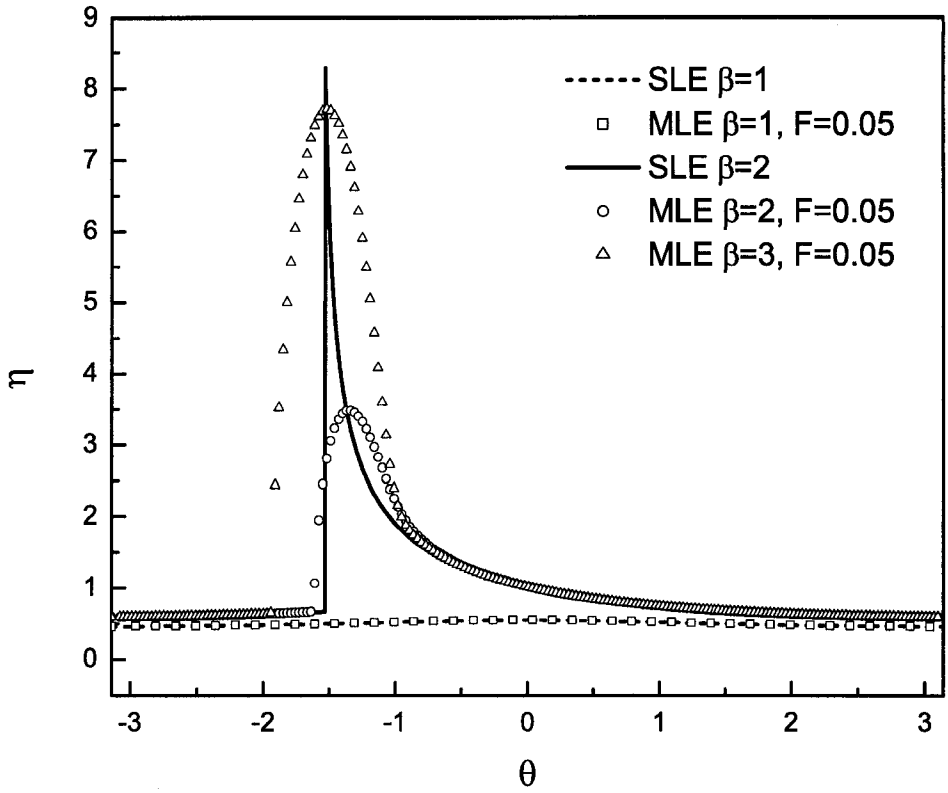

Figure 1.7: The film thickness $\eta(\theta)$ given by the standard lubrication equation (SLE) and the modified lubrication equations (MLE) are compared when $\beta = 1,\ 2$ and 3.

1.2 Film profiles for $\alpha \to 0$ and fixed β

As was said earlier, the solutions of equations (1.11) and (1.13) when $\alpha \to 0$ with F fixed bear no relation to those of the standard lubrication analysis especially considering that the latter does not have a solution for $\alpha < F/\beta^{**}$. We now turn to the case $\alpha \to 0$ with $\beta \equiv F/\alpha$ fixed and examine under what conditions, if any, the solutions of (1.11) and (1.13) asymptote to those of (1.5) and (1.7). We shall examine separately the three cases: **a)** $0 < \beta < \beta^*$; **b)** $\beta^* < \beta < \beta^{**}$; and **c)** $\beta > \beta^{**}$.

Case a ($0 < \beta < \beta^*$) Here, both (1.5) and (1.11), subject to (1.7) and (1.13) respectively, admit symmetric solutions, hence the solution to (1.11) and (1.13) can be constructed simply by means of the regular perturbation expansion. Since $F < 1$,

we expand η and q in a power series of F,

$$\eta = \eta_0 + F\eta_1 + F^2\eta_2^2 + \cdots \tag{1.30}$$

and

$$q = q_0 + Fq_1 + F^2q_2 + \cdots \tag{1.31}$$

then, substitute these into the modified lubrication equation (1.11). The corresponding leading order, $O(1)$, equation is

$$q_0 = \eta_0 - \frac{\eta_0^3}{3}\cos\theta \tag{1.32}$$

subject to

$$\beta = \frac{1}{\pi}\int_{-\pi}^{\pi}\eta_0 \mathrm{d}\theta \tag{1.33}$$

Since β is given, we can solve equation (1.32) to obtain η_0 which has to satisfy equation (1.33). Clearly, the magnitude of η_0 is $O(\beta)$. To next order, $O(F)$, the equation is

$$q_1 = \eta_1\left\{1 - \eta_0^2\cos\theta\right\} + \frac{\eta_0^3}{3\beta}\left\{\eta_0\cos\theta + \eta_0'\sin\theta\right\} \tag{1.34}$$

subject to

$$0 = \int_{-\pi}^{\pi}\eta_1 \mathrm{d}\theta - \frac{1}{2\beta}\int_{-\pi}^{\pi}\eta_0^2 \mathrm{d}\theta \tag{1.35}$$

Since the η_0 and β are known, we can solve for η_1 which satisfies equation (1.35). The other higher order terms in equation (1.30) can be obtained by following a similar procedure. This case will therefore not be pursued any further.

Case b ($\beta^* < \beta < \beta^{**}$) Here, as was already noted in the introduction, the solution to equations (1.5) and (1.7) is asymmetric and has a discontinuity at $\theta = \theta^*$, with the value of θ^*, lying between $-\pi/2$ and 0, being determined by β. For $\alpha \to 0$ and β fixed, we seek therefore to construct an asymptotic solution to equations (1.11) and (1.13) in which (1.5), with $q = 2/3$ and subject to (1.7), serves as the first term of the outer solution valid for $-\pi \leq \theta < \theta_-^*$ and $\theta_+^* < \theta \leq \pi$. Within

the inner region, the last term in (1.11) clearly plays a significant role and hence, following Johnson[6], we require that the corresponding inner solution $\hat{\eta}$ satisfy:

$$\frac{2}{3} = \hat{\eta} - \frac{1}{3}\hat{\eta}^3 \cos\theta^* + \frac{1}{3}\hat{\eta}^3 \frac{\mathrm{d}\hat{\eta}}{\mathrm{d}\psi} \sin\theta^* + O(\alpha) \tag{1.36}$$

with $\psi \equiv (\theta - \theta^*)/\alpha$. As $\psi \to \pm\infty$, the solution of (1.36) clearly matches with $\eta_+(\theta^*)$ and $\eta_-(\theta^*)$, respectively, the higher and lower positive roots of (1.5) at $\theta = \theta^*$ and $q = 2/3$. On the other hand, the solution of (1.36) is not unique given that it is unaffected if an arbitrary constant is added to the definition of ψ [6]. To obtain a unique solution we therefore need to determine the $O(\alpha)$ correction to the outer solution of (1.11). To this end, we let in the outer region $-\pi \leq \theta < \theta_-^*$ and $\theta_+^* < \theta \leq \pi$,

$$\eta = \eta_0(\theta) + \alpha\eta_1(\theta) + \cdots \tag{1.37}$$

where, as before, $\eta_0(\theta)$ satisfies (1.5) with $q = 2/3$ and subject to (1.7). Equation (1.37), when substituted into (1.11) and (1.13) and, in view of the fact that $q = 2/3 + \alpha/3 + \cdots$ (*cf* ref[3] top of p.17) leads to

$$\frac{1}{3} = (1 - \eta_0^2 \cos\theta)\eta_1 + \frac{1}{3}(\eta_0^4 \cos\theta + \eta_0^3 \eta_0' \sin\theta) \tag{1.38}$$

hence,

$$\eta_1 = \frac{1 - \eta_0^4 \cos\theta - \eta_0^3 \eta_0' \sin\theta}{3(1 - \eta_0^2 \cos\theta)} \tag{1.39}$$

everywhere within the outer region. It can easily be shown that η_1, which equals $5/6$ at $\theta = 0$, is continuous everywhere within this outer region.

Finally, on applying equation (1.13) and taking into account that

$$\beta = \frac{1}{\pi}\int_{-\pi}^{\pi} \eta_0 \mathrm{d}\theta$$

we find that

$$0 = \int_{-\pi}^{\theta_-^*} (\eta_1 - \frac{1}{2}\eta_0^2)\mathrm{d}\theta + \int_{\theta_+^*}^{\pi} (\eta_1 - \frac{1}{2}\eta_0^2)\mathrm{d}\theta + \int_{-\infty}^{0} [\hat{\eta} - \eta_-(\theta^*)]\mathrm{d}\psi - \int_0^{\infty} [\eta_+(\theta^*) - \hat{\eta}]\mathrm{d}\psi \tag{1.40}$$

which implicitly determines the unknown constant, for example the value of $\hat{\eta}(0)$, needed for obtaining a unique solution to the inner equation (1.36).

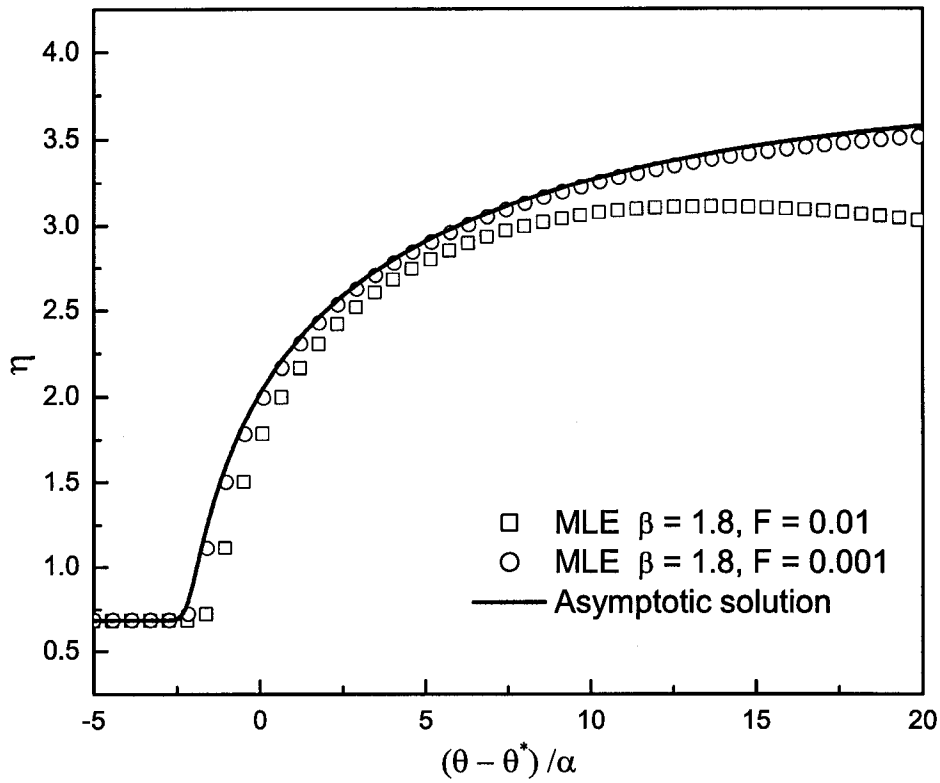

Figure 1.8: The film thickness profiles as obtained from the asymptotic solution of equation (1.36) are compared with those computed from the numerical solution of the modified lubrication equation (MLE) for $\beta = 1.8 < \beta^{**}$.

Figs 1.8-1.9 show several film profiles as obtained from: a) the asymptotic analysis given above; b) the numerical solution of (1.11) and (1.13); and c) the numerical solution of the full two-dimensional Stokes equations using the NEKTON software referred to earlier. Evidently there is good agreement between the three sets thereby leading us to conclude that:

1. The boundary-layer-type equation (1.36), first presented by Johnson [6], correctly describes the film profile in the intermediate region between the higher and lower positive roots of (1.5), with $q = 2/3$, near $\theta = \theta^*$, the point of discontinuity of the film profile as obtained by the standard lubrication analysis,

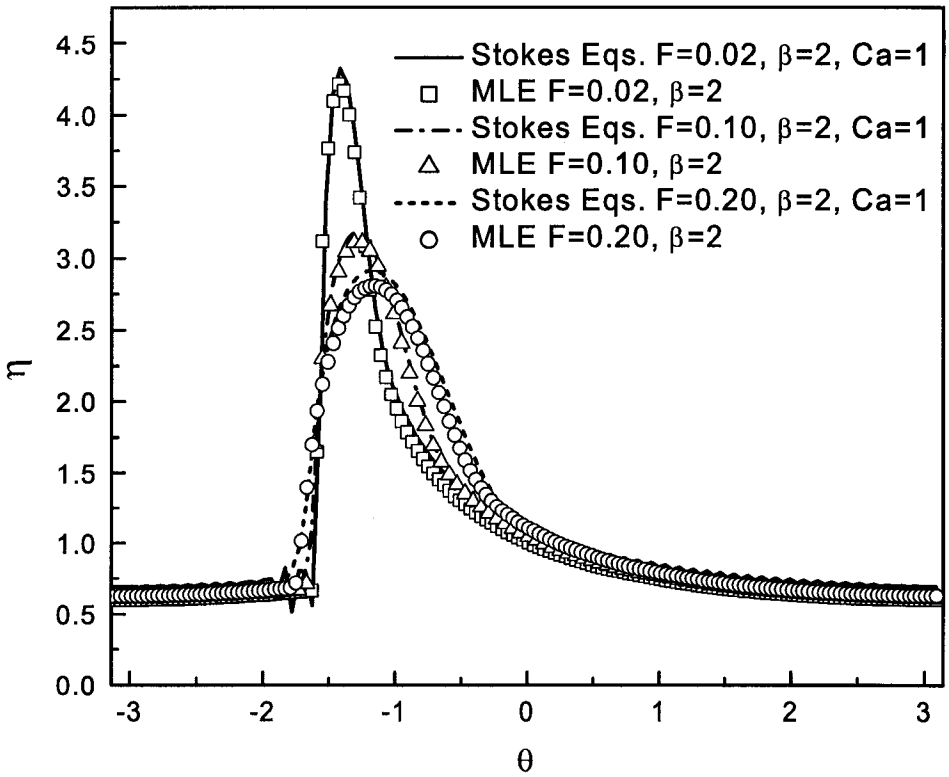

Figure 1.9: The film thickness profiles as obtained from the numerical solutions of the modified lubrication equation (MLE) closely agree with those obtained by solving the two-dimensional Stokes equations for $\beta = 2 < \beta^{**}$ for $F = 0.02,\ 0.10$ and 0.20.

but only under the asymptotic conditions $\alpha \to 0$ and fixed $\beta \equiv F/\alpha$ with $\beta^* < \beta < \beta^{**}$.

2. As was the case $0 < \alpha < \infty$ with $F \leq 0.36$ fixed mentioned in the introduction, the continued good agreement between the solution of (1.11) and (1.13) and that of the full two-dimensional Stokes equations implies that (1.11) subject to (1.13) can be used with confidence for $0 < \alpha < \infty$ for fixed β as well. In fact, it will be shown later on, that this agreement extends for all values of β, i.e. even when $\beta > \beta^{**}$.

The analysis presented above presupposes of course that surface tension effects are negligible. This, according to (1.18), requires that $Ca \gg \alpha^2$ provided that η' and η''' are both $O(\eta)$. This latter condition is not satisfied within the inner region,

however, and, as can easily be seen by comparing (1.17) and (1.36), the surface tension is negligible with in this inner region $\theta + \theta^* \sim O(\alpha)$ only if $Ca \gg 1$, a requirement which, of course, is much more restrictive than that given by (1.18). But the agreement between the asymptotic solutions assuming zero surface tensions and the NEKTON calculations with $Ca = 1$ would seem to indicate that the capillary forces are not as important under these conditions as might have been expected on the basis of the estimate given above.

Case c ($\beta > \beta^{**}$) In this case, equation (1.5) subject to (1.7) does not have a solution and therefore the construction of an asymptotic expansion has to proceed with care. First of all, we note that as $\beta \to \beta^{**}$ from below, the dimensionless film thickness increases and becomes unbounded but integrable at $\theta = -\pi/2$, the point of symmetry of the liquid puddle that forms when the cylinder stops rotating ($\alpha = 0$). Therefore, with $\beta_1 = \beta - \beta^{**} > 0$, we seek an asymptotic solution of (1.11) subject to (1.13) in which the solution of the algebraic equation (1.5) with $q = 2/3$ and $\beta_1 = 0$ serves as the outer solution on either side of the point of discontinuity $\theta = -\pi/2$, plus an asymptotically thin boundary layer within which η increases without bound as $\alpha \to 0$. To this end, let

$$\Phi \equiv \theta + \pi/2$$

in terms of which equation (1.11) becomes,

$$q = \eta - \frac{1}{3}\eta^3\{(1 - \alpha\eta)\sin\Phi + \alpha\eta'\cos\Phi\} \tag{1.41}$$

Letting $\alpha \to 0$, we therefore recover the outer solution

$$\frac{2}{3} = \eta^* - \frac{1}{3}(\eta^*)^3 \sin\Phi$$

for

$$\Phi > 0_+ \text{ and } \Phi < 0_-$$

for which

$$\frac{1}{\pi}\int_{-\pi/2}^{3\pi/2}\eta^* \mathrm{d}\Phi = \beta^{**} \equiv 2.21\ldots$$

We note that, as $\Phi \to 0_+$, $\eta^* \to (3/\Phi)^{1/2}$, and that $\eta^* \to 2/3$ as $\Phi \to 0_-$.

Next, we seek a transformation $\hat{\eta} = \eta\alpha^a$, $\hat{\Phi} = \Phi\alpha^{-b}$, with a and b both positive, such that $\hat{\eta}$ and $\hat{\Phi}$ become $O(1)$ within the boundary layer. In view of (1.41), we are left with two choices:

i) $a = 1/5$, $b = 2/5$ in which case (1.41) becomes

$$\frac{\mathrm{d}\hat{\eta}}{\mathrm{d}\hat{\Phi}} = -\hat{\Phi} + \frac{3}{\hat{\eta}^2} + O(\alpha^{1/5}) \tag{1.42}$$

or

ii) $a = b = 1/3$

$$\frac{\mathrm{d}\hat{\eta}}{\mathrm{d}\hat{\Phi}} = -\hat{\Phi} + O(\alpha^{1/3}) \tag{1.43}$$

The first choice, however, can increase the value of

$$\beta_1 \equiv \beta - \beta^{**} = \frac{1}{\pi}\int_{-\pi/2}^{3\pi/2}(\eta - \eta^*)\mathrm{d}\Phi \tag{1.44}$$

by an amount of at most $O(\alpha^{1/5})$ and, hence, cannot lead to a solution for $\beta_1 = O(1)$. We are left then with the second possibility, equation (1.43), the solution to which is

$$\hat{\eta} = A\left\{1 - \frac{\hat{\Phi}^2}{2A}\right\} \tag{1.45}$$

where, in view of (1.44),

$$A = \frac{1}{2}\left(\frac{3\pi\beta_1}{2}\right)^{2/3} \tag{1.46}$$

with an error of $\mathrm{O}(\alpha^{1/6})$ as can be shown by straightforward analysis involving matching between (1.45) and the outer solution $\eta^* \to (3/\Phi)^{1/2}$ as $\Phi \to 0_+$.

Comparing equation (1.11) with equation (1.5), we find that the maximum value of η, as obtained from the solution of the modified lubrication equation (1.11) when $\beta \geq \beta^{**}$, lies essentially on the η vs. θ curve found from the solution of the standard

lubrication equation (1.5) when $\beta = \beta^{**}$ according to which, as mentioned earlier, $\eta = \left(\frac{3}{\pi/2+\theta}\right)^{1/2} + O(1)$ at $\theta = -\pi/2 + \varepsilon$ with $\varepsilon \to 0$. Therefore, we should center the inner solution, not at $\theta = -\pi/2$ but at $\theta = -\pi/2 + \varepsilon$. Rescaling the variables, η and θ, and comparing with the maximum value of the inner solution (1.45), we obtain

$$\varepsilon = \frac{3}{A^2}\alpha^{2/3} \tag{1.47}$$

provided that $\varepsilon \to 0$. Therefore, the inner solution becomes,

$$\hat{\eta} = A\left\{1 - \frac{(\hat{\Phi} - \varepsilon)^2}{2A}\right\} \tag{1.48}$$

We remark parenthetically that, as can be seen from the analysis given above plus (1.17), the capillary terms remain negligible within this boundary-layer provided that $Ca \gg \alpha^{4/3}$. This is less stringent than the corresponding condition ($Ca \gg 1$) which applies within the boundary-layer of Case b.

The foregoing analysis shows then that, as $\alpha \to 0$, with fixed $\beta_1 = \beta - \beta^{**} > 0$, the film profile is given by: the discontinuous solution of (1.5) with $q = 2/3$ (and with the discontinuity located at $\theta = -\pi/2$ where the largest of the two real roots of (1.5) is infinite), plus a narrow but relatively deep puddle symmetrically placed on either side of $\theta = -\pi/2$ within which the extra fluid given by the positive value β_1 is accumulated. Again, as was the case where $\beta^* < \beta < \beta^{**}$, there is good agreement between the numerical solution of (1.11) and (1.13), the NEKTON solution of the full two-dimensional Stokes equations and the asymptotic solution developed above for $\beta = 3$, as can be seen in Figs 1.10-1.11. It is also clear, however, that the asymptotic analysis applies only for exceedingly small values of α (or for F where β is fixed). For example, for $\beta = 3$ ($\beta_1 = 0.79\ldots$), the asymptotic solution developed above is in good agreement with the numerical solution of (1.11) and (1.13) only if α falls below $3.3\ldots \times 10^{-4}$, corresponding to $F < 10^{-3}$.

We can conclude, therefore that for fixed $\beta > 1.4142\ldots$ and $\alpha \to 0$, the solution to (1.5) and (1.7) together with the asymptotic analysis just presented represents the

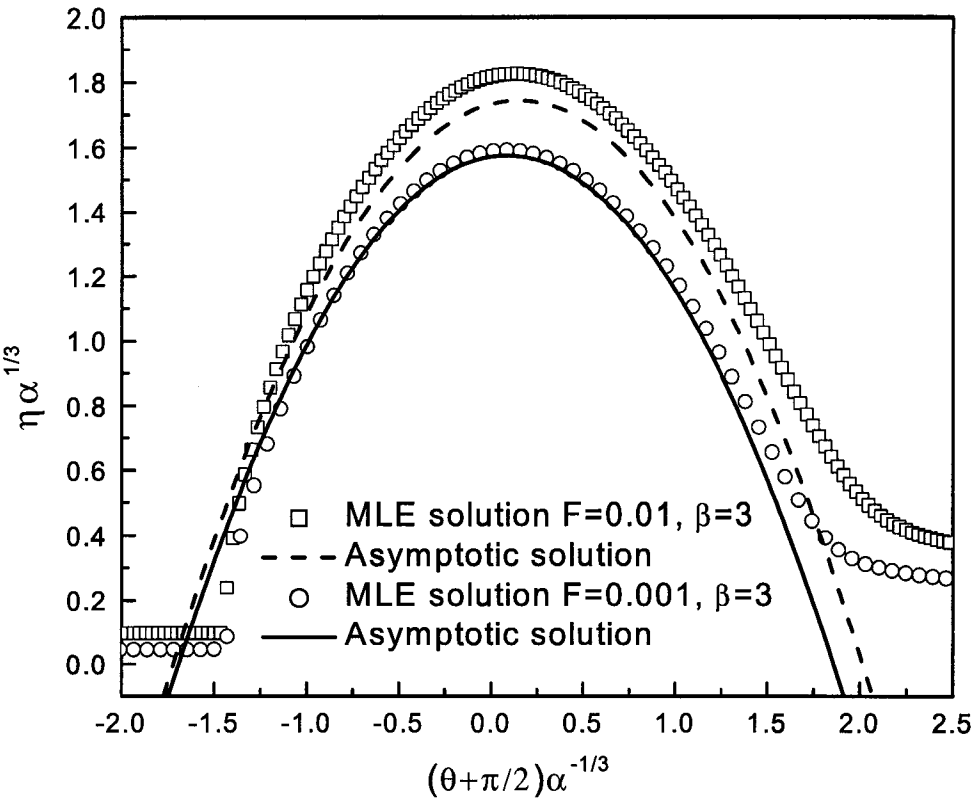

Figure 1.10: The film thickness profiles as obtained from the asymptotic solution of equation (1.48) are compared with those computed from the numerical solution of the modified lubrication equation (MLE) for $\beta = 3 > \beta^{**}$.

salient features of the liquid film profile but under extremely restrictive conditions which typically require very small values of the fill fraction F (or of α). In contrast, as shown in ref[3], the solutions of (1.5) subject to (1.7) and those of (1.11) subject to (1.13), have little in common if F is held fixed and, as α decreases towards zero, β exceeds $\beta^* \equiv 1.4142\ldots$.

For completeness, we also show in Fig 1.12 the film profiles as obtained by solving the full two-dimensional Stokes equations for the case $F = 0.60$. Here, it is interesting to notice that, as α decreases from 0.14 to 0.058, the dimensionless film profile $\eta(\theta)$, which initially is continuous, open and single-valued over the whole range of $-\pi \leq \theta \leq \pi$, becomes closed, double-valued and extends only within the half domain $0 < \theta < \pi$ (or $-\pi < \theta < 0$). Note that the minimum periodicity of $\eta(\theta)$

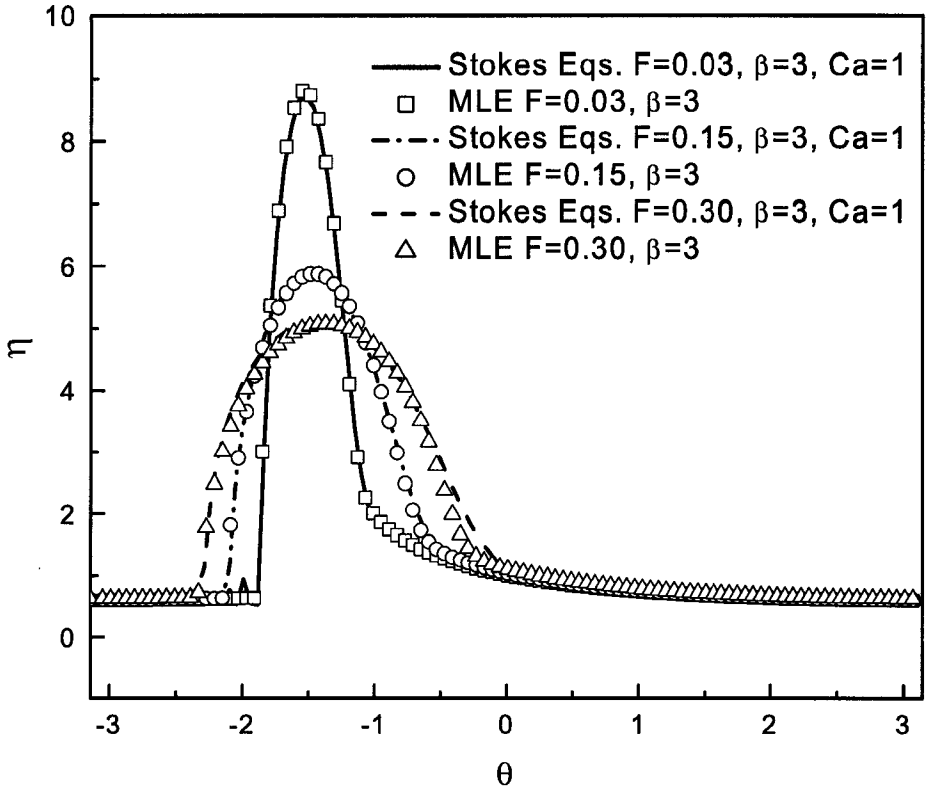

Figure 1.11: The film thickness profiles as obtained from the numerical solutions of the modified lubrication equation (MLE) closely agree with those obtained by solving the two-dimensional Stokes equations for $\beta = 3 > \beta^{**}$ for $F = 0.03,\ 0.15$ and 0.30.

for $\alpha = 0.058$ is now π rather than 2π as was the case of the larger α's. The reason for such a change is as follows:

Due to the reduction of α, more and more liquid stays within the puddle at the bottom of the cylinder until, at some value of α, the depth of the puddle exceeds the radius of the cylinder for such a high fill fraction case. Therefore, during this evolution, the axis of the rotating cylinder, which initially is within the air space, finally becomes submerged with the liquid puddle (*cf* Fig 1.12). After non-dimensionalizing the film thickness $h(\theta)$ to $\eta(\theta)(\equiv h(\theta)/\alpha R)$, we thereby obtain a closed, double-valued profile $\eta(\theta)$ if the axis of the cylinder lies within the puddle; otherwise, the profile $\eta(\theta)$ is open and qualitatively similar to that found by solving

the modified lubrication equation for $F \leq 0.36$. Given, however, that, as shown earlier, the modified lubrication equation has a periodic solution for all α only as long as F does not exceed 0.36, it would be pointless to attempt to compare any further the profiles shown in Fig 1.12 for such a high fill fraction (i.e. $F = 0.60$) with those obtained from the solution of a model equation which relies on the lubrication approximations.

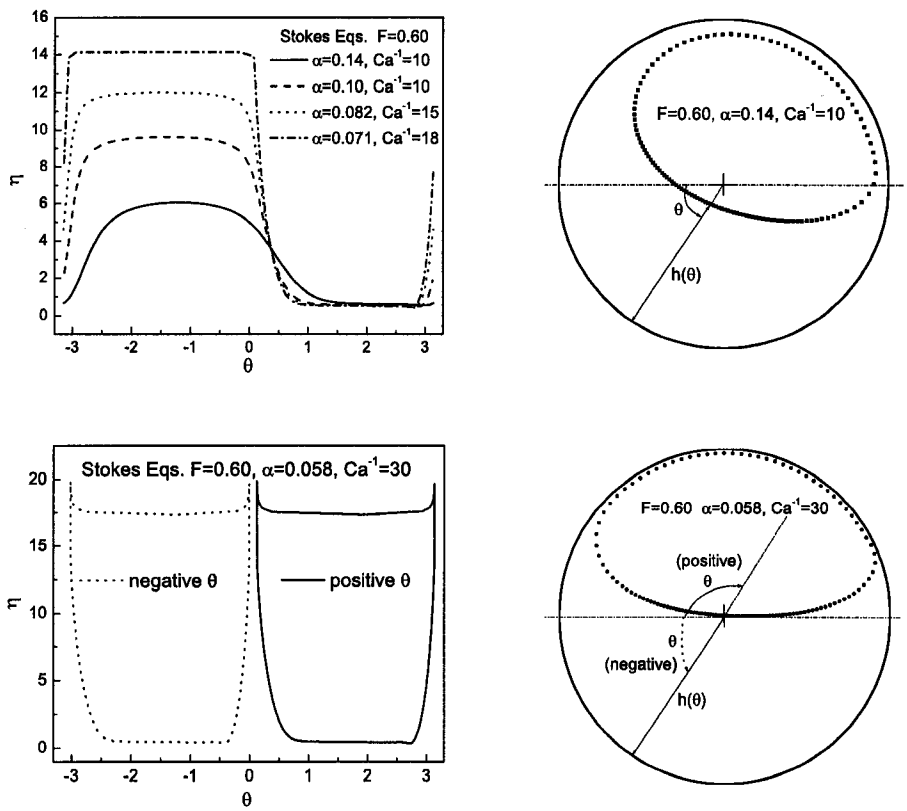

Figure 1.12: The film thickness profiles as obtained by solving the two-dimensional Stokes equations for $F = 0.60 > 0.5$.

1.3 Stability of the two-dimensional steady solutions to two-dimensional disturbances

This issue has already been examined in ref[4] on the basis of the standard lubrication equation (1.5) subject to (1.7), where it was shown that: (a) the symmetric solutions

($\beta < \beta^*$) are neutrally stable; and (b) the asymmetric discontinuous solutions ($\beta^* < \beta < \beta^{**}$) are asymptotically stable. We wish to examine whether these conclusions still apply if the base flow is given by the solutions of equations (1.11) and (1.13) which are everywhere continuous for the whole range of $0 < \beta < \infty$.

Following ref[4], we therefore let $\eta = \eta_0 + \xi$ with $\xi \ll \eta_0$ everywhere and then linearize equations (1.11) and (1.13) to yield

$$q = f(\theta)\xi + \frac{\alpha}{3}\eta_0^3 \frac{\partial \xi}{\partial \theta} \sin\theta \tag{1.49}$$

where

$$f(\theta) \equiv 1 - \eta_0^2 \cos\theta + \frac{4\alpha}{3}\eta_0^3 \cos\theta + \alpha\eta_0^2\eta_0' \sin\theta \tag{1.50}$$

On substituting the above into the kinematic condition

$$(1 - \alpha\eta_0)\frac{\partial \xi}{\partial t} + \frac{\partial q}{\partial \theta} = 0 \tag{1.51}$$

and separating variables by letting

$$\xi = \exp(\lambda t) G(\theta) \tag{1.52}$$

we therefore obtain, for the eigenvalue λ and eigenfunction $G(\theta)$,

$$\lambda(1 - \alpha\eta_0)G + \frac{\mathrm{d}}{\mathrm{d}\theta}(fG) + \frac{\alpha}{3}\frac{\mathrm{d}}{\mathrm{d}\theta}\left[\eta_0^3 \frac{\mathrm{d}G}{\mathrm{d}\theta}\sin\theta\right] = 0 \tag{1.53}$$

which must be solved subject to the periodicity and integral constraints respectively, i.e.

$$G(\theta + 2\pi) = G(\theta) \qquad \text{and} \qquad \int_{-\pi}^{\pi} (1 - \alpha\eta_0) G \mathrm{d}\theta = 0 \tag{1.54}$$

We shall consider separately the case of (a) symmetric profiles ($\beta < \beta^*$) for which f and η_0 are even functions of θ; and (b) asymmetric profiles with $\beta > \beta^*$.

(a) Stability of the homogeneous film (symmetric profile, $\beta < \beta^*$)

Let λ^* and G^* be, respectively, the complex conjugate of the indicated complex quantity. Then, on multiplying (1.53) by fG^* and its conjugate by fG, adding

the two equations followed by integrating this sum from $-\pi$ to π, we obtain after straightforward manipulations that

$$(\lambda+\lambda^*)\int_{-\pi}^{\pi}(1-\alpha\eta_0)f|G|^2\mathrm{d}\theta=\frac{\alpha}{3}\int_{-\pi}^{\pi}\eta_0^3\sin\theta\left\{2f\left|\frac{\mathrm{d}G}{\mathrm{d}\theta}\right|^2+\frac{\mathrm{d}f}{\mathrm{d}\theta}\frac{\mathrm{d}|G|^2}{\mathrm{d}\theta}\right\}\mathrm{d}\theta \quad (1.55)$$

Thus, since the integral on the left-hand side of (1.55) is positive, given that f is everywhere positive, we conclude that λ is complex if $|G|^2$ and $|\mathrm{d}G/\mathrm{d}\theta|^2$ are even functions of θ given that f and η_0 are also even functions. To see whether this is so, we seek to construct a solution of (1.53) and (1.54) by successive approximations in which, to begin with, we neglect the last term in (1.53) [This is permissible given that $\eta_0 \sim O(\beta)$ when $\beta < \beta^*$, hence $\alpha\eta_0^3/3 = O(F\beta^2/3)$ and therefore small for $F \leq 0.36$]. Consequently, to a first approximation,

$$\lambda(1-\alpha\eta_0)G+\frac{\mathrm{d}}{\mathrm{d}\theta}(fG)\cong 0 \quad (1.56)$$

The solution to which, periodic in 2π, is

$$G=\frac{c}{f}\exp\left\{-\lambda\int_0^{\theta}\frac{1-\alpha\eta_0}{f}\mathrm{d}\theta\right\} \quad (1.57)$$

where c is an arbitrary constant (to be set, in most cases and without loss of generality, equal to unity),

$$\lambda=2n\pi i/A \qquad \text{with} \qquad A=\int_{-\pi}^{\pi}\frac{1-\alpha\eta_0}{f}\mathrm{d}\theta=2\int_0^{\pi}\frac{1-\alpha\eta_0}{f}\mathrm{d}\theta$$

and n being a positive integer. [Note that the eigenfunction $G = c/f$ corresponding to $n = 0$, does not satisfy the integral constraint given by equation (1.54).] Clearly, to first approximation, the symmetric flow is neutrally stable as was already shown in ref[4] using, as the base state, that given by the solution of (1.5) and (1.7). Furthermore, we note that the real part of G, as given by (1.57), is even and the imaginary part is odd, hence, as expected from the symmetry of the base film thickness profile η_0, both $|G|^2$ and $|\mathrm{d}G/\mathrm{d}\theta|$ are symmetric and, the right-hand side

of (1.55) vanishes identically. Therefore, the symmetric steady solution remains, neutrally stable even if the analysis is carried out to $O(\alpha)$.

To examine whether this is still the case if the expansion is continued to higher order in α, we formally solve equation (1.53) and find, in addition to the homogeneous term (1.57), the particular solution G_p due to the last term in (1.53)

$$\frac{3fG_p}{\alpha} = -\eta_0^3 \sin\theta \frac{\mathrm{d}G}{\mathrm{d}\theta}$$
$$+\lambda \exp\left\{-\lambda \int_0^\theta \frac{1-\alpha\eta_0}{f}\mathrm{d}\theta\right\} \int_0^\theta \frac{1-\alpha\eta_0}{f} \exp\left\{\lambda \int_0^\theta \frac{1-\alpha\eta_0}{f}\mathrm{d}x\right\} \eta_0^3 \frac{\mathrm{d}G}{\mathrm{d}\theta} \sin\theta \mathrm{d}\theta \quad (1.58)$$

where λ is given by the corresponding expression in (1.57) to insure that f remains periodic in 2π. On substituting the expression for G given in (1.57) to the right-hand side of (1.58), we can easily show that, to $O(\alpha)$, $|G|^2$ and $|\mathrm{d}G/\mathrm{d}\theta|^2$ remain even, hence, as expected, the right-hand side of (1.55) vanishes to $O(\alpha^2)$ and λ remains purely imaginary to this order. In fact, on using successive approximations, it is not difficult to see from (1.57) that the conclusions given above remain valid to all orders in α. Thus, the inclusion of the hydrostatic pressure term which led to the improved version of the lubrication equations, viz, equations (1.11) and (1.13), has not led to a corresponding improvement in the stability characteristics of the symmetric film profiles which, according to the foregoing temporal stability analysis, remain neutrally stable.

In order to arrive at a definite conclusion regarding the stability of the homogeneous film, we therefore turn to the small capillary effects, i.e. the last two terms in equation (1.17) which we have neglected thus far in our analysis. We shall further suppose that $Ca^{-1}\alpha^3 \ll 1$ and, in order to simplify the analysis, we shall also neglect the extra $O(\alpha)$ terms in (1.17) since these only play a minor role as long as the film is homogeneous. Thus, we shall base our analysis on the standard lubrication equation (1.5) to which we add the small capillary terms from (1.17) so that, we

have, in lieu of (1.49),

$$q = f(\theta)\xi + \frac{\alpha^3}{3} Ca^{-1} \eta_0^3 \left(\frac{\partial \xi}{\partial \theta} + \frac{\partial^3 \xi}{\partial \theta^3} \right) \tag{1.59}$$

where

$$f(\theta) = 1 - \eta_0^2 \cos\theta + \alpha^3 Ca^{-1} \eta_0^2 (\eta_0' + \eta_0''')$$

with η_0 being the solution of (1.5) subject to (1.7). By repeating the arguments used previously, we therefore arrive at the equation for the eigenvalue λ and eigenfunction G,

$$\lambda G + \frac{\mathrm{d}}{\mathrm{d}\theta}(fG) + \frac{\alpha^3}{3} Ca^{-1} \frac{\mathrm{d}}{\mathrm{d}\theta} \left\{ \eta_0^3 \left(\frac{\mathrm{d}G}{\mathrm{d}\theta} + \frac{\mathrm{d}^3 G}{\mathrm{d}\theta^3} \right) \right\} = 0 \tag{1.60}$$

hence, in lieu of (1.55), we have

$$(\lambda + \lambda^*) \int_{-\pi}^{\pi} f_0 |G|^2 \mathrm{d}\theta =$$
$$\frac{\alpha^3}{3} Ca^{-1} \int_{-\pi}^{\pi} \eta_0^3 \left[2 f_0 \left| \frac{\mathrm{d}G}{\mathrm{d}\theta} \right|^2 + \frac{\mathrm{d}f_0}{\mathrm{d}\theta} \frac{\mathrm{d}|G|^2}{\mathrm{d}\theta} + \frac{\mathrm{d}(f_0 G)}{\mathrm{d}\theta} \frac{\mathrm{d}^3 G^*}{\mathrm{d}\theta^3} + \frac{\mathrm{d}(f_0 G^*)}{\mathrm{d}\theta} \frac{\mathrm{d}^3 G}{\mathrm{d}\theta^3} \right] \mathrm{d}\theta \tag{1.61}$$

where $f_0 = 1 - \eta_0^2 \cos\theta$.

On letting, *cf* (1.57),

$$G = \frac{1}{f_0} \exp\left\{ -\frac{2n\pi i}{A} \int_0^{\theta} \frac{\mathrm{d}\theta}{f_0} \right\} \qquad \text{with} \qquad A \equiv \int_{-\pi}^{\pi} \frac{\mathrm{d}\theta}{f_0}$$

we can show, after some algebra, that the integral on the right-hand side of equation (1.61) reduces to

$$-4 \left(\frac{2\pi n}{A} \right)^2 \int_0^{\pi} \frac{\eta_0^3}{f_0^5} \left\{ \left(\frac{2\pi n}{A} \right)^2 - f_0^2 - 11 \left(\frac{\mathrm{d}f_0}{\mathrm{d}\theta} \right)^2 + 4 f_0 \frac{\mathrm{d}^2 f_0}{\mathrm{d}\theta^2} \right\} \mathrm{d}\theta \tag{1.62}$$

which, on numerical integration, is found that to be negative for all $0 < \beta < \beta^*$. A plot of the (positive) integral in (1.62) for $n = 1$ is seen plotted vs. β in Fig 1.13. In addition, the asymptotic expression for the real part of the eigenvalue λ (i.e. $(\lambda + \lambda^*)/2$) as $\beta \to 0$ can be derived as follows:

From the standard lubrication equation (1.5) subject to (1.7), we find,

$$\eta_0 = \frac{\beta}{2} + \frac{1}{3} \left(\frac{\beta}{2} \right)^3 \cos\theta + \text{higher order terms in } \beta \tag{1.63}$$

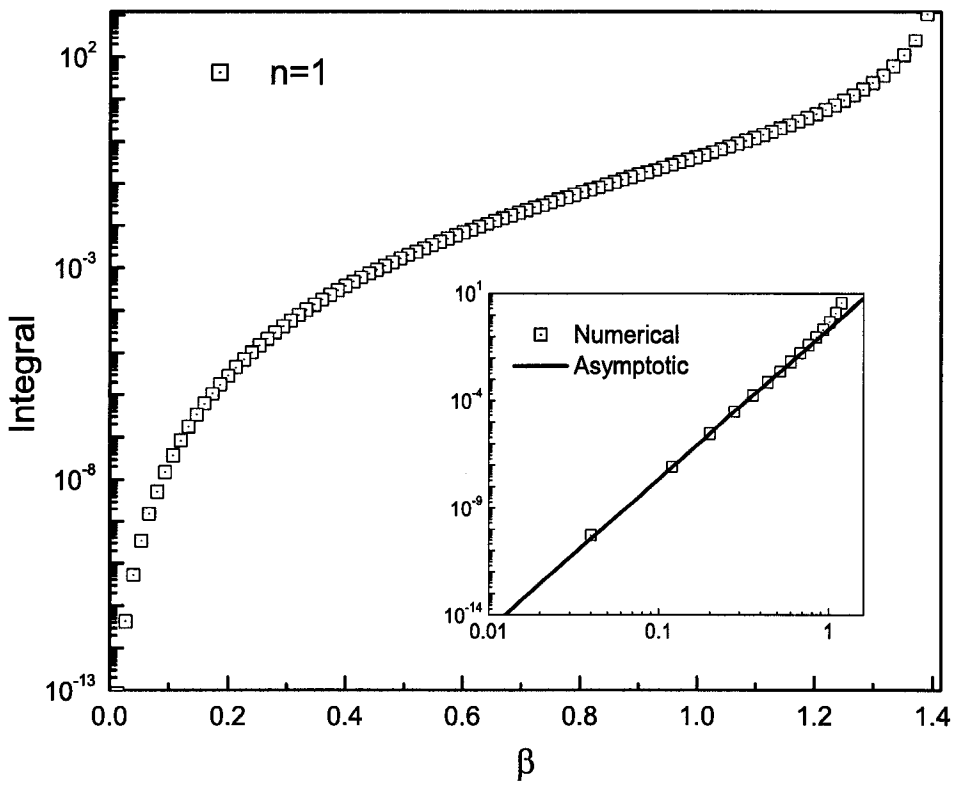

Figure 1.13: The values of the integral in (1.62) for $n = 1$ in the range of $0 < \beta < \beta^* \equiv 1.414\ldots$. In the small window, for small β, the values of the integral given by the asymptotic expression (1.64) are in good agreement with these obtained by numerical integration.

provided that $\beta \ll 1$. On substituting the above into the integral in (1.62), we can show, after some algebra, that, for $n = 1$, the leading order term of the integral is order of $O(\beta^7)$ with its coefficient being $9\pi/2^7$. As shown in Fig 1.13, there is excellent agreement for small β between the values of the integral as obtained by numerical integration and the asymptotic expression quoted above. Therefore, according to equation (1.61), we have,

$$\frac{\lambda + \lambda^*}{2} = -3\alpha^3 Ca^{-1} \left(\frac{\beta}{2}\right)^7 + \text{higher order terms in } \beta \qquad (1.64)$$

This means that, as $\beta \to 0$, the two-dimensional disturbances to the two-dimensional steady-state film decay according to $\exp(-3\alpha^3 Ca^{-1}(\beta/2)^7 t)$, in complete agreement with the results given recently by Hinch and Kelmanson[10]. We see, therefore, that,

according to the foregoing analysis, the homogeneous film is indeed asymptotically stable to small disturbances, but only weekly so, due to the weak capillary forces which have essentially no effect on the structure of the basic flow wherever $\alpha^3 Ca^{-1} \ll 1$. It is surprising that, as $\beta \to 0$, the thin film becomes less stable given that the decay rate of the small disturbances is only $O(\beta^7)$. The physical mechanisms governing such a slow decay involving a delicate interplay between rotation, gravity and surface tension was further discussed in ref[10].

(b) Stability of the inhomogeneous film (asymmetric profile, $\beta > \beta^*$)

The equation for the eigenvalue λ and the eigenfunction $G(\theta)$ is the same as that in the previous case, viz. equation (1.53) for the homogeneous film. But, before solving this equation, we shall study the equation for the eigenvalue λ and the eigenfunction G corresponding to the standard lubrication equation, viz.

$$\lambda G + \frac{\mathrm{d}(fG)}{\mathrm{d}\theta} = 0 \quad \text{with} \quad f = 1 - \eta_0^2 \cos\theta \tag{1.65}$$

which applies everywhere except at the point of discontinuity $\theta = \theta^*$. The eigenfunction G has to satisfy the periodic boundary condition.

To obtain the eigenvalue λ in equation (1.65), we expand both $\eta_0(\theta)$ and the eigenfunction $G(\theta)$ in a power series about the midpoint ($\theta = 0$),

$$\eta_0(\theta) = \sum_0^\infty a_k \theta^k \qquad \text{and} \qquad G(\theta) = \sum_0^\infty b_k \theta^k$$

and substitute these into equation (1.65). The first leading order term ($O(1)$) is

$$(\lambda - 2a_0 a_1) b_0 + (1 - a_0^2) b_1 = 0 \tag{1.66}$$

But since $a_0 = 1$ and $a_1 = -1/\sqrt{6}$ when $\beta > \beta^* \equiv 1.414\ldots$, as can be seen by substituting the power series of η into the standard lubrication equation (1.5) with $q = 2/3$, the second term in equation (1.66) vanishes automatically. Then we obtain one eigenvalue

$$\lambda = 2a_0 a_1 = -\sqrt{\frac{2}{3}} \tag{1.67}$$

In order to obtain all the other eigenvalues, we expand $G(\theta)$ in the general form,

$$G(\theta) = \theta^{n-1} \sum_{0}^{\infty} b_k \theta^k$$

where n is a positive integer, and substitute this together with the expansion of η used previously into equation (1.65). The first leading order term ($O(1)$) and the second leading term ($O(\theta)$) are

$$(n-1)(1-a_0^2)b_0 = 0 \tag{1.68}$$

and

$$(\lambda - 2na_0a_1)b_0 + n(1-a_0^2)b_1 = 0 \tag{1.69}$$

respectively. But, since $a_0 = 1$, equation (1.68) is automatically satisfied, while, from equation (1.69), we obtain all the eigenvalues

$$\lambda = 2na_0a_1 = -\sqrt{\frac{2}{3}}n \tag{1.70}$$

with $n = 1$ clearly giving the maximum eigenvalue, $\lambda = -\sqrt{\frac{2}{3}}$ which we have already obtained (*cf* equation (1.67)).

The general form of the corresponding eigenfunction G for $n = 1$ is

$$G = \frac{c}{f} \exp\left\{-\sqrt{\frac{2}{3}} \int_\theta^\pi \frac{\mathrm{d}t}{f}\right\} \tag{1.71}$$

where c is an arbitrary constant. But, since $f \to -2a_0a_1\theta = \sqrt{\frac{2}{3}}\theta$ as $\theta \to 0$, equation (1.71) needs to be rearranged so it can be applied for all θ.

First, we suppose that $\theta > 0$ and split the integral in equation (1.71) into two parts,

$$\int_\theta^\pi \frac{\mathrm{d}t}{f} = \int_\theta^\pi \sqrt{\frac{3}{2}}\frac{\mathrm{d}t}{t} + \int_\theta^\pi \left\{\frac{1}{f} - \sqrt{\frac{3}{2}}\frac{1}{t}\right\} \mathrm{d}t$$

where the second term on the right-hand side becomes $O(1)$ as $\theta \to 0$. Substituting this into equation (1.71), we obtain

$$G = \frac{c}{\pi}\frac{\theta}{f} \exp\left\{-\sqrt{\frac{2}{3}} \int_\theta^\pi \left(\frac{1}{f} - \sqrt{\frac{3}{2}}\frac{1}{t}\right) \mathrm{d}t\right\} \tag{1.72}$$

which is well-behaved around $\theta \to 0$ and can be shown to satisfy equation (1.65) with $\lambda = -\sqrt{\frac{2}{3}}$ even for $\theta < 0$ except the discontinuity.

Now, let $G(0) = 1$ without losing the generality, hence

$$G = \sqrt{\frac{3}{2}}\frac{\theta}{f} \exp\left\{\sqrt{\frac{2}{3}}\int_0^\theta \left(\frac{1}{f} - \sqrt{\frac{3}{2}}\frac{1}{t}\right) \mathrm{d}t\right\} \tag{1.73}$$

given that, as shown above, $f \to \sqrt{\frac{2}{3}}\theta$ as $\theta \to 0$. However, equation (1.73) only applies for $\theta^* < \theta \leq \pi$. On the other hand, according to equation (1.71), the eigenfunction G with $G(0) = 1$ for $-\pi \leq \theta < \theta^*$ is,

$$G = \frac{c}{f} \exp\left\{\sqrt{\frac{2}{3}}\int_{-\pi}^\theta \frac{\mathrm{d}t}{f}\right\}$$

where $c = f(\pi)G(\pi)$ given that $G(-\pi) = G(\pi)$ and $f(-\pi) = f(\pi)$. Note that on account of f being discontinuous, G is also discontinuous at $\theta = \theta^*$.

Now, returning to equation (1.53), we substitute the power series expansions of η and of G, given previously, into equation (1.53). When $n = 1$, the leading order term ($O(1)$) gives

$$\left\{\lambda(1 - \alpha a_0) - 2a_0a_1\left(1 - \frac{5}{2}\alpha a_0\right)\right\}b_0 + \left\{1 - a_0^2 + \frac{5}{3}\alpha a_0^3\right\}b_1 = 0 \tag{1.74}$$

But since, for an asymmetric base state film profile $\left\{1 - a_0^2 + \frac{5}{3}\alpha a_0^3\right\} = 0$ (*cf* equation (1.29)), we obtain one eigenvalue

$$\lambda = 2a_0a_1\frac{1 - \frac{5}{2}\alpha a_0}{1 - \alpha a_0} \tag{1.75}$$

without solving the whole equation (1.53). When $n \geq 2$, the first leading order term ($O(1)$) and the second leading order term ($O(\theta)$) are

$$(n-1)\left\{1 - a_0^2 + \left(1 + \frac{n}{3}\right)\alpha a_0^3\right\}b_0 = 0 \tag{1.76}$$

and

$$\left\{\lambda(1 - \alpha a_0) - 2a_0a_1\left[n - \frac{\alpha}{2}(n-1) - \frac{\alpha}{2}a_0(n^2 + 3n + 1)\right]\right\}b_0 + \left\{1 - a_0^2 + (4+n)\frac{\alpha}{3}a_0^3\right\}b_1 = 0 \tag{1.77}$$

respectively. But, given that $\left\{1 - a_0^2 + \frac{5}{3}\alpha a_0^3\right\} = 0$, we find that, although, equation (1.76) is automatically satisfied only when $n = 2$, the second term in equation (1.77) does not vanish automatically for any $n \geq 2$. Hence, using this method, we only can obtain one eigenvalue ($n = 1$), viz. equation (1.75). But, in view of our findings regarding the eigenvalues given by the standard lubrication equation, viz. equation (1.67), we can safely take it for granted that the eigenvalue given by equation (1.75) corresponds to the least stable mode and that the remaining eigenvalues, which can only be obtained via a numerical solution of the eigen-equation, can be ignored. Moreover, given that a_0 and a_1 are only weakly dependent on β for $\beta > \beta^*$ and fixed F, it is evident that λ, as given by equation (1.75), is similarly essentially constant — a somewhat surprising result. Moreover, in view of ref[3], $a_0 = 1 + 5\alpha/6 + O(\alpha^2)$ and $a_1 = -1/\sqrt{6} + O(\alpha)$, we have that

$$\lambda = 2a_0 a_1 \frac{1 - \frac{5}{2}\alpha a_0}{1 - \alpha a_0} \cong -\sqrt{\frac{2}{3}} + O(\alpha) < 0 \tag{1.78}$$

Hence, the stability analysis given above shows that the liquid film is indeed asymptotically stable when the film profile becomes asymmetric even for zero surface tension. The same conclusion was reached in ref[4] on the basis of the standard lubrication analysis. Note that, when $\alpha \to 0$ in equation (1.78), the eigenvalue λ becomes equal to $-\sqrt{\frac{2}{3}}$, which is precisely the maximum eigenvalue given by the standard lubrication analysis even though the latter no longer applies when $\beta > \beta^{**}$. This, indeed, is a very curious result. Shown in Fig 1.14, for a particular case, is a plot of the eigenfunction $G(\theta)$ vs. θ showing that the former, is everywhere continuous if we use the modified lubrication equations (1.11) and (1.13). The corresponding eigenfunction, given by equation (1.71) is also plotted. Clearly, the two eigenfunctions are very different even though the corresponding eigenvalues differ by only approximately 6.6% in this case.

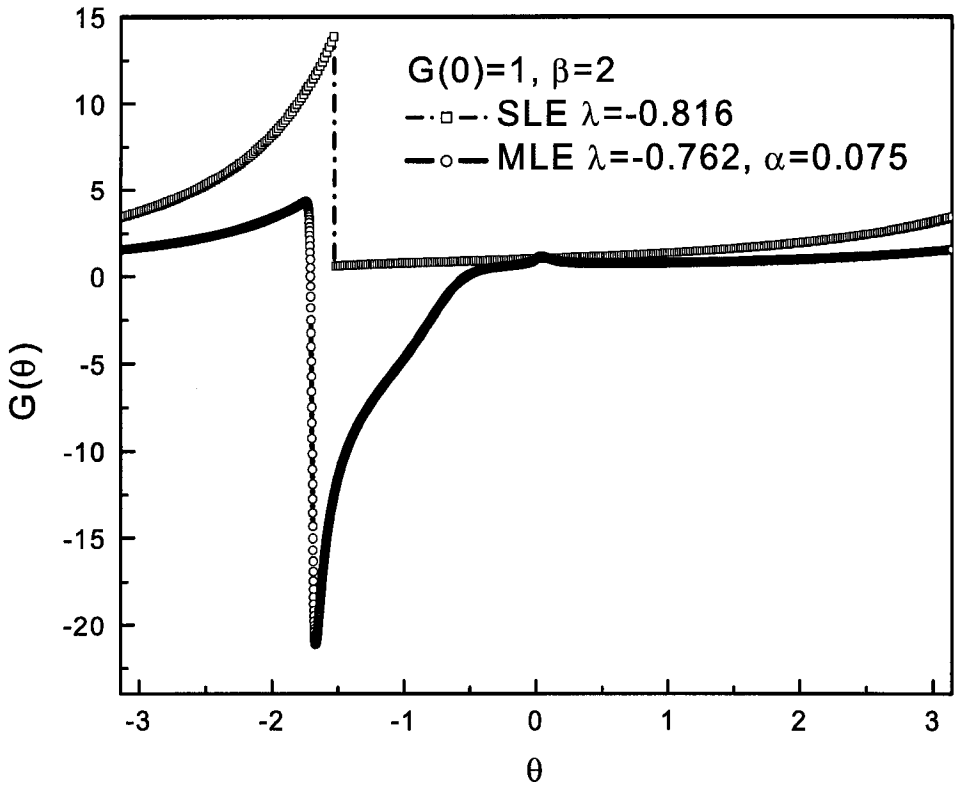

Figure 1.14: The eigenfunction $G(\theta)$, with $G(0) = 1$, as obtained from the modified lubrication (MLE) and the standard lubrication equation (SLE) for $\beta = 2.0$ and $\alpha = 0.075$. Note that the former is continuous whereas the latter is discontinuous.

1.4 Stability of the two-dimensional steady solutions to three-dimensional disturbances

This issue also has been examined in ref [4], on the basis of the standard lubrication equation (1.5) subject to (1.7), where it was shown that the steady flow is neutrally stable and that steady perturbations exist of arbitrary wavelength along the cylinder axis as long as the liquid film profile is symmetric ($\beta < \beta^*$); on the other hand, when the liquid profile is asymmetric ($\beta^* < \beta < \beta^{**}$), the steady solutions are asymptotically stable. Here, using the continuous solutions of the modified lubrication equation (1.11) subject to (1.13), we wish to examine whether or not these conclusions remain valid for the whole range of $0 < \beta < \infty$.

According to ref[4], the dimensionless axial velocity $w(\equiv \hat{w}/\Omega R$ with $\hat{w}$ being

the dimensional one) is given in the thin film approximation by

$$w = \alpha \left(\eta z - \frac{1}{2} z^2 \right) \frac{\partial \eta}{\partial x} \sin\theta \tag{1.79}$$

where $x \equiv \hat{x}/R$ is the dimensionless axial coordinate with $\hat{x}$ being the dimensional one. As shown in ref[4], equation (43), the volume conservation equation for a three-dimensional flow is

$$(1 - \alpha\eta)\frac{\partial \eta}{\partial t} + \frac{\partial q}{\partial \theta} + \frac{\alpha}{3}\frac{\partial}{\partial x}\left(\eta^3 \frac{\partial \eta}{\partial x} \right) \sin\theta = 0 \tag{1.80}$$

This equation can also be derived starting from the MLA. Letting $\eta = \eta_0 + \xi$ with $\xi \ll \eta_0$ and in view of equations (1.49) and (1.50), we therefore arrive at

$$(1 - \alpha\eta_0)\frac{\partial \xi}{\partial t} + \frac{\partial (f\xi)}{\partial \theta} + \frac{\alpha}{3}\frac{\partial}{\partial \theta}\left[\eta_0^3 \frac{\partial \xi}{\partial \theta} \sin\theta \right] + \frac{\alpha}{3}\eta_0^3 \frac{\partial^2 \xi}{\partial x^2} \sin\theta = 0 \tag{1.81}$$

which, on separating variables by letting

$$\xi = \exp(\lambda t) G(\theta) \sin(kx + b) \tag{1.82}$$

where k and b are real constants, becomes

$$\lambda(1 - \alpha\eta_0)G + \frac{\mathrm{d}(fG)}{\mathrm{d}\theta} + \frac{\alpha}{3}\frac{\mathrm{d}}{\mathrm{d}\theta}\left[\eta_0^3 \frac{\mathrm{d}G}{\mathrm{d}\theta} \sin\theta \right] - \frac{\alpha}{3} k^2 \eta_0^3 G \sin\theta = 0 \tag{1.83}$$

The above must be solved for the eigenvalue λ and eigenfunction G subject to the periodicity,

$$G(\theta + 2\pi) = G(\theta)$$

and the integral constraint,

$$\int_{-(\pi l + b)/k}^{(\pi l + b)/k} \sin(kx + b)\mathrm{d}x \int_{-\pi}^{\pi} (1 - \alpha\eta_0) G \mathrm{d}\theta = 0 \quad \text{where } l \text{ is integer.}$$

Obviously, the latter constraint is automatically satisfied for any value of the eigenfunction G. In addition, it can easily be shown that the MLA and, therefore, the kinematic condition (1.80) and the eigen-equation (1.83), are only valid for long wavelength disturbances, specifically for $k < 1/\alpha$.

We shall consider separately the case of **(a)** symmetric profiles ($\beta < \beta^*$) for which f and η_0 are even functions of θ, and **(b)** asymmetric profiles with $\beta > \beta^*$.

(a) Stability of the homogeneous film (symmetric profile, $\beta < \beta^*$)

By means of the same procedure as used previously in the corresponding two-dimensional case ($\beta < \beta^*$), we begin with the first approximation to equation (1.83),

$$\lambda(1-\alpha\eta_0)G + \frac{\mathrm{d}(fG)}{\mathrm{d}\theta} - \frac{\alpha}{3}k^2\eta_0^3 G\sin\theta \cong 0 \tag{1.84}$$

the solution to which, periodic in 2π, is

$$G = \frac{1}{f}\exp\left\{\frac{\alpha}{3}k^2\int_0^\theta \frac{\eta_0^3\sin\theta}{f}\mathrm{d}\theta\right\}\exp\left\{-\lambda\int_0^\theta \frac{1-\alpha\eta_0}{f}\mathrm{d}\theta\right\} \tag{1.85}$$

where

$$\lambda = 2\pi m i/A \qquad \text{with} \qquad A = \int_{-\pi}^{\pi}\frac{1-\alpha\eta_0}{f}\mathrm{d}\theta = 2\int_0^{\pi}\frac{1-\alpha\eta_0}{f}\mathrm{d}\theta$$

and m is zero or any positive integer. When $m = 0$, there exists a time-independent perturbation with arbitrary dependence on x,

$$\xi = G\sin(kx+b) \tag{1.86}$$

where

$$G = \frac{1}{f}\exp\left\{\frac{\alpha}{3}k^2\int_0^\theta \frac{\eta_0^3\sin\theta}{f}\mathrm{d}\theta\right\}$$

Obviously, the above expression for G automatically satisfies the periodicity and integral constraints, in contrast to the corresponding two-dimensional case, i.e. $G = 1/f$, which cannot satisfy the integral constraint (1.54).

Let λ^* and G^* be, respectively, the complex conjugate of the indicated complex quantity. Performing the same operation as shown in section 1.3, we obtain that

$$(\lambda+\lambda^*)\int_{-\pi}^{\pi}(1-\alpha\eta_0)f|G|^2\mathrm{d}\theta = \frac{\alpha}{3}\int_{-\pi}^{\pi}\eta_0^3\sin\theta\left\{2f\left|\frac{\mathrm{d}G}{\mathrm{d}\theta}\right|^2 + \frac{\mathrm{d}f}{\mathrm{d}\theta}\frac{\mathrm{d}|G|^2}{\mathrm{d}\theta} + 2k^2 f|G|^2\right\}\mathrm{d}\theta \tag{1.87}$$

Since η_0, $|G|^2$ and $|\mathrm{d}G/\mathrm{d}\theta|$ are symmetric (this was demonstrated in detail in section 1.3 dealing with the two-dimensional case), the right-hand side of equation (1.87) vanishes. Therefore, the symmetric steady solution in three dimensions remains neutrally stable even if the analysis is carried out to $O(\alpha)$.

Now, let us consider the effects of surface tension. Taking account of the capillary contribution arising from the film thickness variation along axial direction, we extend the expression for the hydrostatic pressure in the two-dimensional case, i.e. equation (1.16), to this axially non-uniform case as

$$p = \alpha(z-\eta)\sin(\theta) - \alpha^3 Ca^{-1}\left(\eta + \frac{\partial^2\eta}{\partial\theta^2} + \frac{\partial^2\eta}{\partial x^2}\right) \tag{1.88}$$

Then, by repeating the steps used earlier in the two-dimensional case, we base our analysis on the standard lubrication equation (1.5) to which we add the small capillary terms from equations (1.17) so that, we have (*cf* equation 1.59)),

$$q = f(\theta)\xi + \frac{\alpha^3}{3}Ca^{-1}\eta_0^3\left(\frac{\partial\xi}{\partial\theta} + \frac{\partial^3\xi}{\partial\theta\partial x^2} + \frac{\partial^3\xi}{\partial\theta^3}\right) \tag{1.89}$$

where

$$f(\theta) = 1 - \eta_0^2\cos\theta + \alpha^3 Ca^{-1}\eta_0^2(\eta_0' + \eta_0''') \tag{1.90}$$

with η_0 being the solutions of the standard lubrication equation (1.5) subject to (1.7). By repeating the arguments used previously in the two-dimensional case (*cf* equation (1.60)), we arrive at the equation for the eigenvalue λ and the eigenfunction $G(\theta)$,

$$\lambda G + \frac{\mathrm{d}}{\mathrm{d}\theta}(fG) + \frac{\alpha^3}{3}Ca^{-1}\frac{\mathrm{d}}{\mathrm{d}\theta}\left\{\eta_0^3\left[(1-k^2)\frac{\mathrm{d}G}{\mathrm{d}\theta} + \frac{\mathrm{d}^3G}{\mathrm{d}\theta^3}\right]\right\} - \frac{\alpha}{3}k^2\eta_0^3 G\sin\theta$$
$$-\frac{\alpha^3}{3}Ca^{-1}k^2\eta_0^3\left\{(1-k^2)G + \frac{\mathrm{d}^2G}{\mathrm{d}\theta^2}\right\} = 0 \tag{1.91}$$

Note that the last term on the left-hand side of the above equation results from the modification of the axial velocity due to the pressure (1.88). Hence, in lieu of (1.87),

we have

$$(\lambda+\lambda^*)\int_{-\pi}^{\pi} f_0|G|^2\mathrm{d}\theta = \frac{\alpha^4k^2}{3Ca}\int_{-\pi}^{\pi} 2\eta_0^5(\eta_0'+\eta_0''')|G|^2\sin\theta\mathrm{d}\theta - \frac{\alpha^3k^4}{3Ca}\int_{-\pi}^{\pi} 2\eta_0^3 f_0|G|^2\mathrm{d}\theta$$
$$+\frac{\alpha^3k^2}{3Ca}\int_{-\pi}^{\pi}\eta_0^3\left\{2f_0|G|^2 - 2f_0\left|\frac{\mathrm{d}G}{\mathrm{d}\theta}\right|^2 - \frac{\mathrm{d}f_0}{\mathrm{d}\theta}\frac{\mathrm{d}|G|^2}{\mathrm{d}\theta} + f_0G^*\frac{\mathrm{d}^2G}{\mathrm{d}\theta^2} + f_0G\frac{\mathrm{d}^2G^*}{\mathrm{d}\theta^2}\right\}\mathrm{d}\theta$$
$$+\frac{\alpha^3}{3Ca}\int_{-\pi}^{\pi}\eta_0^3\left\{2f_0\left|\frac{\mathrm{d}G}{\mathrm{d}\theta}\right|^2 + \frac{\mathrm{d}f_0}{\mathrm{d}\theta}\frac{\mathrm{d}|G|^2}{\mathrm{d}\theta} + \frac{\mathrm{d}(f_0G)}{\mathrm{d}\theta}\frac{\mathrm{d}^3G^*}{\mathrm{d}\theta^3} + \frac{\mathrm{d}(f_0G^*)}{\mathrm{d}\theta}\frac{\mathrm{d}^3G}{\mathrm{d}\theta^3}\right\}\mathrm{d}\theta \quad (1.92)$$

where $f_0 = 1-\eta_0^2\cos\theta$. The first term on the right-hand side of the above equation involving $O(\alpha^4)$ can be neglected provided that $\alpha \ll 1$ together with $k^2 \sim O(1)$ or less. [Note that, in order that α always satisfies the condition $\alpha \ll 1$ for all $\beta < \beta^*$, we have to take $F \to 0$ as $\beta \to 0$.] Under these conditions, the expression for G is, to first order, (*cf* (1.85))

$$G = \frac{1}{f_0}\exp\left\{-\frac{2m\pi i}{A}\int_0^{\theta}\frac{1}{f_0}\mathrm{d}\theta\right\} \quad \text{with} \quad A = \int_{-\pi}^{\pi}\frac{1}{f_0}\mathrm{d}\theta \qquad (1.93)$$

and m being zero or any positive integer.

On inserting the expression for G given above into (1.92), we found, using numerical integration, that when m in (1.93) is any positive integer, the sum of all the terms on the right-hand side of equation (1.92), except that involving $O(\alpha^4)$ which is neglected, is negative for $k > 0$ and becomes increasingly more negative with increasing k; however, when $m = 0$ (i.e. $G = 1/f_0$), the sum has a positive maximum, thereby implying that, according to our linear analysis, the homogeneous film is asymptotically unstable to small axial disturbances having a wavelength of the order of the cylinder radius, if we include the very weak capillary effects. Such a family of eigenvalue profiles is shown in Fig 1.15 for three typical cases $\beta = 0.13$, 0.67 and 1.23. Clearly, the magnitude of the most rapidly growing disturbance for $m = 0$ decreases with a decrease in the value of β implying that the symmetric profiles should be more unstable at the larger value of β. In addition, by means of a method similar to that described in the corresponding two-dimensional case (*cf*

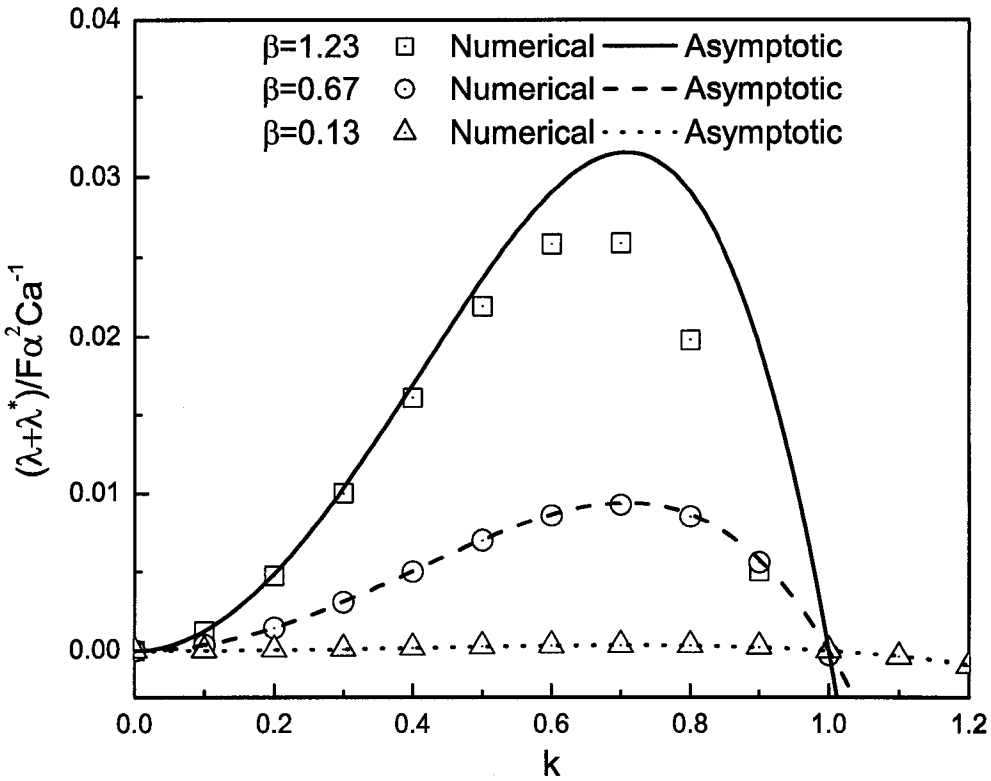

Figure 1.15: The real part of the eigenvalue λ has a positive maximum when $m = 0$ in (1.93) with the magnitude of the most rapidly amplified disturbance increasing with an increase in the value of β. As $\beta \to 0$, the values of the real part of λ for $m = 0$ predicted by the asymptotic expression in equation (1.94) are in close agreement with those obtained by numerical calculation from equation (1.92).

equation (1.63)), we can also obtain the asymptotic expression for the real part of the eigenvalue λ for $m = 0$, i.e.,

$$\frac{\lambda + \lambda^*}{2} = \frac{1}{3}k^2(1-k^2)\alpha^3 Ca^{-1}\left(\frac{\beta}{2}\right)^3 + \text{higher order terms in } \beta \qquad (1.94)$$

which, as shown in Fig 1.15, closely matches the value of $(\lambda + \lambda^*)$ calculated numerically from equation (1.92) when $\beta \to 0$. In fact, when $m = 0$, the eigenvalue λ is real and so is the corresponding eigenfunction G. Therefore, as $\beta \to 0$, we can expand λ and G in a power series in β, i.e.

$$\lambda = 0 + \lambda^a\left(\frac{\beta}{2}\right)^3 + \lambda^b\left(\frac{\beta}{2}\right)^4 + \text{higher order terms in } \beta$$

and

$$G = \frac{1}{f_0} + G^a \left(\frac{\beta}{2}\right)^3 + G^b \left(\frac{\beta}{2}\right)^4 + \text{higher order terms in } \beta$$

with

$$\frac{1}{f_0} = 1 + \left(\frac{\beta}{2}\right)^2 \cos\theta + \frac{2}{3}\left(\frac{\beta}{2}\right)^4 \cos^2\theta + \text{higher order terms in } \beta$$

and substitute them together with the expression for η in (1.63) into equation (1.91). Then, it is a straightforward matter to show that the first leading order term involving λ^a gives

$$\lambda^a = \frac{1}{3}k^2(1-k^2)\alpha^3 Ca^{-1}$$

which is in complete agreement with equation (1.94), with the corresponding G^a being

$$G^a = \frac{\alpha}{3}k^2(\cos\theta - 1)$$

Also, the next order in λ ($O(\beta^4)$) is zero, i.e. $\lambda^b = 0$, with the corresponding G^b being

$$G^b = \frac{\alpha}{12}k^2(\cos 2\theta - 1)$$

Note that, according to equation (1.94), the corresponding wavenumber k of the most rapidly growing disturbance (i.e. the location where the eigenvalue λ vs. k has a positive maximum) is found to equal $\sqrt{2}/2$ with the corresponding wavelength being $2R\sqrt{2}\pi$. Since the wavelength of such a disturbance is of the order of the cylinder radius, we believe that the mechanism for the instability, just presented, of a homogeneous liquid film to axial disturbances due to surface tension, is closely related to that of the well-known Rayleigh-Taylor instability of a stationary liquid film coating the surface of a non-rotating cylinder in the absence of gravity. [After finishing the analysis given above, we were reminded that, Hosoi & Mahadevan [11] also examined this axial stability problem by means of a numerical linear analysis starting from the lubrication equations very similar to ours but including inertia effects, and concluded that the flow should remain stable as long as inertial effects are

weak. In view of our results, however, it would appear that some of the calculations of ref[11] could have been marred by numerical inaccuracies.]

(b) Stability of the inhomogeneous film (asymmetric profile, $\beta > \beta^*$)

We begin with equation (1.83) for the eigenvalue λ and the eigenfunction $G(\theta)$ and expand both $\eta_0(\theta)$ and $G(\theta)$ in a power series about $\theta = 0$, as was done earlier in the corresponding two-dimensional case. Then, we substitute these into equation (1.83). The first and second leading order terms that we obtain are exactly the same as those in the two-dimensional case, i.e. equations (1.76) and (1.77), and therefore the expression for the maximum eigenvalue λ is, as before,

$$\lambda = 2a_0 a_1 \frac{1 - \frac{5}{2}\alpha a_0}{1 - \alpha a_0} \cong -\sqrt{\frac{2}{3}} + O(\alpha) < 0.$$

Interestingly, this maximum eigenvalue λ is independent of k, that is, the wavelength of the small axial disturbance, and is also essentially independent of β. This result shows that the two-dimensional steady solutions are asymptotically stable to axial perturbations for $\beta > \beta^*$ even for zero surface tension.

1.5 Discussion

First of all we show, on the basis of the modified lubrication equation, that the discontinuous solution of the standard lubrication equation for $\beta > 1.414\ldots$ represent correctly of the asymmetric film thickness profiles but only under the restrictive condition: $\alpha \to 0$ with β fixed. On the other hand, as shown previously [3], the solutions to the standard lubrication equation fail to represent the film thickness profiles when α is decreased with $F = \alpha\beta$ fixed, especially given that equation (1.5) subject to (1.7) has no physically acceptable solution when $\beta > 2.21\ldots$.

Secondly, according to the stability analysis given by the modified lubrication equation for these two-dimensional rimming flows, we find that, as shown previously [4] on the basis of the standard lubrication theory, the asymmetric profiles

are asymptotically stable to small two-dimensional as well as axial disturbances. In addition, we can obtain the maximum eigenvalue of these asymmetric profiles (i.e. the negative eigenvalue with the smallest absolute value) by simply expanding the corresponding eigen-equations about $\theta = 0$ instead of solving the full eigen-equation. It is surprising that this maximum eigenvalue is essentially independent of β and becomes equal to the maximum eigenvalue given by the standard lubrication equation as $\alpha \to 0$ even though the corresponding two eigenfunctions are substantially different.

On the other hand, again in conformity with ref[4], the symmetric profiles are found to be neutrally stable to small two-dimensional as well as axial disturbances if surface tension effects are neglected. When these effects are included in the stability analysis, however, the film thickness profiles are found to become asymptotically stable to small two-dimensional disturbances with the magnitude of the least stable eigenvalue increasing monotonically with β for $0 < \beta < \beta^*$, and to become asymptotically unstable to small, long wavelength, axial disturbances with the magnitude of the most rapidly amplified disturbance increasing monotonically with β for $\beta < \beta^*$. This implies that, when the surface tension is included, the symmetric profiles at the larger value of β should be more stable to two-dimensional disturbances, but should become more unstable to axial disturbances. When we performed experiments in a long cylinder (i.e. aspect ratio $L/R \gg 1$) with a very viscous fluid ($\mu = 4000cP$), we found the expected stable flows for $\beta > 1.6$, and also a variety of time dependent flows in the range $0.7 < \beta < 1.6$, which, however, seem to become stable for $\beta < 0.7$ (see also ref[4]). These experimental observations are consistent with our stability analysis. [Note that this instability requires a very long time to evolve given that $\alpha \ll 1$ and $\alpha^2 Ca^{-1} \ll 1$. Moreover, according to Fig 1.15, the magnitude of the most rapidly amplified disturbance for $\beta = 0.67$ is only one fourth of that for $\beta = 1.23$. Therefore, when β becomes even smaller (e.g. $\beta = 0.13$), this instability

is unlikely to be observed throughout the duration of an experiment.]

According to ref[4], however, there exists another possibility which can accounts for the instability when β falls in the range of $0.7 < \beta < 1.6$, due to extremely small deviations ($\leq 0.1^0$) of the cylinder's axis from the horizontal. We, therefore, turn next to consider the rimming flow in a rotating cylinder with a small inclination of $O(\delta)$ which generates a gravity induced axial flow. Thus, the expression for w (*cf* equation (1.79)), the axial component of the fluid velocity becomes,

$$w = \left\{ \alpha \frac{\partial \eta}{\partial x} \sin\theta + \delta \right\} \left(\eta z - \frac{1}{2} z^2 \right) \tag{1.95}$$

with the corresponding axial volumetric flow rate being given by

$$J = \int_{-\pi}^{\pi} \int_{0}^{\eta} w \mathrm{d}z = \frac{\alpha}{3} \int_{-\pi}^{\pi} \eta^3 \frac{\partial \eta}{\partial x} \sin\theta \mathrm{d}\theta + \frac{\delta}{3} \int_{-\pi}^{\pi} \eta^3 \mathrm{d}\theta \tag{1.96}$$

Steady state can only be achieved if J vanishes for all $0 \leq x \leq L$ where L denotes the length of the cylinder.

Now, due to the inclination, the liquid fill fraction at every cross section, referred to as F_{local}, will no longer be uniform but will be increasing monotonically with x and similarly for $\beta_{local} \equiv F_{local}/\alpha$, if the lower end of the cylinder is at $x = L$.

Under these conditions, the first term on the right-hand side of equation (1.96) is obviously zero everywhere where the film thickness profile is symmetric ($\beta_{local} < \beta^* = 1.414\ldots$), but, as found by numerical calculation, it is negative and decreasing monotonically with x wherever $\beta_{local} > \beta^*$ and $\mathrm{d}\beta_{local}/\mathrm{d}x > 0$. On the other hand, the second term is clearly always positive and, again as found by numerical calculation, is increasing monotonically with x over the whole range $0 < \beta_{local} < \infty$ if $\mathrm{d}\beta_{local}/\mathrm{d}x > 0$. Thus, if the minimum value of $\beta_{local} > \beta^*$, the film thickness at every cross section of the cylinder is asymmetric, and, therefore, the two terms on the right-hand side of equation (1.96) being, respectively, (a) negative and decreasing monotonically with x; and (b) positive and increasing monotonically with x,

can balance each other thereby allowing the net volumetric flow rate J to vanish at every cross section and a stable steady state to be achieved. But if the minimum value of β_{local} is less than $\beta^* = 1.414\ldots$, the film profile at the higher end will be symmetric, and, therefore, the first term on the right-hand side of equation (1.96) will be zero near $x = 0$, while the second term will be positive thereby insuring that a net volumetric flow rate towards the lower end will always exist. Under this situation, the flow will be always be time dependent and will never reach steady state. But this type of unsteady flow is almost impossible to observe during an experiment until a transition zone is created between the symmetric film profiles at one end and the asymmetric film profiles at the other. The reason for this is that there exists a distinction between these two type of film profiles, in that whereas the asymmetric profiles vary sharply over a restricted range of θ (referred to as a "bump"), the symmetric profiles are everywhere homogeneous. It is obvious that the time for the appearance of the transition zone will depend on the initial value of β along the length of the cylinder. For example, if, initially, β is much less than β^*, the whole inclined cylinder will be coated initially by a homogeneous film rendering it impossible to determine whether the flow in the cylinder is unsteady or not at least until such time when the film profiles at the lower end become asymmetric (24 hours or more for $\beta = 0.4$); on the other hand, if the initial value of β is relatively close to β^* (e.g. $0.7 < \beta < 1.6$), the transition zone will appear quite a bit sooner following the start of the experiment, so that this type of unsteady flow could be observed within a reasonable period of time (i.e. 8 hours for $\beta = 1.0$).

By using the arguments given above, we can also explain why the flow in the rotating cylinder with a small inclination is steady as long as, everywhere, $\beta_{local} > \beta^*$ and is unsteady for β around and below β^*. Specifically, for $\beta < \beta^*$, since the flow can never reach steady in the portion of the inclined cylinder where the film profiles are symmetric, a net volumetric flow rate towards the lower end will

always exist so that the transition zone (i.e. the region between the symmetric and asymmetric film profiles) should always move towards the higher end, consistent with the experimental observations (*cf* Fig 16 in ref[4]). However, according to the experimental observations in ref[4], for $0.7 < \beta < 1.6$, the axial motion of the transition zone may be very complicated rather than being unidirectional as was mentioned earlier. Specifically, when β is within such a range, the transition zone was found to move back and forth along the cylinder with some periodicity, contrary to the predictions of our arguments. [The relation between the periodicity and β was investigated experimentally in detail in ref[4].] Clearly, a satisfactory explanation for all the complex experimental phenomena referred to above must await the results of further studies.

Chapter 2

Experimental investigations

2.1 Introduction

When an initially homogeneous suspension containing neutrally buoyant particles is sheared in a partially filled horizontal Couette device [1] or in a partially filled horizontal single cylinder [2], the particles are found to segregate into bands separated by regions of low conentration or even pure liquid. Although numerous systematic experiments in the partially filled horizontal single cylinder have been performed by Tirumkudulu [12], the mechanism responsible for this segregation has remained elusive up to now.

Here, we first repeated some of the experiments recorded in Tirumkudulu's thesis and confirmed his previous findings. Then, we performed a large variety of new experiments in order to understand the whole process of particle segregation and shall describe each of them in detail in the following section.

2.2 Experiments with single cylinder

2.2.1 Previous experimental work

Previous experiments by Tirumkudulu [12] were performed in a cylinder which was supported horizontally by axial shafts, one coupled directly to a variable speed motor (0 to 120 rpm), the other hollow, allowing the filling and emptying of the cylinder (*cf* Fig 2.1). The liquid for the suspension consisted of a mixture of 77.4% Triton X-100, 13.4% zinc chloride ($ZnCl_2$), and 9.2% water (with the percentages based on mass) having a viscosity of 4000 cP (at 23^0C) and a density of 1.172 g/cm^3. Acrylic spherical particles of two different diameters, viz. 463 ± 37.5 μm and 60 ± 15 μm were used and the density and refractive index (RI = 1.49) of the suspending liquid were matched with those of the particles. In all the experiments, 5% to 15% of the particles were colored red for visibility.

Seven dimensionless parameters were identified as influencing the observed phe-

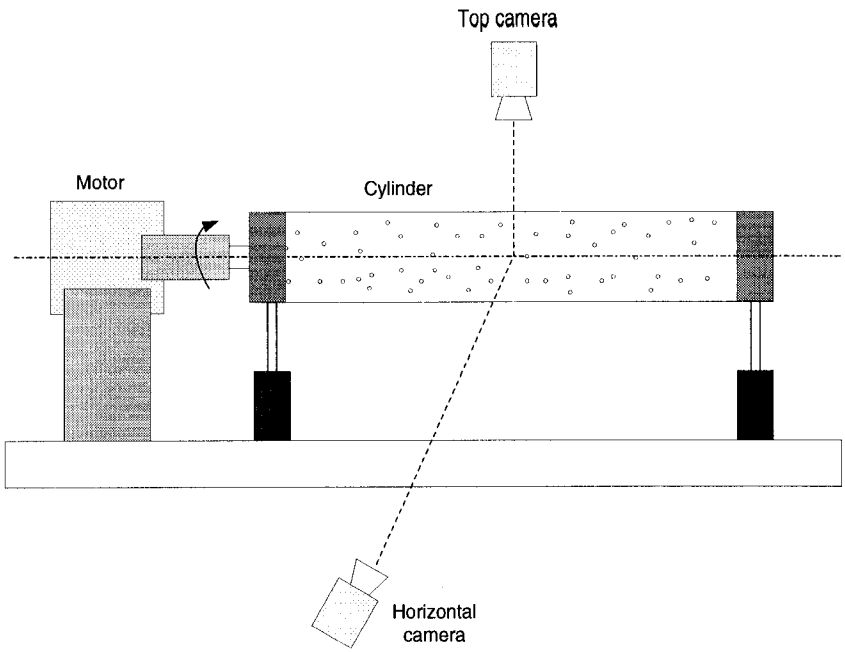

Figure 2.1: Sketch of the experimental setup

nomena, specifically: $Re \equiv \Omega \rho h_0^2/\mu$, $\alpha \equiv \sqrt{\Omega \mu/\rho g R}$, F, $Ca \equiv \Omega R \mu/\sigma$, L/R, $h_m/2\hat{a}$ and ϕ, where Re is the Reynolds number, Ω is the angular velocity of the cylinder, h_0 is the mean thickness of the film, ρ is the density of the suspension, μ is the effective viscosity of the suspension, α^2 measures the ratio of the viscous to the gravitational forces, R is the inner radius of the cylinder, g is the gravity constant, F is the fill fraction of the suspension, Ca is the capillary number referring to the relative importance of the viscous to the surface tension forces, σ is the surface tension, L is the length of the cylinder, $\eta_m = h_m/\alpha R$ is the minimum dimensionless thickness with h_m being the minimum film thickness, $a = \hat{a}/\alpha R$ is the dimensionless particle radius with $\hat{a}$ being the dimensional particle radius, and ϕ is the particle concentration. The effective viscosity of the suspension, μ, was calculated by means of a standard correlation [13]:

$$\mu = \mu_f \left(1 + \frac{1.5\phi}{1 - \frac{\phi}{\phi_m}}\right)^2, \qquad \phi_m = 0.58 \tag{2.1}$$

where μ_f is the pure fluid viscosity, and ϕ_m is the solid volume fraction beyond which the suspension can no longer flow. Note that the value of $\beta \equiv F/\alpha$ can be computed for the experiments since the volume of the suspension, the geometry of the cylinder, the properties of the liquid and the operating conditions needed for obtaining the fill fraction F and α are all known.

Since the Reynolds number was always less than 10^{-2} in all the experiments, inertial effects were assumed negligible. The capillary number Ca ranged from 0.05 to 7.3 and α from 0.03 to 0.26. The suspension concentration ϕ was varied from 1% to 15% and the fill fraction F from 0.15 to 0.75. The experiments were performed in cylinders having the following inner radii and aspect ratios (L/R): 5 cm (6.0), 1.27 cm (6.0, 22.4) and 0.635 cm (6.0, 45.6). The main conclusions to be drawn from these earlier experiments [12] are as follows:

- *It appears that particle segregation will occur only when a region of recirculating flow is present at the bottom of the cylinder.*
- *The degree of particle segregation depends primarily on* α, F *and* $h_m/2\hat{a}$.
  - *For* $F < 0.4$, *clear segregation was achieved for* $1.6 < \beta < 2.3$ *and* $h_m/2\hat{a} < 15$.
  - *For* $F \approx 0.15$ *and* $0.7 < \beta < 1.6$, *particles segregated only within a portion of the cylinder while the rest of the cylinder was coated with a homogeneous suspension.*
  - *For large values of* $h_m/2\hat{a}(\approx 25)$, *a significant number of particles remained in the low concentration region even for* $\beta < 2.0$.
- *Increasing the total particle concentration* (ϕ) *led to shorter segregation times.*
- *The dimensionless wavelength* (l/R) *of the pattern, with* l *being the average center to center distance between the neighboring high concentration bands,*

was found to decrease with an increase in the capillary number (Ca).

- *The aspect ratio (L/R) was found to have a significant effect on the wavelength for cylinders of small aspect ratio (relative to the dimensionless wavelengths).*
- *A secondary flow exists between the high and the low concentration regions.*
- *Film thickness measurements showed that the local fill fraction in the high concentration region was considerably higher than that in the low concentration region.*

2.2.2 Repeating the previous experiments

We repeated some of the previous experiments and observed results similar to those recorded in the thesis of Tirumkudulu [12]. Specifically, in some of these experiments, complete segregation was reached in the sense that no particles were present in the low concentration region, but, in some, the segregation was incomplete in that a significant number of particles remained in the low concentration region even after the experiments were run for 24 hours or more. These two types of segregation are shown in Fig 2.2. It appears that there exists a critical value of β which demarcates the regions of complete and incomplete degree of particle segregation. In general, the particle segregation became incomplete as β increased beyond this critical value.

As noted by Tirumkudulu[12], the high concentration bands can move along the axis of the cylinder due to small misalignments of the cylinder axis about the horizontal. As a result, it is difficult to make a rigorous quantitative comparison between different experiments, especially as concerns the wavelength. However, we have confirmed the previous experimental observation that, the dimensionless wavelength, l/R, was found to be an increasing function of the dimensionless surface tension parameter $\gamma(\equiv \sigma/\rho g R^2)$. Note that, γ is actually an inverse Bond number (*cf* equation (1.18)). Since γ is independent of the operational parameter Ω, it is

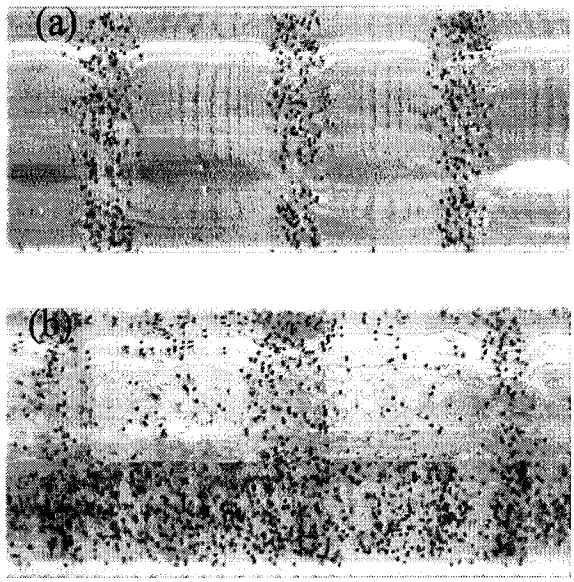

Figure 2.2: Two different kinds of particle segregation along the cylinder ($L = 30$ cm, $R = 1.27$ cm): (a) complete segregation ($F = 0.4$, $\beta = 1.8$ and $\phi = 5\%$), and (b) incomplete segregation ($F = 0.5$, $\beta = 3.2$ and $\phi = 10\%$).

more convenient for us to analyze the dependence of the dimensionless wavelength on γ instead of on Ca. The relation between these two dimensionless parameters is

$$\gamma \equiv \frac{\sigma}{\rho g R^2} = \frac{\alpha^2}{Ca} \tag{2.2}$$

When the experiments were performed in cylinders having inner radii: 5 cm, 1.27 cm and 0.635 cm, and on using a value for the surface tension $\sigma = 0.032$ N/m at $T = 23^o$C, the corresponding dimensionless surface tension parameter γ was found to equal 0.0011, 0.017 and 0.069 respectively for the same mixed suspensions of spherical acrylic particles dispersed in the density-matched liquid (Triton Mixture). As seen in Fig 2.3, the dimensionless wavelength (l/R) of the pattern obviously increases with a decrease in the radius of the cylinder R, or conversely, with an increase in the dimensionless parameter γ.

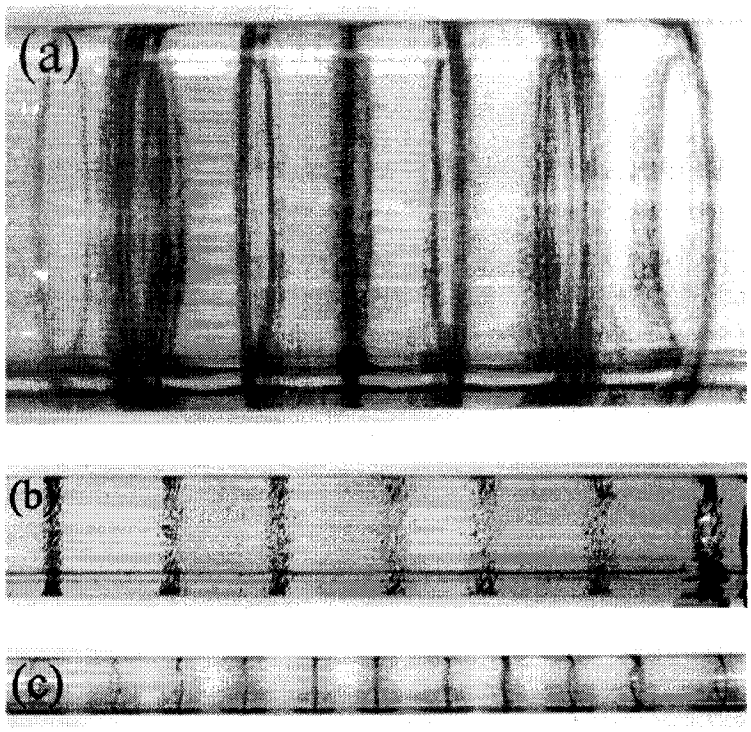

Figure 2.3: A set of photographs showing that the dimensionless wavelength of the band pattern which increases with a decrease in the radius of the cylinder for $F = 0.18$, $\beta = 0.18$ and $\phi = 1\%$. (a) $R = 5$ cm, (b) $R = 1.27$ cm, (c)$R = 0.635$ cm

2.2.3 High fill fraction and high concentration experiments

We also performed some experiments with a high fill fraction ($F = 0.5$ or 0.75) and a high concentration ($\phi = 10\%$) using the longer cylinder ($L = 30$ cm) with the intermediate inner radius ($R = 1.27$ cm). During those experiments, we observed some new phenomena as follows:

- When the cylinder, containing a high fill fraction ($F = 0.75$), was rotated very slowly (around 1 rpm) so that the value of β was very large ($\beta \approx 10$) in the sense that a huge recirculating flow was present at the bottom of the cylinder, no obvious bands could be discerned along the cylinder even after the experiment was run for a whole day, as shown in Fig 2.4(A)&(B).

- By increasing the rotation speed Ω by an order of magnitude (around 10 rpm),

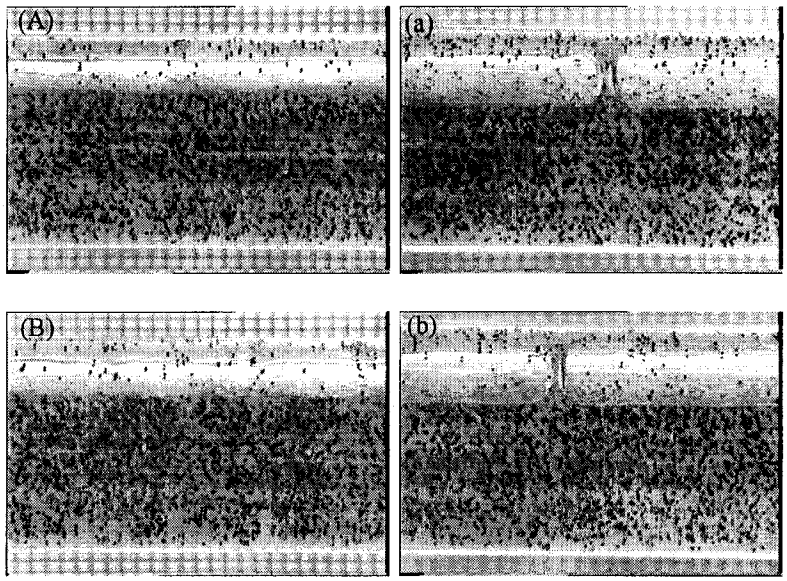

Figure 2.4: A set of photographs showing the absence of particle segregation in the high fill fraction, low rotation speed experiments (L = 30 cm, R = 1.27 cm). (A)→(B) No obvious band is discerned along the cylinder even after one day ($F = 0.75$, $\beta = 9.7$ and $\phi = 10\%$). (a)→(b) During the experiment, the initially continuous air gap at the top of the cylinder is split by the suspension, and the location where the local fill fraction equals unity has changed with time along the length of the cylinder ($F = 0.75$, $\beta = 5.9$ and $\phi = 10\%$).

the flow became unsteady in the sense that the initially continuous air gap at the top of the cylinder was divided by the suspension into several unstable bubbles, which could either merge together to form larger ones or be split again into smaller bubbles. Such an instability along the whole cylinder is shown only partially in Fig 2.4(a)&(b). In fact, a similar behavior were also observed by Benjamin and Pathak [14] in the case of a pure fluid where, beyond a critical rotation speed, the initial air space near the top of the cylinder was found to break suddenly into two or more parts.

- By increasing the rotation speed Ω even further (around 25 rpm), the air bubbles separated by the suspension became steady and the particles segregated near the two ends of each air bubble, as shown in Fig 2.5, thereby reducing the particle concentration within the central portion of the liquid column (where the local fill

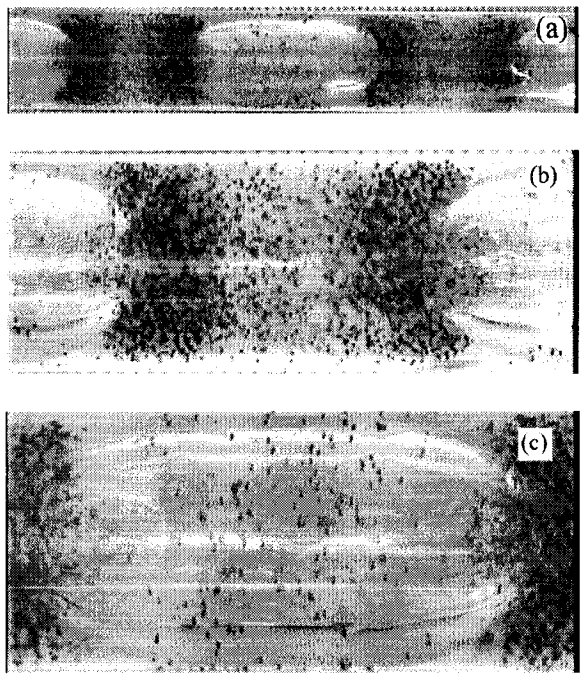

Figure 2.5: A set of photographs showing the segregation phenomenon in the high fill fraction experiment ($F = 0.50$, $\beta = 1.30$, $\phi = 10\%$, $L = 30$ cm, $R = 1.27$ cm). (a) The initial continuous air space at the top of the cylinder is divided into three air bubbles by the suspension. (b) The particles segregate near both ends of each air bubble. (c) Some particles stay in the uniform thin film surrounding the center portion of each bubble.

fraction is unity) below its initial value (*cf* Fig 2.5(b)). Also, only a few particles remained within the thin film (which is homogeneous owing to the small value of the local β) surrounding the central portion of each air bubble (*cf* Fig 2.5(c)).

2.2.4 Bidisperse suspension experiments

We constructed the bidisperse suspension by dispersing two different particle sizes in the Triton-100 mixture. Here, the concentration of the larger particles ($2\hat{a} = 463 \pm 37.5$ μm) was the same as that of the smaller ones ($2\hat{a} = 60 \pm 15$ μm), viz. $\phi_l = \phi_s = 1\%$. By performing experiments with this suspension in a cylinder ($L = 30$ cm and $R = 1.27$ cm), we observed some fine structures for $F = 0.2$ which were very sensitive to the value β, as shown in Fig 2.6. Specifically, when

$\beta = 1.74$, several groups of bands formed along the cylinder, each of which was comprised of three bands with the one in the center containing both larger and smaller particles, while the other two, of equal width on each side, only contained smaller particles. No particles were present in the regions between any two adjacent band groups as well as between the three bands in each group (*cf* Fig 2.6(B) for the magnification of one of the band groups, but the individual small particles (60 μm) are still too small to be discerned clearly). In contrast, when $\beta = 1.86$, all the

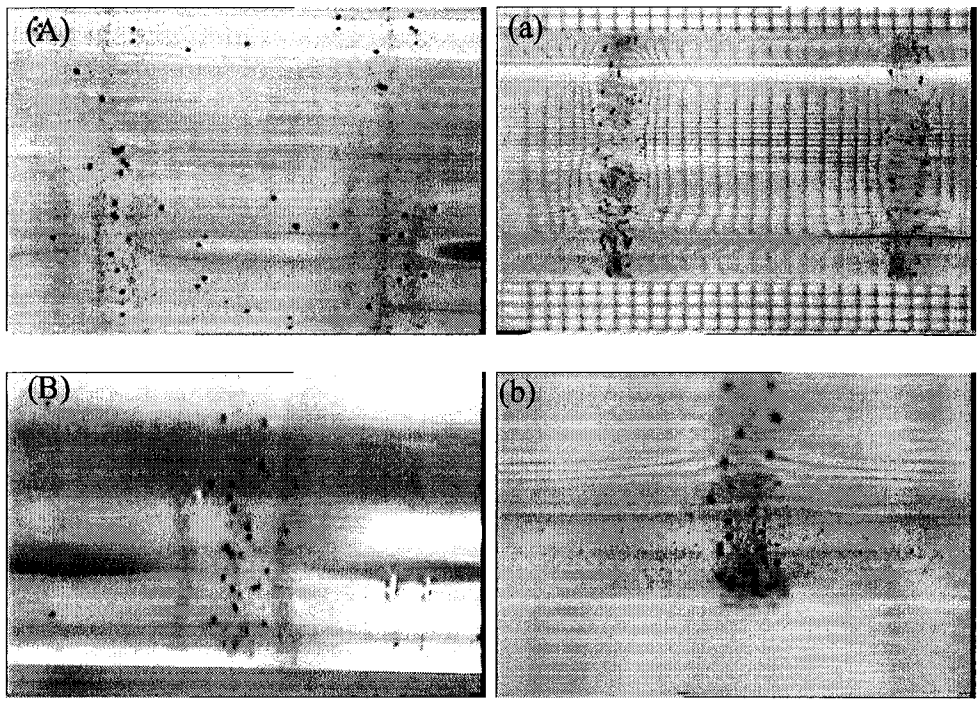

Figure 2.6: A set of photographs showing the fine structure of the bands in a bidisperse suspension: (A)&(B) $F = 0.2$, $\beta = 1.74$ and $\phi_l = \phi_s = 1\%$; (a)&(b) $F = 0.2$, $\beta = 1.86$ and $\phi_l = \phi_s = 1\%$.

bands contained both larger and smaller particles. But, even though all the larger particles had segregated completely, a number of smaller particles were still left in the recirculating flow region close to the bands (*cf* Fig 2.6(b) for the magnification of one of the bands). In both the experiments described above, the time required for the segregation of the smaller particles was similar to that of the larger ones.

2.2.5 Experiments with $\beta \ll \beta^+$

As we know, from the analysis presented earlier pertaining to the rimming flow of a particle-free liquid (*cf* chapter 1), no recirculating flow is expected to be present at the bottom of the cylinder when $\beta < \beta^+ \sim 1.6$. Ideally, we would have liked

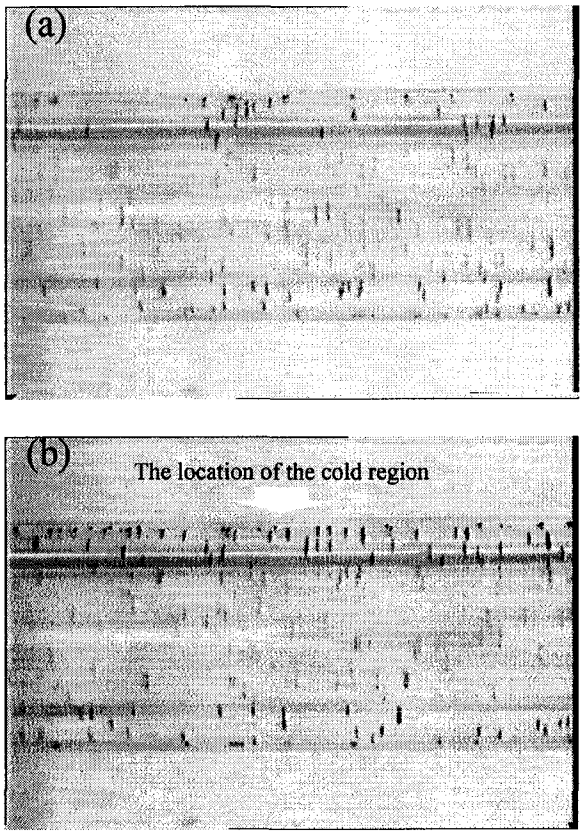

Figure 2.7: A set of photographs showing the lack of particle segregation along the cylinder ($F = 0.20$, $\beta = 0.23$, $\phi = 5\%$, $L = 28.5$ cm and $R = 1.27$ cm). (a) No bands can be discerned along the cylinder, even when (b) a piece of ice had been placed on the outer wall of the cylinder midway along its length.

to have studied a larger class of profiles without a puddle, i.e. for $\beta < \beta^+$, but, unfortunately, for values of β between β^+ and 0.7, the flow, even for a particle-free liquid, becomes irregular, time dependent and very susceptible to minute misalignments of the cylinder axis from the horizontal[4]. Moreover, in chapter1, we showed that such a homogeneous liquid film is unstable to axial disturbances due to surface tension effects (Rayleigh-Taylor instability). Hence, within that range of β, we

could not perform meaningful experiments over the long periods of time required to test for the possible creation of particle segregation, even going to extreme efforts in aligning the cylinder. [Note that the time dependent flows referred to above evolve over long periods[4] and may, in the short run, appear to be steady[15].] Thus, in order to avoid those complex flows, the experiments had to be performed with β kept below 0.7. [Even though there also exists the Rayleigh-Taylor instability for $\beta < 0.7$, this instability, as discussed in chapter1, requires such long time to evolve that it is unlikely to be discerned throughout the duration of the experiment.] Using a single cylinder ($L = 30$ cm and $R = 1.27$ cm) with the suspension containing the larger particles ($2\hat{a} = 463$ μm), it was found that no bands formed along the cylinder even if a piece of ice was placed on the outer wall of the cylinder (*cf* Fig 2.7). This result was quite surprising when compared to that obtained previously for $\beta > \beta^+$, in which the first band formed very quickly at that portion of the cylinder that had been cooled by placing a piece of ice[12]. We also repeated these experiments with the bidisperse suspension referred to above and found that, again, no particle bands appeared along the cylinder either with or without the presence of the ice.

2.2.6 Experiments with $\beta > \beta^+$ in which larger particles were introduced into the suspension

It is difficult to predict the location of a band along the cylinder unless one introduces a disturbance, e.g. as was said earlier, by placing a piece of ice at some spot. Similarly, we found that the band formed at the same location where a larger particle (3 mm in diameter and having a density twice that of the liquid) was introduced in advance into the suspension consisting of 430 μm particles. [Note that the larger particle kept on staying out of the puddle and circulating without being affected by the segregation.] This whole process as recorded from the bottom of the cylinder is illustrated in Fig 2.8. We then repeated this experiment but with five larger particles

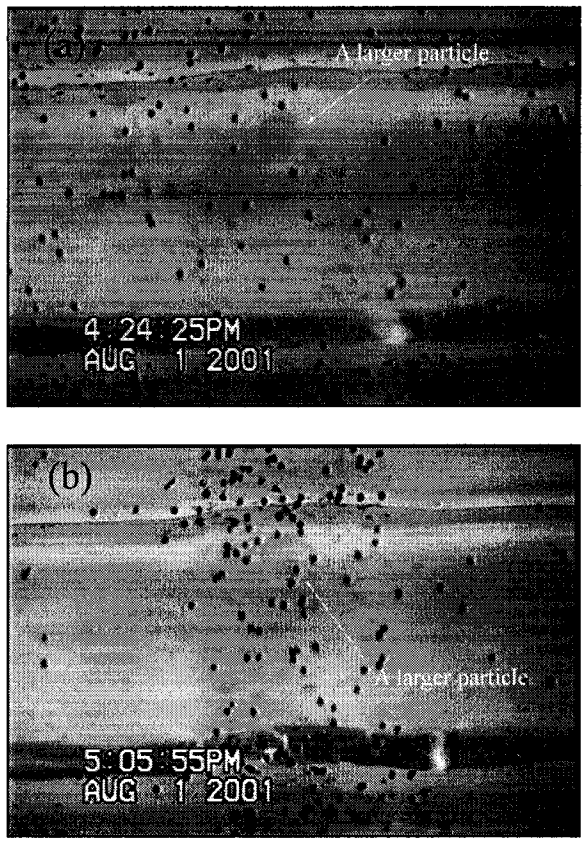

Figure 2.8: A set of photographs taken from the bottom of the cylinder show particle segregation induced by the presence of a larger particle which is darkened on the print. ($F = 0.40$, $\beta = 1.8$, $\phi = 5\%$, $L = 28.5$ cm and $R = 1.27$ cm)

spread separately along the cylinder, and found that five bands now formed at the locations containing the larger particles. When we introduced twenty one such large particles into the suspension, these were not initially distributed uniformly along the cylinder, hence, some of them were close enough to one another that it was possible for one of the bands to contain one or more of the large particles. Again, the bands formed at the location occupied the large particles. Although the band containing several large particles formed faster than that with fewer, the band width was approximately the same in both cases. Also, when we replaced the large particle by a particle cluster in the suspension, we observed similar results, in which the band formed at the same spot where a particle cluster was initially introduced.

2.2.7 Single particle experiments with $\beta > \beta^+$

In order to further investigate the process of particle trapping and segregation, we performed a few single particle experiments in which one particle was introduced into a pure liquid with an imposed axial viscosity variation.

On way of achieving the flow field for this kind of experiment was to cool one portion of the fluid in the rotating cylinder by placing a piece of ice on the outer wall. Here, the experiment was performed in the cylinder of radius 1.27 cm and length 30 cm, with initial values of F and β equal to 0.2 and 1.92 respectively. After the rimming flow had reached a steady state, we introduced a single particle ($2\hat{a} = 463\mu$m) in the circumferential flow region close to the center of the cool region, and found that, although, this particle remained in the circumferential flow, it moved towards the center of the cool region where it remained (*cf* Fig 2.9).

Since the effective viscosity of the suspension is an increasing function of the particle concentration, we also can vary the liquid viscosity by adding particles only in one portion of the liquid in the rotating cylinder. Here, choosing the same cylinder as in the previous case, we put enough particles ($2\hat{a} = 463$ μm) into one portion of the liquid to create a region of locally higher viscosity than in the surrounding particle-free liquid. After the flow had reached a steady state, we introduced one particle ($2\hat{a} = 463$ μm) in the recirculating flow close to the high concentration region. After some time, this particle moved away from the high concentration region (high viscosity region) toward the low concentration region (*cf* Fig 2.10).

These two experiments reveal that, in the presence of an axial variation of viscosity, two opposite axial flows coexist as long as a puddle appears at the bottom of the cylinder. Specifically, the fluid in the puddle moves on average towards the lower viscosity region while, that the fluid in the circumferential flow, moves on average towards the higher viscosity region.

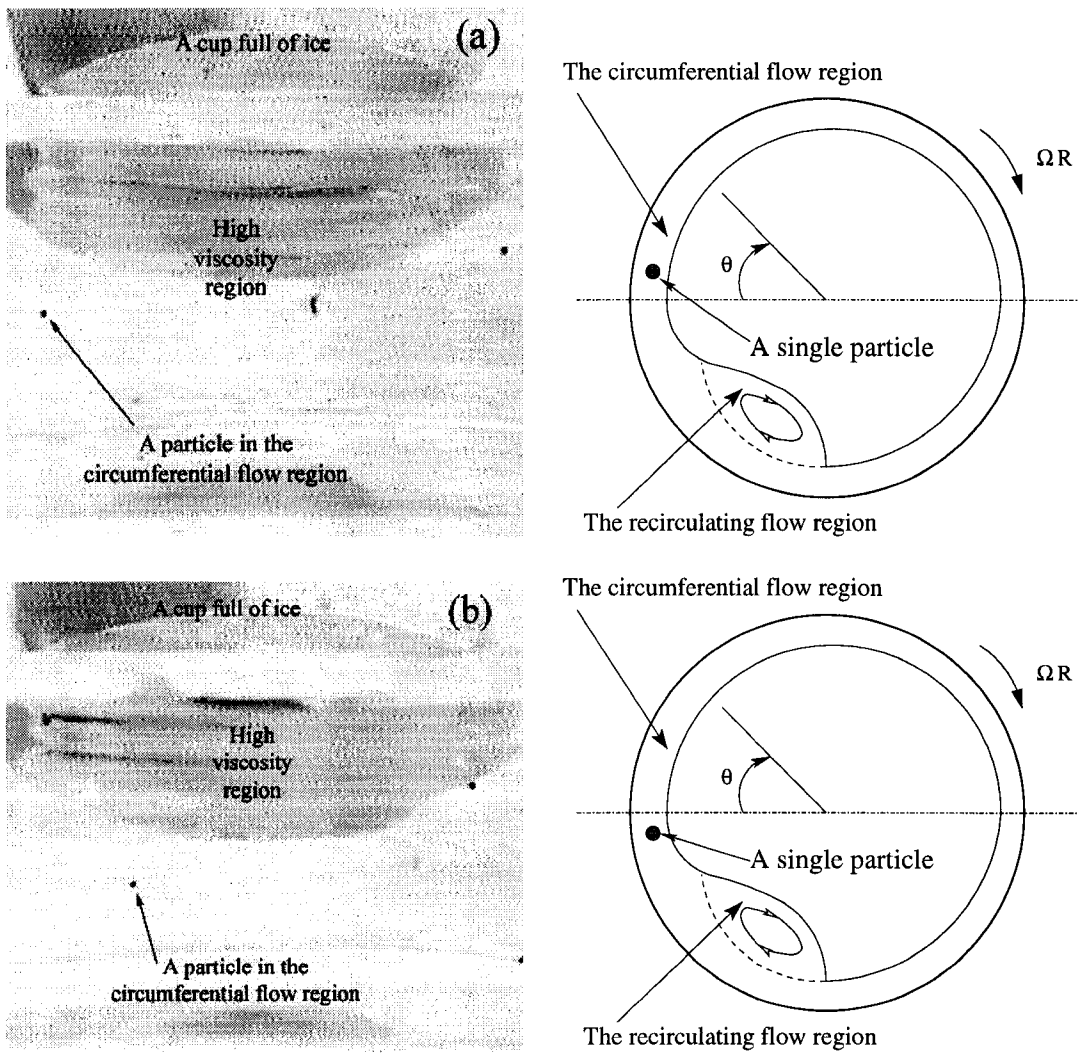

Figure 2.9: A set of photographs showing the axial motion of a single particle in the film with an imposed axial viscosity variation: (a)→(b) A single particle in the circumferential flow region has moved to the cooler region.($F_{initial} = 0.2$, $\beta_{initial} = 1.92$, $L = 30$ cm and $R = 1.27$ cm)

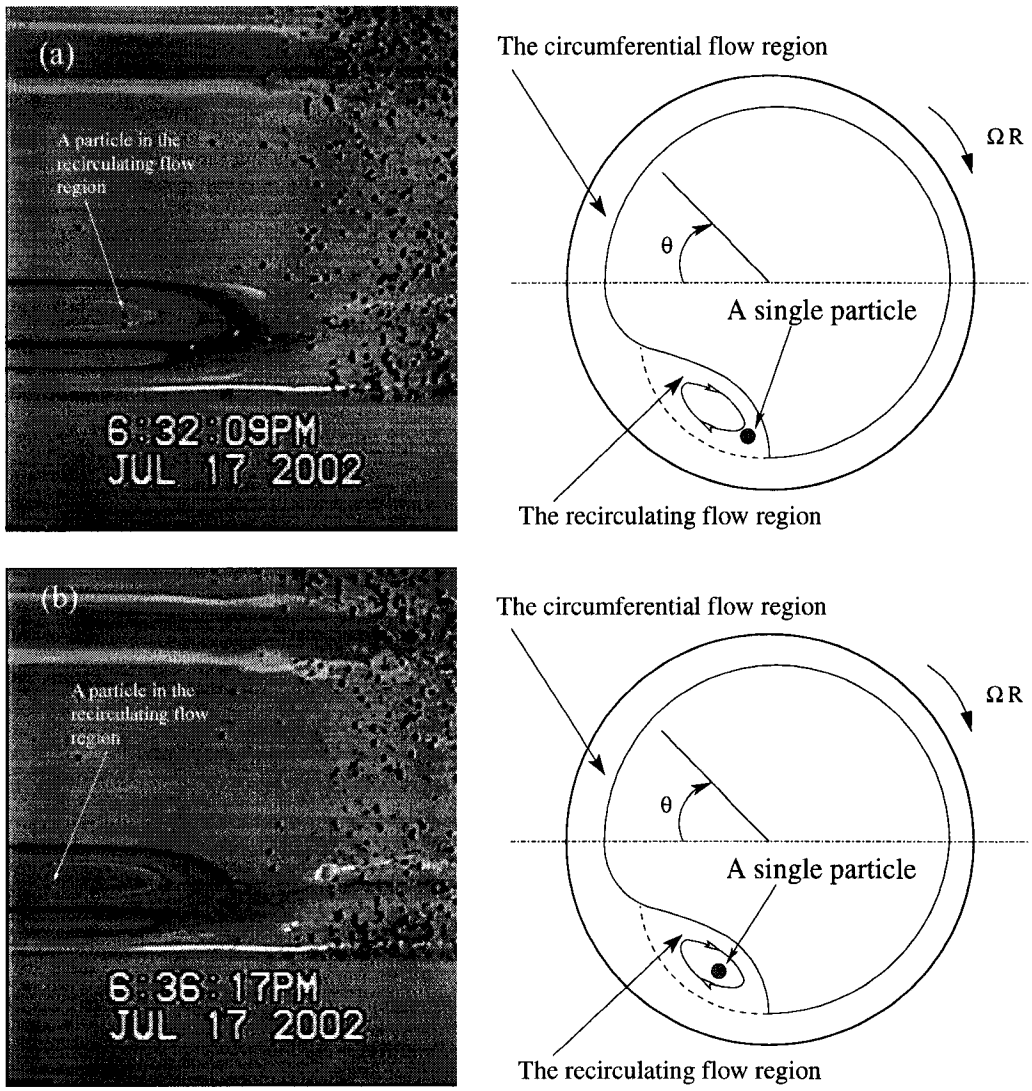

Figure 2.10: A set of photographs showing the axial motion of a single particle in the film with an imposed axial viscosity variation: (a)→(b) A single particle in the recirculating flow region has moved away from the high concentration region. ($F_{initial} = 0.2$, $\beta_{initial} = 1.8$, $L = 30$ cm and $R = 1.27$ cm)

2.2.8 Experimental observations of the suspension flow in the recirculating region

Since the recirculating flow is near the bottom of the cylinder, it could be fully observed only if the camera was placed under the cylinder. Here, the radius and length of the cylinder which was used were respectively 1.27 cm and 28.5 cm, and the diameter of the particles in the suspension was 463 μm. First, we focused on the recirculating flow in the band and found that, for smaller initial values of β (e.g. $\beta < 2.0$), no obvious recirculating flow was present at the center of the band even though a recirculating flow existed in the low concentration region (*cf* Fig 2.11); but, for larger initial values of β (e.g. $\beta > 3.0$), a recirculating flow was present along the whole cylinder but its size was smaller in the band than outside of it (*cf* Fig 2.12). It was quite surprising to observe that the particle in the recirculating flow region (puddle) moved away from the particle band (*cf* Fig 2.12).

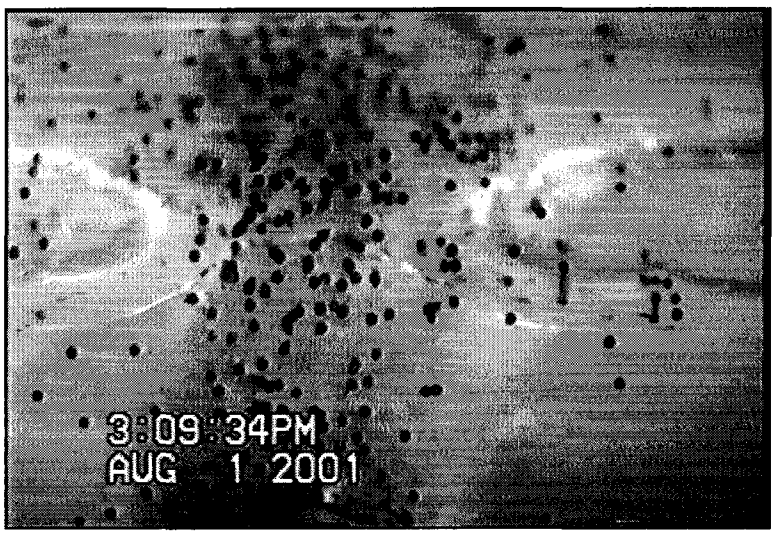

Figure 2.11: A photograph taken from the bottom of the cylinder showing the absence of a recirculating flow region at the center of the particle band.

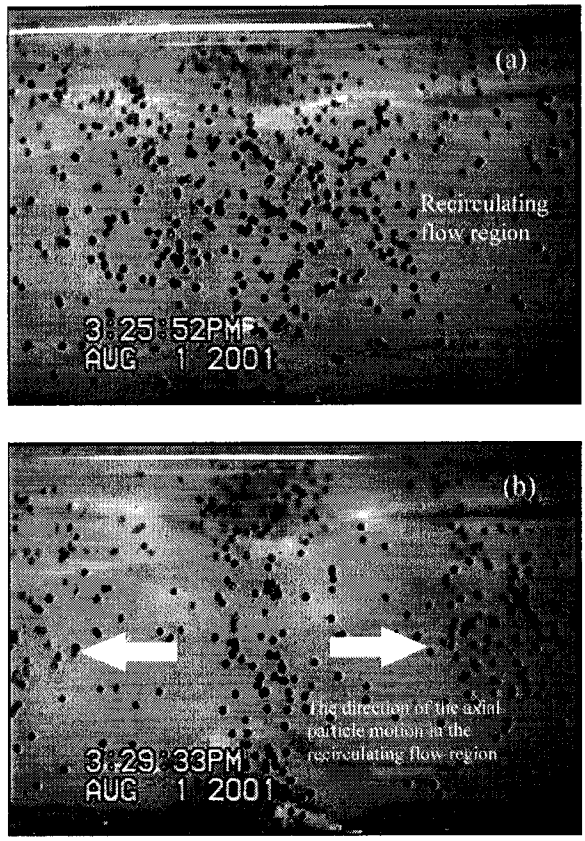

Figure 2.12: A set of photographs taken from the bottom of the cylinder showing the axial motion of particles in the recirculating flow region (puddle): $(a) \rightarrow (b)$ the particles in the puddle have moved away from the band to the low concentration region.

2.2.9 Low fill fraction and low concentration experiments

Here, we focus on the experiments which were performed with very low particle volume fractions ($\phi = 1\%$) and low fill fractions ($F = 0.18 \sim 0.2$) to observe the whole band formation process where, in order to observe every particle within the suspension, all of them were colored red.

The experiments were performed in a 30 cm long circular Plexiglas cylinder with end plates and inner radius 1.27cm. To monitor qualitatively the cross-sectional particle concentration distribution, one camera was placed at the top of the center of the cylinder, while the other one was placed in front of the cylinder to record the

variation of the axial particle concentration distribution (*cf* Fig 2.1).

First, we performed experiments with a suspension which was initially uniform everywhere and for values of β in the range $\beta^+ < \beta < 2.1$, which implies that there is a small recirculating flow near the bottom of the cylinder. We found that within a relatively short period of time (within 3 hours at a rotating speed of 3 RPM) following the start of the experiments, all the particles initially present in the recirculating flow region (puddle) had moved into the circumferential flow region (*cf* Fig 2.13). At that time, no bands had appeared along the cylinder as yet, that is, the concentration along the cylinder appeared to be uniform except for the absence of particles within the recirculating flow region. After about 10 hours, some bands began to appear at the center of the cylinder. Usually, it took at least 24 hours to reach the final stage, i.e. complete segregation, in which the bands were separated by regions of essentially particle-free liquid.

These experiments were also repeated but with $\beta > 2.1$ for which a large region of recirculating flow was present at the bottom of the cylinder. We found that, even though during the process of band formation, the particle concentration within the recirculating flow region was observed to have decreased from the its initial value, a number of particles always remained there. After one day or more, several bands formed along the cylinder but a significant number of particles still remained in the low concentration regions, this being referred to as an incomplete segregation.

These two processes are sketched in Figs 2.13-2.14. These experimental results reveal that the whole process of particle segregation occurs in two stages. Specifically, at first, particles in the recirculating flow region move into the circumferential flow region within a relatively short period of time. As a result of this **radial particle segregation** in the early stages of the experiment, the particle concentration in the circumferential flow region becomes higher than that in the recirculating region. Then, particles in the circumferential flow region move axially

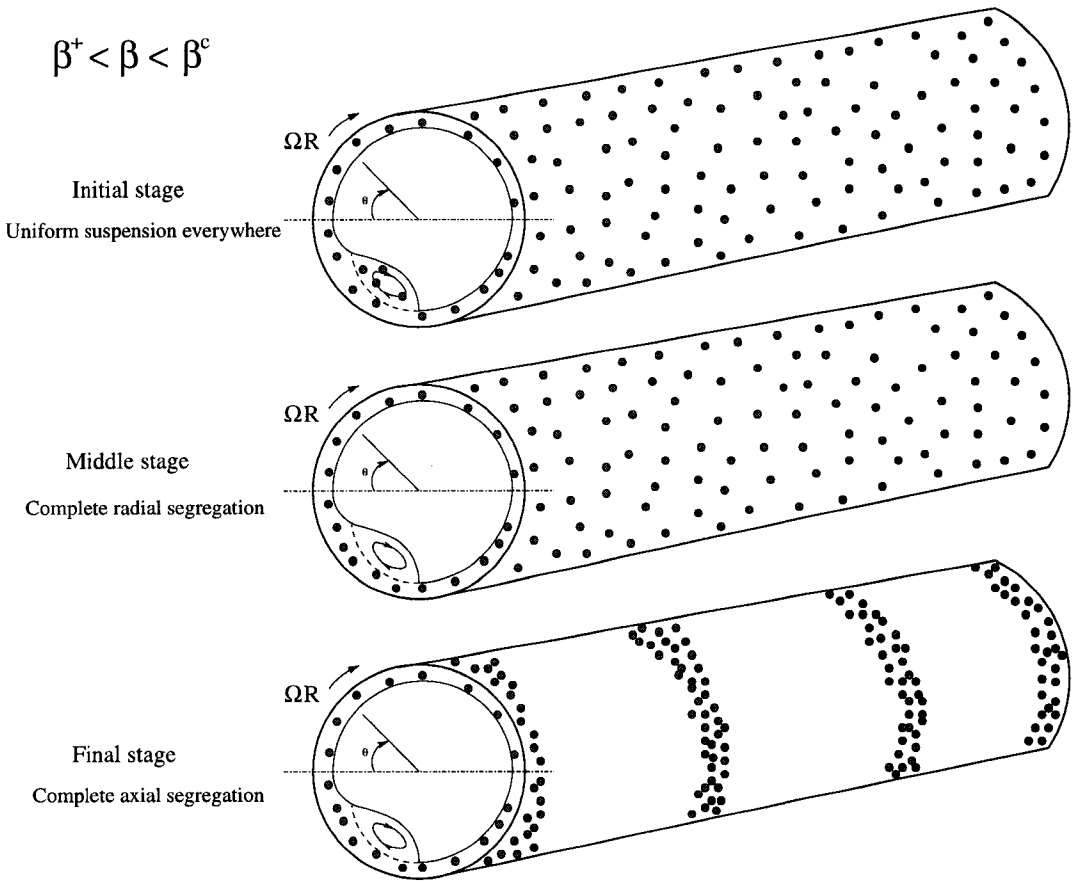

Figure 2.13: Sketch of the process of band formation when $\beta^+ < \beta < \beta^c$

to the local higher concentration region to form bands, a process to be referred to as **axial particle segregation**. The time required for the first stage is an order of magnitude shorter than that for the second. (Note that for large β, the two stages overlap during the band formation.)

Using the top camera, we can observe this whole process of particle migration from the recirculating flow region into the circumferential flow region. We find that when a particle in the recirculating region moves near the stagnation point close to $\theta = 0$, its velocity is, of course, close to zero. But when some rapidly moving particles in the circumferential flow region move past this stagnation point, they entrain this essentially stationary particle which then crosses the dividing streamline into the circumferential flow region. In contrast, when our experiments were performed

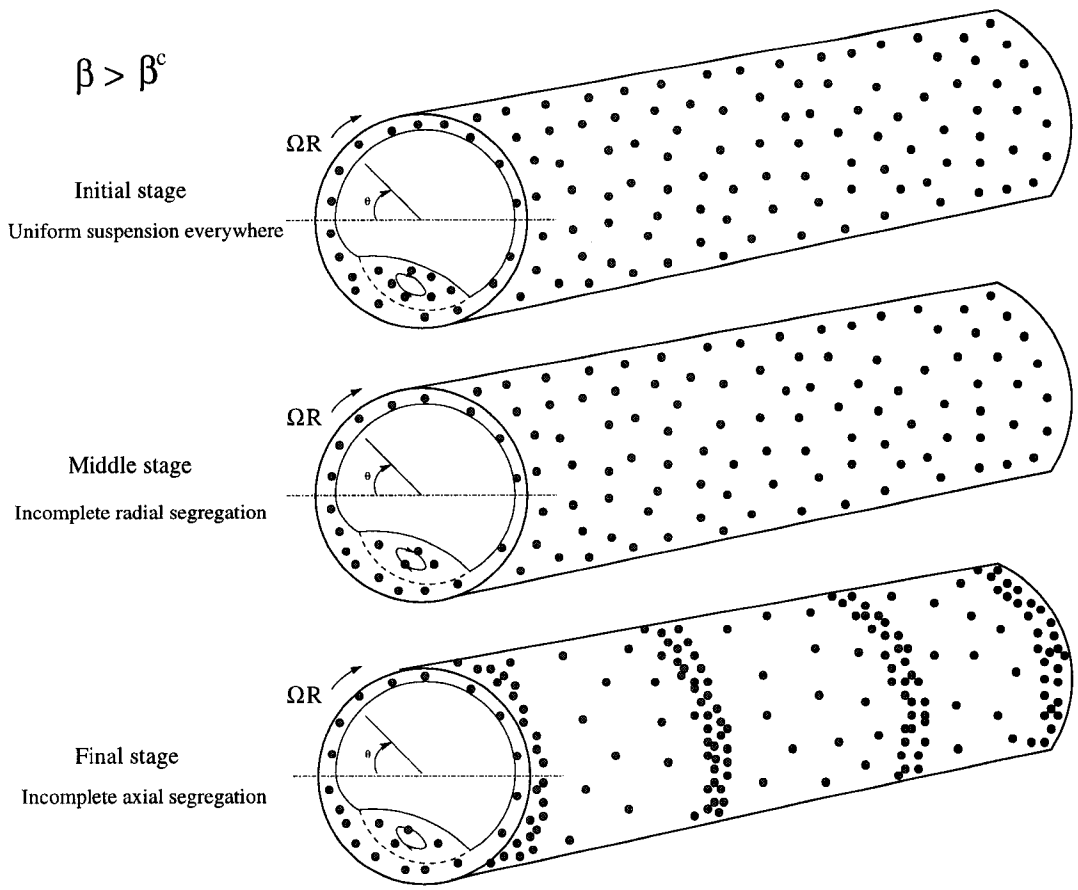

Figure 2.14: Sketch of the process of band formation when $\beta > \beta^c$

using a single particle which was placed within the recirculating region, we found that this particle remained there forever. We can conclude therefore that the particle migration from the recirculating region to the circumferential flow region results from the interaction between the particles in the recirculation region and the particles in the circumferential flow region. Since the inter-particle interaction depends on the particle size and the distance between the particles, the degree of radial particle segregation and the time required to achieve radial segregation depends on these two factors. Thus, when we fix the fill fraction F and decrease α by slowing down the rotating speed (Ω) of the cylinder, β will increase, which implies that the size of the recirculating region as well as the average distance between the particles in the recirculating region and those in the circumferential flow both become larger.

As a result, the strength of the interaction between the particles in the recirculating flow region and those in the circumferential flow region decreases monotonically as $\beta \to \infty$ with fixed F. Hence, it is likely that, for a given suspension, there is a critical value of β, to be referred to as β^c, which can be used to mark the boundary between complete and partial radial particle segregation. The experimental results reported here show that $\beta^c \approx 2.1$ for the suspension with the 463 μm particles. In addition, when the size of the particles in the suspension decreases, this type of inter-particle interaction also becomes weaker so that one should expect that, for a fixed particle volume fraction, β^c should fall below 2.1 if smaller particles were used (i.e. $2\hat{a} = 60\mu$m instead of $2\hat{a} = 463\mu$m) in the sense that, a number of particles would be expected to remain in the recirculating region even when $\beta < 2.1$ if the particles in suspension we made smaller than $2\hat{a} = 463\mu$m. Another possibility for the smaller particle case is that smaller particles leave the puddle just as the larger ones do but more slowly so that it takes almost forever for them to reach complete axial segregation.

It is interesting to note that, from our experiments, this value of β^c is also essentially equal to the critical value of β which demarcates the boundary between the complete and incomplete axial particle segregation[12].

2.3 Conclusions

We first confirmed the previous experimental work by Tirumkudulu [12] by repeating a number of the experiments recorded in his thesis and then performed a number of new experiments which allow us to arrive at the following conclusions:

- Particle bands do not form along the cylinder in the presence of a huge recirculating region (e.g. $\beta \sim 10$) as well as in the absence of a recirculating flow at the bottom of the cylinder ($\beta < \beta^+$). In the latter case, there is no particle

segregation even when an axial variation of viscosity is introduced along the cylinder.

- When they do form, the bands are located in the region where the effective viscosity of the suspension has a local maximum.

- In a bidisperse suspension, particles can segregate into several groups of bands, each of which consists of three sub-bands. The larger particles only appear at the center sub-band but the time required for the segregation of both kinds of particles is similar.

- In the presence of an axial variation of viscosity, a particle in the recirculating flow region moves towards the low viscosity region, whereas a particle in the circumferential flow moves toward the high viscosity region.

- When starting with a suspension having uniform particle concentration, the particles in the recirculating flow migrated into the circumferential flow region at the start of the experiments (i.e. radial particle segregation), and that the time required for this process was an order of magnitude shorter than that required for the band formation (i.e. axial particle segregation).

- There exists a critical value of β, to be referred to as β^c, which can be used to mark the boundary between complete and incomplete radial as well as axial particle segregation.

Chapter 3

Theory of particle segregation in rimming flows of suspensions containing neutrally buoyant particles

3.1 Introduction

Recently, a new phenomenon was discovered which, until now, remained unexplained, in which an initially uniform suspension of neutrally buoyant particles within a partially filled rotating cylinder is found to segregate into bands of particles separated by regions of essentially particle-free liquid [2]. In order to arrive at an explanation, we first construct a simple model on the basis of the modified lubrication equation for describing the free surface profiles of the three-dimensional flows generated by an imposed axial variation of the fluid viscosity, and show that the free surface profiles thereby obtained agree with those determined by solving numerically the three-dimensional Stokes equations with the FIDAP software (Fluent. Inc). Since particle concentration fluctuations always exist along the rotating cylinder, which, in turn, lead to axial fluctuations in the effective viscosity of the suspension, this simple model could be applied to represent the effect of axial disturbances to the suspension flow in the rotating cylinder. Moreover, on the basis of this model, we calculate the axial volumetric flow rate of a suspension in the dilute limit, in which the flow field is not influenced by the presence of the particles. We show that, in the absence of a recirculating flow near the bottom of the cylinder, the net axial volumetric flow rate of particles always vanishes even in the presence of a viscosity variation along the cylinder. On the other hand, in the presence of such a recirculating flow, we find that, although the net axial volumetric flow rate of the particles similarly again vanishes if the concentration of the suspension at every cross section is kept uniform, there does exist a net axial volumetric flow rate of particles in the direction of increasing viscosity if the concentration in the circumferential thin film flow is higher than that in the region of recirculating flow, i.e. within the "puddle" (*cf* Fig 3.1 to view these two flow regions). On the basis of these calculations and the experiment finding about the radial particle segregation

described in chapter 2, we shall then provide an explanation for the segregation phenomenon referred to above. Moreover, we shall carry out a linear stability analysis for dilute suspensions having radial segregation and show that such a particle distribution is unstable to axial perturbations with the surface tension being responsible for the selection of the wavelength of the most rapidly amplified disturbance. The calculated and measured spacings between the bands are in good agreement.

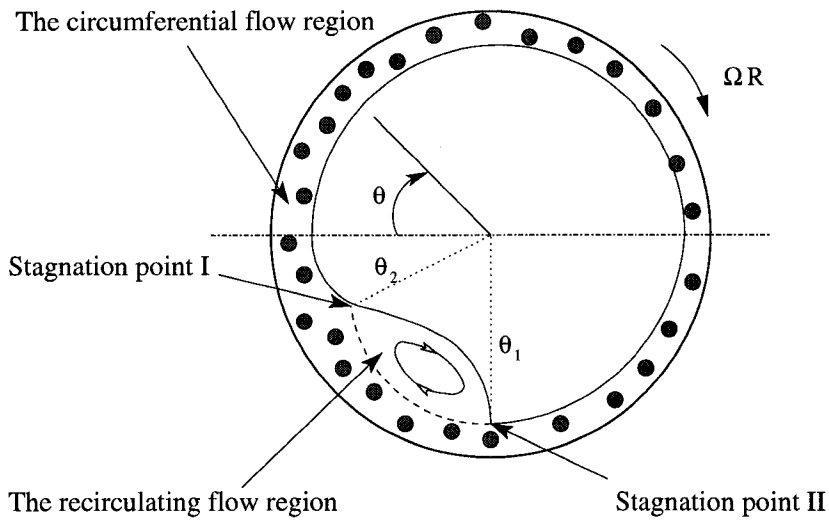

Figure 3.1: Sketch of the two flow regions at a cross section of the rotating cylinder.

3.2 A model of the three-dimensional rimming flow with an axially varying viscosity

In a two-dimensional rimming flow, the modified lubrication equation can be used to characterize accurately the film profiles over a broad range of α, $0 < \alpha \equiv \sqrt{\Omega\mu/\rho Rg} < \infty$, even when the fill fraction F is as large as 36% (*cf* chapter 1). Recall that this modified lubrication equation is

$$q = \eta - \frac{\eta^3}{3}\{(1-\alpha\eta)\cos\theta - \alpha\eta'\sin\theta\} \tag{3.1}$$

where θ is the angular coordinate, η is a dimensionless film thickness and q, which must be obtained as part of the solution, refers to the dimensionless volumetric flow rate per unit axial distance. In addition, η is required to be periodic in 2π and to satisfy

$$\beta \equiv F/\alpha = \frac{1}{\pi}\int_{-\pi}^{\pi}\left(1-\frac{\alpha}{2}\eta\right)\eta \mathrm{d}\theta \tag{3.2}$$

Suppose now that the viscosity μ varies with the axial coordinate x and therefore the film thickness η also varies with x. Letting

$$\alpha \equiv \sqrt{\frac{\Omega\mu_m}{Rg\rho}} \tag{3.3}$$

where μ_m is the minimum viscosity, we obtain (*cf* chapter 1), the corresponding momentum equation along the θ direction

$$\bar{\mu}\frac{\partial^2 v}{\partial z^2} = \cos\theta + \frac{\alpha}{1-\alpha z}\left\{(z-\eta)\cos\theta - \frac{\partial\eta}{\partial\theta}\sin\theta\right\} \tag{3.4}$$

or

$$(1-\alpha z)\bar{\mu}\frac{\partial^2 v}{\partial z^2} = (1-\alpha\eta)\cos\theta - \alpha\frac{\partial\eta}{\partial\theta}\sin\theta$$

where $\bar{\mu} \equiv \mu/\mu_m$ is the dimensionless viscosity, $v \equiv \hat{v}/\Omega R$ is the dimensionless angular component of the velocity, $z \equiv (R-r)/\alpha R$ is the dimensionless distance from the rotating cylindrical boundary with r being the radial coordinate. As in the two-dimensional case (*cf* equation (1.9) in chapter 1), this equation is also subject to two boundary conditions, specifically, the no-slip condition at the rotating solid wall requiring $v = 1$ at $z = 0$ and the zero shear stress condition on the free surface implying $\partial v/\partial z = 0$ at $z = \eta$. Hence, provided that $\alpha z \ll 1$, the solution to this equation is

$$v = 1 - \frac{1}{\bar{\mu}}\left(\eta z - \frac{z^2}{2}\right)\left\{(1-\alpha\eta)\cos\theta - \alpha\frac{\partial\eta}{\partial\theta}\sin\theta\right\} \tag{3.5}$$

so that the relationship between the flow rate q and the film thickness η becomes

$$q \equiv \int_0^{\eta} v \mathrm{d}z = \eta - \frac{\eta^3}{3\bar{\mu}}\left\{(1-\alpha\eta)\cos\theta - \alpha\frac{\partial\eta}{\partial\theta}\sin\theta\right\} \tag{3.6}$$

subject to

$$\beta \equiv F/\alpha = \frac{1}{\pi L}\int_{-L/2}^{L/2}\int_{-\pi}^{\pi}\eta \mathrm{d}\theta \mathrm{d}x - \frac{\alpha}{2\pi L}\int_{-L/2}^{L/2}\int_{-\pi}^{\pi}\eta^2 \mathrm{d}\theta \mathrm{d}x \tag{3.7}$$

where L is the length of the cylinder. We can also define the value of β at every cross section of the cylinder as

$$\beta_{local}(x) \equiv F_{local}/\alpha = \frac{1}{\pi}\int_{-\pi}^{\pi}\eta \mathrm{d}\theta - \frac{\alpha}{2\pi}\int_{-\pi}^{\pi}\eta^2 \mathrm{d}\theta \tag{3.8}$$

where F_{local} is the fill fraction at every cross section of the cylinder, so that β, the average value of $\beta_{local}(x)$ over the cylinder, becomes

$$\beta \equiv F/\alpha = \frac{1}{L}\int_{-L/2}^{L/2}\beta_{local}(x)\mathrm{d}x$$

According to the lubrication analysis in this three-dimensional flow[4], the leading order term of the dimensionless pressure without considering the surface tension effects is

$$p = \alpha(z-\eta)\sin\theta \tag{3.9}$$

the form of which is the exactly same as that for the two-dimensional case (*cf* equation (1.8) in chapter 1). Therefore, we obtain the momentum equation along the axial direction,

$$\bar{\mu}\frac{\partial^2 w}{\partial z^2} = \frac{\partial p}{\partial x} = -\alpha\frac{\partial \eta}{\partial x}\sin\theta \tag{3.10}$$

where $x \equiv \hat{x}/R$ is the dimensionless distance in the axial direction with $\hat{x}$ being the corresponding dimensional distance. This equation is subject to two boundary conditions:

$$w = 0 \quad \text{at} \quad z = 0, \quad \text{and} \quad \frac{\partial w}{\partial z} = 0 \quad \text{at} \quad z = \eta$$

Therefore, the dimensionless axial velocity becomes

$$w = \frac{\alpha}{\bar{\mu}}\frac{\partial \eta}{\partial x}\left(\eta z - \frac{1}{2}z^2\right)\sin\theta \tag{3.11}$$

and hence, on applying the volumetric conservation equation, we find that [4]:

$$(1-\alpha\eta)\frac{\partial\eta}{\partial t}+\frac{\partial q}{\partial\theta}+\frac{\alpha}{3}\frac{\partial}{\partial x}\left(\frac{\eta^3}{\bar{\mu}}\frac{\partial\eta}{\partial x}\right)\sin\theta=0 \tag{3.12}$$

When the flow reaches steady state, the time-dependent term in equation (3.12) vanishes. Then, by integrating the remaining terms of that equation with respect to θ, from $-\pi$ to π, we obtain

$$\int_{-\pi}^{\pi}\frac{\partial q}{\partial\theta}\mathrm{d}\theta+\frac{\alpha}{12}\frac{\partial}{\partial x}\left\{\frac{1}{\bar{\mu}}\frac{\partial}{\partial x}\int_{-\pi}^{\pi}\eta^4\sin\theta\mathrm{d}\theta\right\}=0 \tag{3.13}$$

But since the flow rate q is periodic in the angular coordinate, the above equation reduces to

$$\frac{\alpha}{12}\frac{1}{\bar{\mu}}\frac{\mathrm{d}}{\mathrm{d}x}\int_{-\pi}^{\pi}\eta^4\sin\theta\mathrm{d}\theta=\text{constant independent of } x \tag{3.14}$$

Actually, the left-hand side of equation (3.14) denotes the axial fluid volumetric flow rate, viz.

$$J=\int_{-\pi}^{\pi}\mathrm{d}\theta\int_0^{\eta}w\mathrm{d}z=\frac{\alpha}{12}\frac{1}{\bar{\mu}}\frac{\mathrm{d}}{\mathrm{d}x}\int_{-\pi}^{\pi}\eta^4\sin\theta\mathrm{d}\theta \tag{3.15}$$

which must vanish at steady state. Therefore,

$$\int_{-\pi}^{\pi}\eta^4\sin\theta\mathrm{d}\theta=A\quad\text{which is a constant (independent of x).} \tag{3.16}$$

As we shall show presently, the condition given above in equation (3.16) allows us to complete the solution of (3.6) subject to (3.7) and to determine $F_{local}(x)$ or, alternatively, $\beta_{local}(x)$.

Next, let us suppose, for the sake of simplicity, that the third term on the left-hand side of equation (3.12) is an order of magnitude smaller than the second term, e.g. that either $\bar{\mu}$ varies on a length scale much larger than R or that the value of $\alpha/12$ is small. In this case we have, again from equation (3.12), that, at steady state, $q_\theta\approx 0$, i.e. q is, to a first approximation, independent of θ. We therefore let $\bar{\mu}(0)=1$, solve equation (3.6) for a given q and calculate the constant A in equation (3.16). Then, for a different value of x (corresponding to a different value

of $\bar{\mu}(x)$), we solve equation (3.6) subject to (3.16) (for the same value of A). After obtaining $\eta(\theta, x)$ and, by means of equation (3.8), the profile of $\beta_{local}(x)$ or that of F_{local}, we use equation (3.7) to determine the relation between A and the a priori specified value of F or β.

The general numerical procedure outlined above is straightforward and allows us to obtain the steady three-dimensional free surface shape if the film profiles $\eta(\theta, x)$ are everywhere asymmetric about $\theta = 0$ so that A is everywhere non-zero. However, the technique fails for symmetric profiles given that the integral in equation (3.16) vanishes identically for any value of β_{local} provided, of course, that this value of β_{local} is consistent with the existence of a symmetric profile. But, under this condition, first, we integrate equation (3.12) with respect to θ from $-\pi$ to π,

$$\int_{-\pi}^{\pi}(1-\alpha\eta)\frac{\partial\eta}{\partial t}\mathrm{d}\theta+\int_{-\pi}^{\pi}\frac{\partial q}{\partial\theta}\mathrm{d}\theta+\frac{\alpha}{3}\int_{-\pi}^{\pi}\frac{\partial}{\partial x}\left(\frac{\eta^3}{\bar{\mu}}\frac{\partial\eta}{\partial x}\right)\sin\theta\mathrm{d}\theta=0 \tag{3.17}$$

Since the flow rate q is periodic in 2π and η is symmetric about $\theta = 0$, the second and third terms in equation (3.17) are equal zero. Therefore,

$$\frac{\partial}{\partial t}\int_{-\pi}^{\pi}\left(1-\frac{1}{2}\alpha\eta\right)\eta\mathrm{d}\theta=0 \tag{3.18}$$

and in view of equation (3.8),

$$\frac{1}{\pi}\frac{\partial}{\partial t}\int_{-\pi}^{\pi}\left(1-\frac{1}{2}\alpha\eta\right)\eta\mathrm{d}\theta=\frac{\partial\beta_{local}}{\partial t}=0 \tag{3.19}$$

which implies that β_{local}, as well as the local fill fraction F_{local}, remain at their initial, and presumable known values even in the presence of the three-dimensional steady flow which is created by the imposed axial variation of the viscosity. Therefore, we can solve equation (3.6) subject to (3.8) for any value of x and then obtain the steady-state symmetric profiles $\eta(\theta, x)$.

In order to check the reliability of the model described above, we also solved the full three-dimensional Stokes equation using the FIDAP software (Fluent, Inc.) for

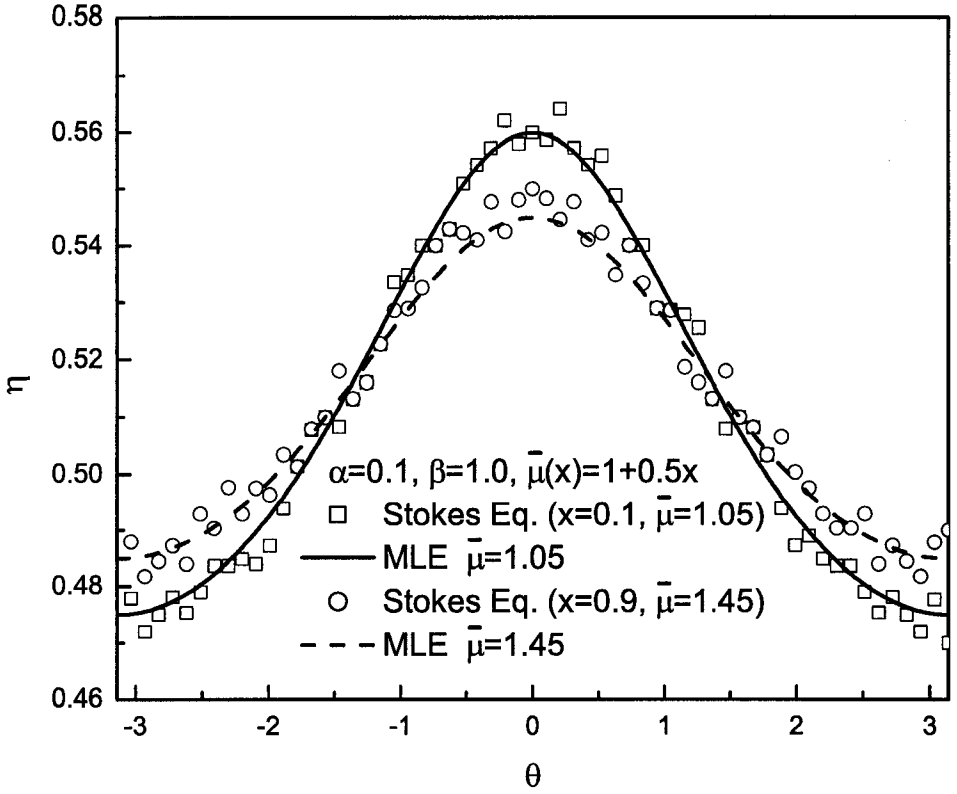

Figure 3.2: The film profiles at different locations ($x = 0.1$ and $x = 0.9$) along the cylinder. Comparison between the numerical solutions of the three-dimensional Stokes equations with $\gamma = 10^{-2}$ and those of the modified lubrication model with $\gamma = 0$ for the case of an axially varying viscosity of the form $\bar{\mu}(x) = 1 + 0.5x$, $0 \leq x \leq 1$: symmetric profiles for an axial uniform fill fraction $F = 0.1$ and $\alpha = 0.1$.

both symmetric and asymmetric film profiles. A comparison of the dimensionless steady-state film profiles at different values of x with $\bar{\mu}(x) = 1 + 0.5x$ obtained from the solution to the Stokes equations and from the model is plotted in Fig 3.2 for an initially symmetric and axially uniform film with $\beta = 1$, $F = 0.1$ ($\alpha = 0.1$), $\gamma = 10^{-2}$, and, in Fig 3.3, for an initially asymmetric and axially uniform film with $\beta = 1.9$, and average fill fraction $F = 0.19$ ($\alpha = 0.1$), $\gamma = 10^{-2}$. Clearly, the agreement is satisfactory in both cases even though the surface tension effects are neglected in the model equation (3.6).

According to this model, it is not possible for rimming flows with an axially varying viscosity to reach a steady state unless the film profiles are everywhere ei-

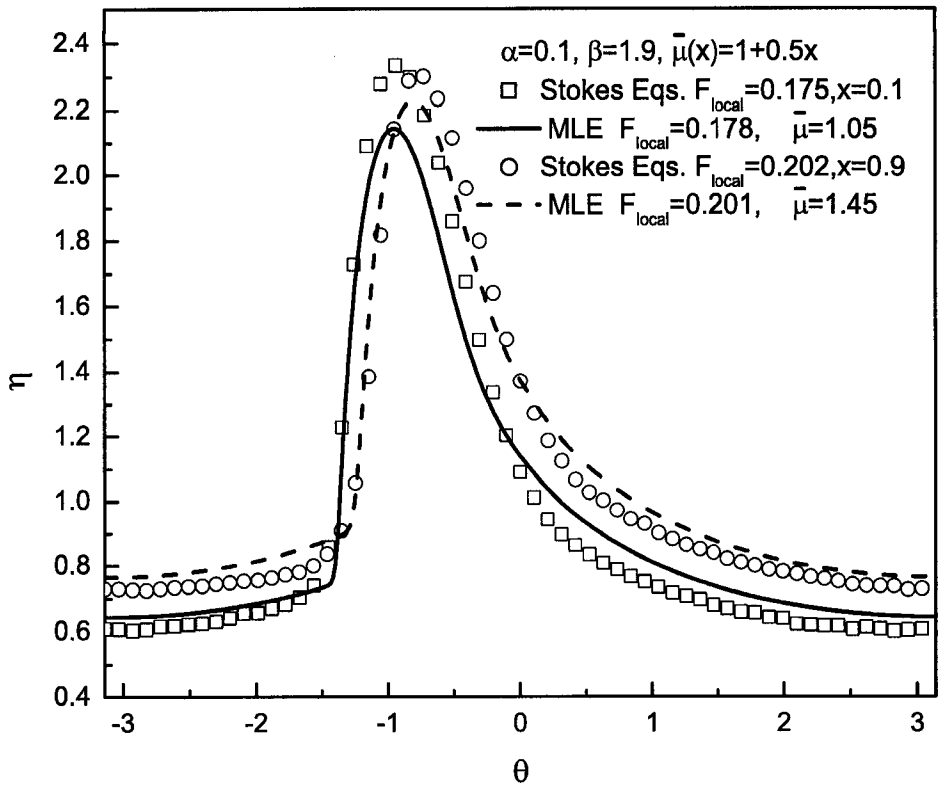

Figure 3.3: The film profiles at different locations ($x = 0.1$ and $x = 0.9$) along the cylinder. Comparison between the numerical solutions of the three-dimensional Stokes equations with $\gamma = 10^{-2}$ and those of the modified lubrication model with $\gamma = 0$ for the case of an axially varying viscosity of the form $\bar{\mu}(x) = 1 + 0.5x$, $0 \leq x \leq 1$: asymmetric profiles for an average fill fraction $F = 0.19$ and $\alpha = 0.1$.

ther symmetric or asymmetric for, otherwise, the integral in equation (3.16) cannot remain independent of x. It is worth noting, however, that, although for the symmetric profiles, $\beta_{local}(x)$ as well as $F_{local}(x)$ remain at their initial values, the steady free surface shapes will differ from those given initially. This is shown in Fig 3.2 where the steady symmetric film profiles are no longer axially uniform, as was the case initially, thereby implying the existence of an axial flow generated by the axially varying viscosity.

In summary then, based on the modified lubrication analysis, we have proposed a model describing rimming flows with an axially varying viscosity and have shown that the solutions of the resulting model equations capture the essential features

of the three-dimensional film profiles in both the symmetric and asymmetric cases, and also, that these profiles are in close agreement with those computed by solving numerically the full three-dimensional Stokes equations.

3.3 The axial particle volumetric flow rate in a film with a prescribed axial viscosity variation

As was already shown in chapter 1, in the two-dimensional rimming flow there exists a critical value of β, referred to as $\beta^+ \approx 1.6 + O(\alpha)$, which is a weak function of α that can be used to determine whether or not there is a recirculating flow near the bottom of cylinder. Thus, when $\beta > \beta^+$, the two-dimensional rimming flow can be divided into two flow regions, viz. the recirculating flow region ($\eta^* < z \leq \eta$) and the circumferential flow region ($0 \leq z < \eta^*$) as shown in Fig 3.4. Similarly, there also exists a corresponding critical value β^+ in the three-dimensional flow described above which can be obtained as follows:

We first note that the value of $\beta^+ \sim 1.6$ for the constant viscosity case can be obtained from the standard lubrication theory, i.e. equations (1.5) and (1.7) in chapter 1, which also follow from equations (3.6) and (3.8) given above by setting $\alpha = 0$ and $\bar{\mu} = 1$. This implies that, for $\bar{\mu} \neq 1$, we could set $\alpha = 0$ in equation (3.6) and (3.8), let $q \equiv \bar{q}\sqrt{\bar{\mu}}$, $\eta \equiv \bar{\eta}\sqrt{\bar{\mu}}$, $\beta \equiv \bar{\beta}\sqrt{\bar{\mu}}$ and thereby eliminate $\bar{\mu}$ giving that, in general, $\beta^+ \sim 1.6\sqrt{\bar{\mu}}$. We therefore conclude that a recirculating flow will be present near the bottom of the cylinder if $\beta_{local} > 1.6\sqrt{\bar{\mu}}$. (Actually, equations (3.6) and (3.8) can be transformed into the same form as the modified lubrication equations (3.1) and (3.2) by letting $\bar{\alpha} \equiv \alpha\sqrt{\bar{\mu}}$ and similarly for the other variables as indicated above.)

Thus, when $\beta_{local} > 1.6\sqrt{\bar{\mu}}$, we can divide the axial volumetric flow rate, J, into

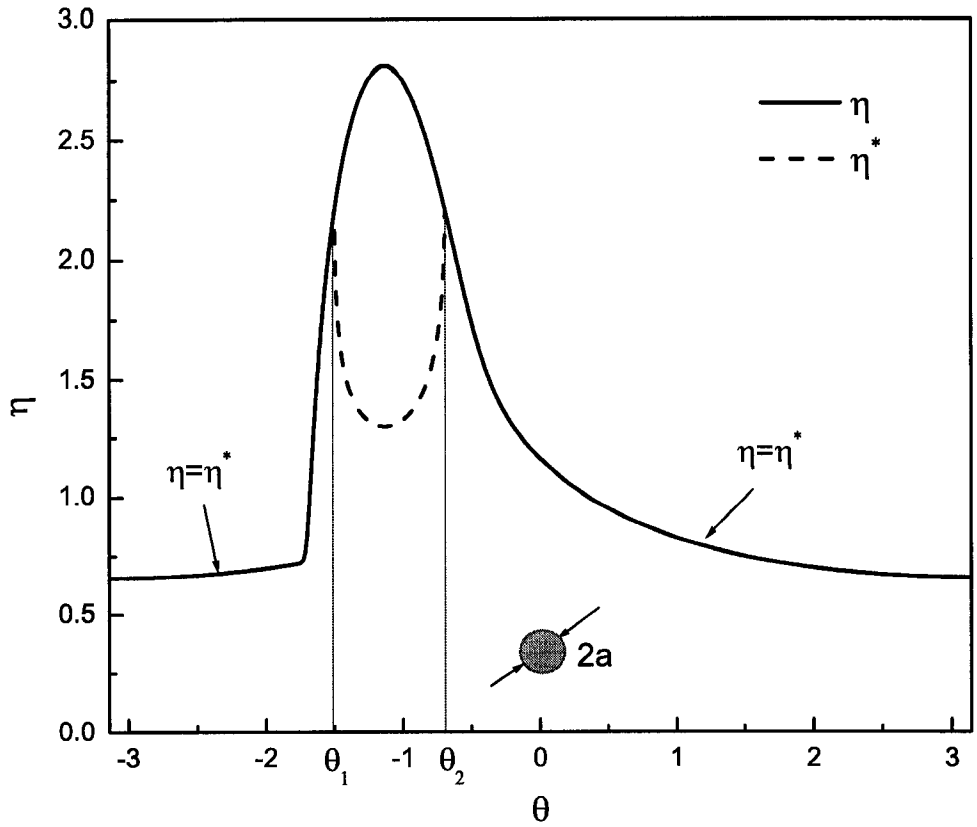

Figure 3.4: Sketch of the dimensionless particle size, the dimensionless film thickness profile η and the corresponding profile for η^* which refers to the lower boundary of the recirculating flow region.

two parts: the flow rate in the circumferential region, J^c,

$$J^c \equiv \int_{-\pi}^{\pi}\int_{0}^{\eta^*} w\mathrm{d}\theta\mathrm{d}z = \frac{\alpha}{\bar{\mu}}\int_{-\pi}^{\pi}\left\{\frac{1}{2}\eta(\eta^*)^2 - \frac{1}{6}(\eta^*)^3\right\}\frac{\partial\eta}{\partial x}\sin\theta\mathrm{d}\theta \tag{3.20}$$

and that in the recirculating region, J^r,

$$J^r \equiv \int_{-\pi}^{\pi}\int_{\eta^*}^{\eta} w\mathrm{d}\theta\mathrm{d}z = J - \frac{\alpha}{\bar{\mu}}\int_{-\pi}^{\pi}\left\{\frac{1}{2}\eta(\eta^*)^2 - \frac{1}{6}(\eta^*)^3\right\}\frac{\partial\eta}{\partial x}\sin\theta\mathrm{d}\theta \tag{3.21}$$

But since $J = 0$ at steady state, we have that $J^r = -J^c$. In order to calculate J^c, we have to know the film profiles $\eta(\theta, x)$ and the lower boundary of the recirculating flow region $\eta^*(\theta, x)$. We first can obtain the free surface profiles $\eta(\theta, x)$ by following the procedure described after equation (3.16) at section 3.2 of the present chapter.

Next, we combine equations (3.5) and (3.6) to yield,

$$v = 1 - \left(\eta z - \frac{z^2}{2}\right)\frac{3(\eta - q)}{\eta^3} \tag{3.22}$$

and make use of the definition,

$$q \equiv \int_0^{\eta} v\mathrm{d}z \equiv \int_0^{\eta^*} v\mathrm{d}z = \eta^* - \left\{\frac{1}{2}\eta(\eta^*)^2 - \frac{1}{6}(\eta^*)^3\right\}\frac{3(\eta - q)}{\eta^3} \tag{3.23}$$

which can be solved for η^* given that $\eta(\theta, x)$ and q are already known. As mentioned earlier, q, to first approximation, is independent of θ provided that the axial flow is quite weak, that is, the original three-dimensional rimming flow can been treated as a quasi-two-dimensional flow. Under this situation, η^* in equation (3.23) can still be referred to as the lower boundary of the recirculating flow region. Note that η and η^* differ only within that range of θ where a puddle exists (*cf* Fig 3.4). Therefore, we can use equations (3.20) to calculate J^c, the axial volumetric flow rate in the circumferential flow region, as well as that in the recirculating region $J^r = -J^c$.

By numerical calculation, we find that, within the range of monotonically increasing $\bar{\mu}(x)$, J^c is positive at steady state and therefore, J^r is equal but opposite in sign, which means that the fluid in the recirculating region and that in the circumferential flow region move, respectively, towards the lower and higher viscosity region with the same axial volumetric flow rate. The film profiles and the integrand on the right-hand side of equation (3.20) are plotted vs. θ in Fig 3.5, for $\beta = 2.10$ and $\alpha = 0.1$ and for a particular function $\bar{\mu}(x)$, where we see that both β_{local} and F_{local} increase monotonically with x, but that the recirculating flow region becomes smaller implying that the effective β ($\equiv \beta_{local}/\sqrt{\bar{\mu}}$) decreases monotonically with x. Such a reduction in the size of the "puddle" along the direction of increasing viscosity can also be clearly discerned from the velocity profiles as obtained from the FIDAP software (Fluent Inc.) which we used to solve the three-dimensional Stokes equations (*cf* Fig 3.6). [Unfortunately, the FIDAP software (Fluent Inc.)

is not set up to give us directly the lower boundary of the puddle because, what this software does, is to generate the three-dimensional flow field from which it is not possible to extract with any confidence its two-dimensional projection along the plane perpendicular to the cylinder axis.]

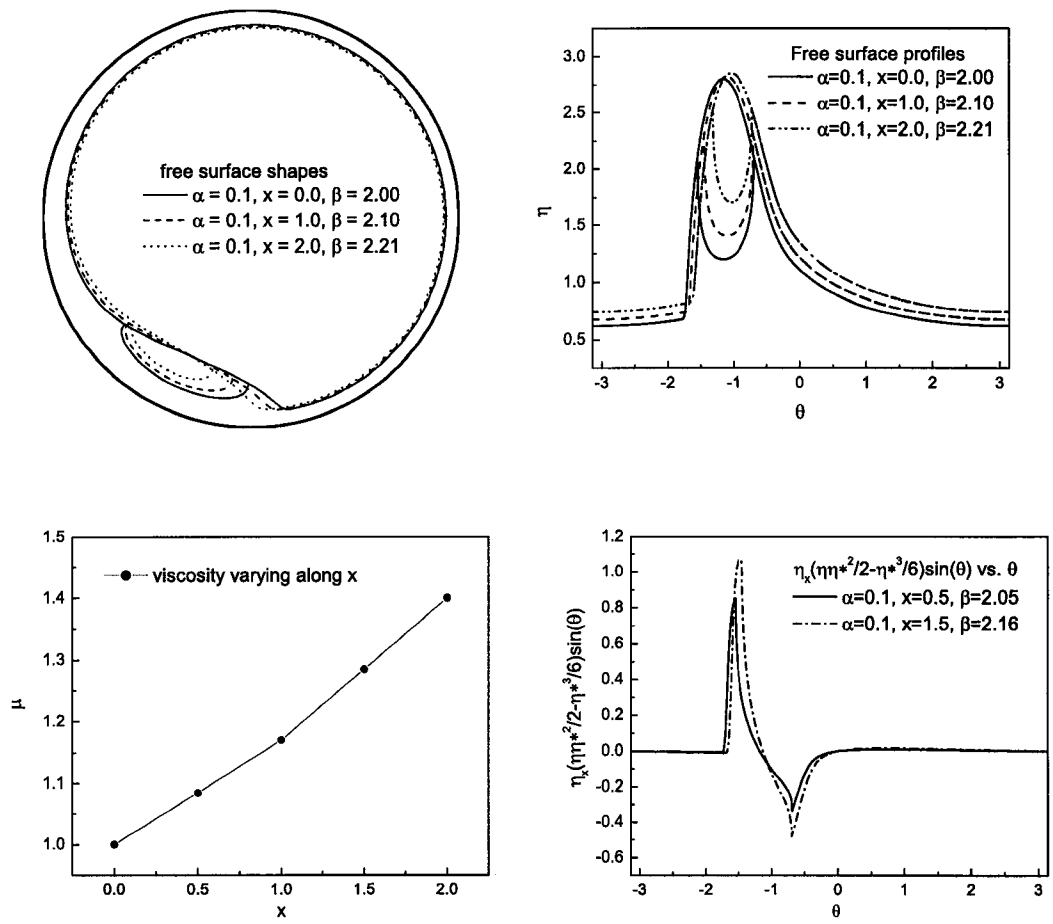

Figure 3.5: The film profiles and the integrand in equation (3.20) at different cross sections with the viscosity varying along the cylinder.

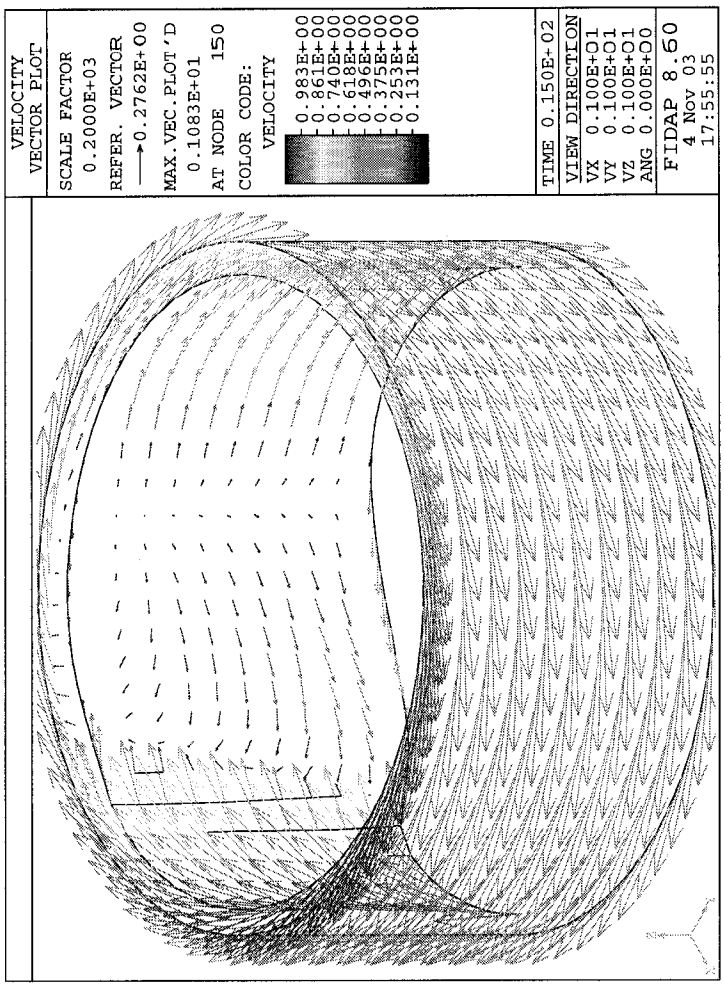

Figure 3.6: The velocity profiles obtained by solving the three-dimensional Stokes equations with $\beta = 2.15$, $F = 0.215$ ($\alpha = 0.1$), $\gamma = 10^{-2}$ and $\bar{\mu}(Z) = 1 + 0.5Z$ ($0 \leq Z \leq 1$). Note that, the direction of the increasing viscosity in this plot is along the axis Z rather than x as was in other places.

Now let us replace the pure fluid by a suspension of neutrally buoyant particles which is so dilute that the flow field is not influenced by their presence and suppose that the fluid viscosity is a prescribed function of the axial coordinate x. Then the axial particle flow rate is

$$J_p \equiv \int_{-\pi}^{\pi} \mathrm{d}\theta \int_0^{\eta} \phi w_p \mathrm{d}z \tag{3.24}$$

where w_p is the particle axial velocity in this flow field and ϕ is the particle volume fraction. In a manner analogous to that used for the pure fluid, we split the total

axial particle flow rate at every cross section of the cylinder into two parts: the axial particle flow rate in the recirculating flow region, J_p^r, and that in the circumferential flow region, J_p^o,

$$J_p^r \equiv \int_{-\pi}^{\pi}\int_{\eta^*}^{\eta} \phi^r w_p \mathrm{d}\theta\mathrm{d}z \tag{3.25}$$

and

$$J_p^o \equiv \int_{-\pi}^{\pi}\int_{0}^{\eta^*} \phi^c w_p \mathrm{d}\theta\mathrm{d}z \tag{3.26}$$

where, ϕ^r and ϕ^c are the particle volume fractions in the recirculating flow region and in the circumferential flow region respectively. Therefore, the total axial particle volumetric flow rate, equation (3.24), becomes

$$J_p = J_p^r + J_p^o = \int_{-\pi}^{\pi}\int_{\eta^*}^{\eta} \phi^r w_p \mathrm{d}\theta\mathrm{d}z + \int_{-\pi}^{\pi}\int_{0}^{\eta^*} \phi^c w_p \mathrm{d}\theta\mathrm{d}z \tag{3.27}$$

As mentioned before, in the pure fluid case, the axial volumetric flow rate of the fluid at any cross section of cylinder is zero when the flow has reached steady state, viz.

$$J = J^r + J^c = \int_{-\pi}^{\pi}\int_{\eta^*}^{\eta} w \mathrm{d}\theta\mathrm{d}z + \int_{-\pi}^{\pi}\int_{0}^{\eta^*} w \mathrm{d}\theta\mathrm{d}z = 0 \tag{3.28}$$

If we suppose now that ϕ^c and ϕ^r are independent of z and θ, multiply equation (3.28) by $-\phi^c$ and then add the result to equation (3.27), we obtain a new form for the particle volumetric flow rate,

$$J_p = \int_{-\pi}^{\pi}\int_{\eta^*}^{\eta} (\phi^r w_p - \phi^c w) \mathrm{d}\theta\mathrm{d}z + \int_{-\pi}^{\pi}\int_{0}^{\eta^*} \phi^c (w_p - w) \mathrm{d}\theta\mathrm{d}z \tag{3.29}$$

When the particles are small relative to the minimum film thickness, (i.e. if $a \equiv \hat{a}/\alpha R \ll \eta_m$ where $\hat{a}$ is the particle radius, *cf* Fig 3.4), $w_p \sim w$ everywhere except within a thin $O(a)$ layer close to the wall where w_p effectively vanishes. Consequently, the second term on the right hand side of equation (3.29) gives a negative contribution to J_p which however, is only $O(a^2)$ given that w is proportional to z within this thin $O(a)$ layer. Hence, on setting $w_p \sim w$ in the integrand of the first

term on the right-hand side of equation (3.29) and taking account of equations (3.28) and (3.20), the expression for J_p reduces to

$$J_p \approx (\phi^c - \phi^r)J^c = (\phi^c - \phi^r)\frac{\alpha}{\bar{\mu}}\int_{-\pi}^{\pi}\left\{\frac{1}{2}\eta(\eta^*)^2 - \frac{1}{6}(\eta^*)^3\right\}\frac{\partial\eta}{\partial x}\sin(\theta)\mathrm{d}\theta \qquad (3.30)$$

where $\bar{\mu}$ is the dimensionless viscosity of the suspension taken to be an effective Newtonian fluid. As was said earlier, the value of J^c is positive at steady state within the range of monotonically increasing $\bar{\mu}$, hence the sign of J_p is equal to that of $(\phi^c - \phi^r)$. Specifically, when $\phi^r < \phi^c$, the axial particle volumetric flow rate, J_p, is positive, implying a net particle flow rate towards the *high* viscosity region; but if $\phi^r = \phi^c$, then J_p vanishes even in the presence of an axially varying viscosity. These conclusions apply of course as long as the particles are so small that their "slip" velocity relative to the fluid is negligible beyond the $O(a)$ thin layer adjacent to the wall.

Now let us analyze the axial particle flow rate under the condition that there is no recirculating flow near the bottom of the cylinder and the film profile is everywhere symmetric about $\theta = 0$. In this case, given that, according to our observations, the particle volume fraction ϕ appears to be uniform throughout the cross-section of the film in the absence of the puddle,

$$J_p = \phi\int_{-\pi}^{\pi}\int_0^{\eta}(w_p - w)\mathrm{d}\theta\mathrm{d}z \qquad (3.31)$$

where ϕ is the particle volume fraction in the thin film and assumed to be independent of z and θ. But, if η is symmetric, w is odd (*cf* equation (3.11)) and w_p should similarly be odd, thereby implying that

$$J_p = 0 \qquad (3.32)$$

no matter how $\bar{\mu}(x)$ varies with x. We conclude that therefore, that, for homogeneous films ($\beta < 1.4\sqrt{\bar{\mu}}$), no particle segregation should be expected to occur.

Actually, there is a small range in β within which the film profile is asymmetric but without a recirculating flow being present near the bottom of the cylinder ($\beta^* < \beta < \beta^+$). When the particles are small relative to the minimum film thickness, however, we find, on using the same assumption about "slip" velocity as that for $\beta > \beta^+$ case, that J_p is negative but its magnitude is $O(a^2)$, thereby implying that

$$J_p \approx 0 \tag{3.33}$$

Note that all the conclusions made above require that the flow field of liquid reaches steady state. In fact, according to equation (3.19), the value of β_{local} and also F_{local} are indepent of time if the initial film profiles are symmetric. Hence, for $\beta < \beta^*$, there is no axial mass transport for any time so that particle segregation should not occur even when the viscosity varies along the cylinder.

3.4 Explanation for particle band formation

We shall now provide an explanation for the particle segregation based on the the calculated results about the axial particle volumetric flow rate together with the experimental findings about the radial particle segregation described in chapter 2.

From the experimental observations in chapter 2, we know that the particles in the recirculating region move into the circumferential flow region so that their volume fraction in the former is lower than in the latter. As mentioned before, particle concentration fluctuations are always present along the cylinder which in turn induce axial variations in the suspension effective viscosity. Consequently, according to equation (3.30),

$$J_p \approx (\phi^c - \phi^r) J_f^o = (\phi^c - \phi^r) \frac{\alpha}{\bar{\mu}} \int_{-\pi}^{\pi} \left\{ \frac{1}{2} \eta (\eta^*)^2 - \frac{1}{6} (\eta^*)^3 \right\} \frac{\partial \eta}{\partial x} \sin\theta \mathrm{d}\theta,$$

an axial particle volumetric flow rate is induced towards the more viscous region, viz. the region with the higher particle concentration, thereby further enhancing the

initial particle concentration fluctuations until, eventually, the bands appear along the cylinder.

Since, according to our experimental observations, the time for the first stage (the particle radial particle segregation) is an order of magnitude shorter than that for the second stage (the particle axial particle segregation), the whole time for the band formation is approximatively equal to the time for the second stage to set in which, in turn, is inversely proportional to the axial particle flow rate J_p. From equation (3.30), we can obtain the information of the time for band formation, viz.

- When the difference between ϕ^c, the particle concentration in the circumferential flow region and that in the recirculating region, ϕ^r, increases, the time required for the band formation is shortened (all other variables being the same).

- The suspension should require less time to segregate if the total particle concentration is increased given that, J_p is, to a first approximation, proportional to ϕ and that, as shown previously, J^c and therefore J_p increase with an increase in the gradient of the effective viscosity.

- The dimensionless time required for particle segregation is a very weak function of the particle size. This fact can be used to explain why the time required to achieve complete segregation did not change significantly when the particle size was increased by almost an order of magnitude (#52 and #77 in Table 3.1).

As mentioned in chapter 2, there exists a value of $\beta = \beta^c$ which can be used to determine qualitatively the degree of radial particle segregation as well as that of the degree of axial particle segregation (e.g. $\beta^c \approx 2.1$ for a low concentration suspension with $2\hat{a} = 463\mu$m). The reason for this is as follows:

When $\beta^+ < \beta < \beta^c$, the suspension in the cylinder can achieve complete radial particle segregation in the sense that no particles remain in the recirculating region.

On this situation, equation (3.30) becomes

$$J_p = \phi^c \frac{\alpha}{\bar{\mu}} \int_{-\pi}^{\pi} \left\{ \frac{1}{2}\eta(\eta^*)^2 - \frac{1}{6}(\eta^*)^3 \right\} \frac{\partial \eta}{\partial x} \sin\theta \mathrm{d}\theta \tag{3.34}$$

Therefore, an axial particle volumetric flow rate from the lower to the higher conentration region always exists unless no particles are left in the circumferential flow within the lower concentration region. Hence, all the particles at the region just referred to definitely move into the bands and the axial particle segregation becomes complete. On the other hand, when $\beta > \beta^c$, some particles always remain within the recirculating region throughout the duration of the experiments even though a number of particles initially present have already migrated out (incomplete radial particle segregation). Therefore, according to equation (3.30), some particles in the circumferential flow at the lower concentration region move into the higher concentration region to form bands. As a result of this axial particle migration, the concentration in the circumferential flow at the lower concentration region decreases until, at some point, the cross-sectional concentration at the lower concentration region becomes uniform again. But the suspension is then so dilute that any further radial particle segregation is unlikely to occur. Hence, the axial particle volumetric flow rate vanishes, implying that no further axial particle segregation can occur. Therefore, since at this stage some particles have remained within the low concentration regions, the axial particle segregation is incomplete.

Now let us explain the experimental phenomena in the absence of a "puddle" at the bottom of the cylinder, i.e. for $\beta < \beta^+$.

In view of the analysis in section 3.3 leading to equations (3.32) and (3.33), particle segregation should not occur along the cylinder as long as the suspension can be modeled as an effective Newtonian fluid which is permissible provided that ϕ is relatively small, say less than about 0.2. [More concentrated suspensions exhibit non-Newtonian effects, in particular normal stresses, which can induce instabilities

in similar systems even if the particle concentration is uniform[16].] Nevertheless, when we performed experiments with a suspension with a value of β within the range, approximately $0.7 - 1.5$, particle segregation was observed but only within a section of the cylinder while the rest of the region remained coated with a homogeneous suspension. As mentioned earlier, for β within this range, rimming flows are very sensitive to extremely small deviations of the cylinder's axis ($\leq 0.1^0$) from the horizontal [4], and hence, it is almost impossible to keep β_{local} uniform along the cylinder during the experiment. In fact, since, after the start of an experiment in a rotating cylinder with a very small inclination, the value of β_{local} at the lower end would be expected to eventually exceed β^+ thereby creating a "puddle", the appearance of bands at the lower end of the cylinder is entirely consistent with the predictions of our analysis. On the other hand, the value of β_{local} at the higher end would be expected to fall even further below β^* thereby creating a homogeneous film profile where, according to our arguments, particle segregation cannot occur. This theoretical prediction is consistent with the experimental findings in the sense that, for β sufficiently below β^+ where the film profile is both quasi-steady and homogeneous, no bands were found to form along the cylinder even when the viscosity was increased locally by placing a piece of ice on the outer wall of the rotating cylinder.

The arguments given above, which are consistent with the main conclusions of our experimental work as well as Tirumkudulu's which are listed in chapter 2, will be rendered more quantitative by means of a linear stability analysis based on the modified lubrication equation described in the preceding section 3.2 which will also lead to a prediction of the expected wavelength of the particle bands along the cylinder.

3.5 Stability analysis of a dilute suspension

As already mentioned, the particle segregation leading to the formation of bands appears to proceed in two stages, viz. first, a radial particle segregation followed by an axial particle segregation. As a result of the radial particle segregation, the particle concentration in the circumferential flow region (ϕ^c) is higher than that in the recirculating flow (ϕ^r) at every cross section, but the axial concentration is still essentially uniform. In order to simplify the analysis, we shall only deal with the case of complete radial segregation i.e. $\phi^r = 0$ and shall further suppose that the suspension is initially very dilute, i.e. $\phi \sim 0.01$. Note that if ϕ refers to the initial particle concentration throughout the film, then after the completion of the radial particle segregation, ϕ^c will still be approximately equal to ϕ given that, for a typical case ($\alpha = 0.1$, $\beta = 1.8$), the region occupied by the recirculating flow is, according to the "modified lubrication analysis" (MLA), only about 3% of the total volume of the suspension.

3.5.1 MLA for complete radial segregation

First we provide a detailed derivation of a special modified lubrication equation which is used to characterize the film profile of the suspension having complete radial particle segregation.

Choose the pure liquid viscosity for the reference viscosity, express α in terms of this reference viscosity (*cf* equation (3.3) for the expression of α). Consequently, within the puddle ($\eta^* < z \leq \eta$ and $\theta_1 < \theta < \theta_2$), $\bar{\mu} = 1$, whereas, $\bar{\mu} > 1$ within the circumferential flow region ($0 < z \leq \eta^*$ for $\theta_1 < \theta < \theta_2$ and $0 < z \leq \eta$ for $-\pi < \theta < \theta_1$ plus $\theta_2 < \theta < \pi$) (*cf* Fig 3.4). Let the dimensionless angular velocity within the puddle be denoted by v^*, and that within the circumferential flow region

by v. Then, the boundary conditions for $\theta_1 < \theta < \theta_2$ become

$$v = 1 \quad \text{at} \quad z = 0; \qquad \frac{\partial v^*}{\partial z} = 0 \quad \text{at} \quad z = \eta$$

and

$$v = v^* \quad \text{at} \quad z = \eta^*; \qquad \frac{\partial v^*}{\partial z} = \bar{\mu}\frac{\partial v}{\partial z} \quad \text{at} \quad z = \eta^*$$

but remain the same for the other region ($-\pi < \theta < \theta_1$ plus $\theta_2 < \theta < \pi$) as those for the pure liquid case, i.e.

$$v = 1 \quad \text{at} \quad z = 0; \qquad \frac{\partial v}{\partial z} = 0 \quad \text{at} \quad z = \eta$$

Now, according to the "modified lubrication analysis"(MLA) with $\gamma = 0$, i.e. equation (3.4), the expressions for v and v^* satisfying the above boundary conditions are

$$v = 1 - \frac{1}{\bar{\mu}}\left(\eta z - \frac{z^2}{2}\right)\left\{(1 - \alpha\eta)\cos\theta - \alpha\frac{\partial \eta}{\partial \theta}\sin\theta\right\} \tag{3.35}$$

and

$$v^* = 1 + \left\{\left(1 - \frac{1}{\bar{\mu}}\right)\left(\eta\eta^* - \frac{(\eta^*)^2}{2}\right) - \left(\eta z - \frac{z^2}{2}\right)\right\}\left\{(1 - \alpha\eta)\cos\theta - \alpha\frac{\partial \eta}{\partial \theta}\sin\theta\right\} \tag{3.36}$$

Therefore,

$$q \equiv \int_0^{\eta^*} v\mathrm{d}z = \eta^* - \frac{1}{3\bar{\mu}}\left\{\frac{3}{2}\eta(\eta^*)^2 - \frac{1}{2}(\eta^*)^3\right\}\left\{(1 - \alpha\eta)\cos\theta - \alpha\frac{\partial \eta}{\partial \theta}\sin\theta\right\} \tag{3.37}$$

and

$$\int_{\eta^*}^{\eta} v^*\mathrm{d}z = 0 = \eta - \eta^*$$
$$-\frac{1}{3\bar{\mu}}\left\{\frac{3}{2}(\eta^*)^3 - \frac{9}{2}\eta(\eta^*)^2 + 3\eta^2\eta^* + \bar{\mu}(\eta - \eta^*)^3\right\}\left\{(1 - \alpha\eta)\cos\theta - \alpha\frac{\partial \eta}{\partial \theta}\sin\theta\right\} \tag{3.38}$$

Combining equations (3.37) and (3.38), we obtain,

$$q = \eta - \frac{1}{3\bar{\mu}}\left\{\eta^3 + (\bar{\mu} - 1)(\eta - \eta^*)^3\right\}\left\{(1 - \alpha\eta)\cos\theta - \alpha\frac{\partial \eta}{\partial \theta}\sin\theta\right\} \tag{3.39}$$

Note that when $\bar{\mu} = 1$, i.e. if $\phi^c = \phi^r = 0$, equation (3.39) reduces to that for the pure liquid case (*cf* the modified lubrication equation (MLE) (3.6)).

Next, by the similar procedure as shown above, we shall modify the expression for w, the axial velocity component due to the complete radial segregation. Let w and w^* refer to the axial velocity in the circumferential and recirculating flow regions respectively. Then the boundary conditions for w and w^* within the region $\theta_1 < \theta < \theta_2$ become

$$w = 1 \quad \text{at} \quad z = 0; \qquad \frac{\partial w^*}{\partial z} = 0 \quad \text{at} \quad z = \eta$$

and

$$w = w^* \quad \text{at} \quad z = \eta^*; \qquad \frac{\partial w^*}{\partial z} = \bar{\mu}\frac{\partial w}{\partial z} \quad \text{at} \quad z = \eta^*$$

According to the MLA (*cf* equation (3.10)), the expressions of w and w^* satisfying the above boundary conditions are

$$w = \frac{\alpha}{\bar{\mu}}\left\{\eta z - \frac{1}{2}z^2\right\}\frac{\partial \eta}{\partial x}\sin\theta \tag{3.40}$$

and

$$w^* = \alpha\left\{\left(\eta z - \frac{1}{2}z^2\right) + \left(1 - \frac{1}{\bar{\mu}}\right)\left(\frac{1}{2}(\eta^*)^2 - \eta^*\eta\right)\right\}\frac{\partial \eta}{\partial x}\sin\theta \tag{3.41}$$

Therefore,

$$W \equiv \int_0^{\eta^*} w\mathrm{d}z + \int_{\eta^*}^{\eta} w^*\mathrm{d}z = \frac{\alpha}{3}\frac{\eta^3}{\bar{\mu}}\left\{1 + (\bar{\mu} - 1)\left(1 - \frac{\eta^*}{\eta}\right)^3\right\}\frac{\partial \eta}{\partial x}\sin\theta \tag{3.42}$$

3.5.2 Mass conservation

Letting $\phi^c = \phi$, we begin with the overall mass conservation equation for the *particle* phase across the cylinder at location x,

$$\frac{\partial}{\partial t}\left\{\phi\int_{-\pi}^{\pi}\left(1 - \frac{\alpha}{2}\eta^*\right)\eta^*\mathrm{d}\theta\right\} + \frac{\partial J_p}{\partial x} = 0 \tag{3.43}$$

where J_p is given by equation (3.34) with ϕ^c having been replaced by ϕ, together with the mass conservation equation for the suspension with complete radial segregation viewed as an effective Newtonian fluid with a concentration dependent relative viscosity $\bar{\mu}(\phi)$,

$$(1-\alpha\eta)\frac{\partial \eta}{\partial t}+\frac{\partial q}{\partial \theta}+\frac{\partial W}{\partial x}=0 \tag{3.44}$$

where the expressions for q and W are given in equations (3.39) and (3.42) respectively. Since, as stated above, equation (3.43) refers to an overall, rather than to a local particle conservation balance, equations (3.34) and (3.43) imply that ϕ is a function only of x and t, and that other modes of particle transport besides bulk convection, e.g. shear-induced diffusion which, anyhow, is negligible if ϕ is small, can safely be ignored.

3.5.3 Linear stability analysis

Since the suspension is very dilute, the relationship between the effective relative viscosity, $\bar{\mu}$, and the concentration, ϕ, is described by Einstein's well-known expression,

$$\bar{\mu}=1+\frac{5}{2}\phi \tag{3.45}$$

We let $\phi=\phi_0+\zeta$ with $|\zeta|\ll\phi_0$ and correspondingly $\eta=\eta_0(\theta)+\xi$ with $|\xi|\ll\eta_0$, $\eta^*=\eta_0^*(\theta)+\xi^*$ with $|\xi|^*\ll\eta_0^*$, and $q=q_0+\delta$ with $|\delta|\ll q_0$ everywhere (the subscript 0 refers to the initial axially uniform state in which $\phi=\phi_0$ throughout the circumferential flow region, and $\phi=0$ within the puddle), and then linearize equations (3.43) and (3.44) to yield

$$\frac{\partial \zeta}{\partial t}\int_{-\pi}^{\pi}\left(1-\frac{\alpha}{2}\eta_0^*\right)\eta_0^*\mathrm{d}\theta+\phi_0\int_{-\pi}^{\pi}(1-\alpha\eta_0^*)\frac{\partial \xi^*}{\partial t}\mathrm{d}\theta$$
$$=-\phi_0\frac{\alpha}{\bar{\mu}_0}\int_{-\pi}^{\pi}\left\{\frac{1}{2}\eta_0(\eta_0^*)^2-\frac{1}{6}(\eta_0^*)^3\right\}\frac{\partial^2\xi}{\partial x^2}\sin\theta\mathrm{d}\theta \tag{3.46}$$

and

$$(1-\alpha\eta_0)\frac{\partial \xi}{\partial t}+\frac{\partial \delta}{\partial \theta}+\frac{\alpha}{3\bar{\mu}_0}\eta_0^3\sin\theta\frac{\partial^2\xi}{\partial x^2}=0 \tag{3.47}$$

where

$$\delta = f_0\xi$$
$$+\frac{\alpha}{3\bar{\mu}_0}\eta_0^3\frac{\partial\xi}{\partial\theta}\sin\theta + \frac{5\zeta}{2}\frac{\eta_0^3}{3\bar{\mu}_0}\left[\frac{1}{\bar{\mu}_0} - \left(1-\frac{\eta_0^*}{\eta_0}\right)^3\right]\left\{(1-\alpha\eta_0)\cos\theta - \alpha\frac{\mathrm{d}\eta_0}{\mathrm{d}\theta}\sin\theta\right\}$$
$$-\frac{\bar{\mu}_0-1}{3\bar{\mu}_0}\left\{3(\eta_0-\eta_0^*)^2(\xi-\xi^*) - \frac{5\zeta}{2\bar{\mu}_0}(\eta_0-\eta_0^*)^3\right\}\left\{(1-\alpha\eta_0)\cos\theta - \alpha\frac{\mathrm{d}\eta_0}{\mathrm{d}\theta}\sin\theta\right\}$$
$$+\alpha\frac{\bar{\mu}_0-1}{3\bar{\mu}_0}(\eta_0-\eta_0^*)^3\left\{\xi\cos\theta + \frac{\partial\xi}{\partial\theta}\sin\theta\right\} \tag{3.48}$$

and

$$f_0(\theta) \equiv 1 - \frac{1}{\bar{\mu}_0}\eta_0^2\cos\theta + \frac{4\alpha}{3\bar{\mu}_0}\eta_0^3\cos\theta + \frac{\alpha}{\bar{\mu}_0}\eta_0^2\frac{\mathrm{d}\eta_0}{\mathrm{d}\theta}\sin\theta$$

But, since $\phi_0 \sim 0.01$, $(\bar{\mu}_0 - 1) \sim O(\phi_0) \sim 0$, and therefore the second term on the left-hand side of equation (3.46) as well as the last two terms on the right-hand side of equation (3.48) can be neglected. Consequently, equations (3.46) and (3.47) can be simplified into

$$\frac{\partial\zeta}{\partial t}\int_{-\pi}^{\pi}\left(1-\frac{\alpha}{2}\eta_0^*\right)\eta_0^*\mathrm{d}\theta = -\phi_0\frac{\alpha}{\bar{\mu}_0}\int_{-\pi}^{\pi}\left\{\frac{1}{2}\eta_0(\eta_0^*)^2 - \frac{1}{6}(\eta_0^*)^3\right\}\frac{\partial^2\xi}{\partial x^2}\sin\theta\mathrm{d}\theta \tag{3.49}$$

and

$$(1-\alpha\eta_0)\frac{\partial\xi}{\partial t} + \frac{\partial(f_0\xi)}{\partial\theta} + \frac{\alpha}{3}\frac{\partial}{\partial\theta}\left[\eta_0^3\sin\theta\frac{\partial\xi}{\partial\theta}\right] + \frac{\alpha}{3}\eta_0^3\sin\theta\frac{\partial^2\xi}{\partial x^2}$$
$$= -\frac{5}{2}\zeta\frac{\mathrm{d}\eta_0}{\mathrm{d}\theta} + \frac{5}{2}\zeta\frac{\mathrm{d}}{\mathrm{d}\theta}\left[(\eta_0-q_0)\left(1-\frac{\eta_0^*}{\eta_0}\right)^3\right] \tag{3.50}$$

where

$$f_0(\theta) \equiv 1 - \eta_0^2\cos\theta + \frac{4\alpha}{3}\eta_0^3\cos\theta + \alpha\eta_0^2\frac{\mathrm{d}\eta_0}{\mathrm{d}\theta}\sin\theta = \frac{3q_0}{\eta_0} - 2 + \frac{\alpha}{3}\eta_0^3\cos\theta \tag{3.51}$$

and

$$q_0 = \eta_0 - \frac{\eta_0^3}{3}\left\{(1-\alpha\eta_0)\cos\theta - \alpha\frac{\mathrm{d}\eta_0}{\mathrm{d}\theta}\sin\theta\right\} \tag{3.52}$$

Next, we separate variables by letting

$$\zeta = \epsilon\exp(\lambda t)\sin(kx+b) \tag{3.53}$$

and

$$\xi = \epsilon G(\theta) \exp(\lambda t) \sin(kx + b) \tag{3.54}$$

and thereby obtain for the growth constant λ and the function $G(\theta)$,

$$\lambda = \alpha k^2 \phi_0 \frac{\int_{-\pi}^{\pi} \left\{ \frac{1}{2}\eta_0(\eta_0^*)^2 - \frac{1}{6}(\eta_0^*)^3 \right\} G \sin\theta \mathrm{d}\theta}{\int_{-\pi}^{\pi} \left(1 - \frac{\alpha}{2}\eta_0^*\right) \eta_0^* \mathrm{d}\theta} \tag{3.55}$$

and

$$(1 - \alpha\eta_0)\lambda G + \frac{\mathrm{d}(f_0 G)}{\mathrm{d}\theta} + \frac{\alpha}{3}\frac{\mathrm{d}}{\mathrm{d}\theta}\left[\eta_0^3 \sin\theta \frac{\mathrm{d}G}{\mathrm{d}\theta}\right] - \frac{\alpha}{3}k^2\eta_0^3 \sin\theta G = -\frac{5}{2}\frac{\mathrm{d}\eta_0}{\mathrm{d}\theta} + \frac{5}{2}\frac{\mathrm{d}}{\mathrm{d}\theta}\left[(\eta_0 - q_0)\left(1 - \frac{\eta_0^*}{\eta_0}\right)^3\right] \tag{3.56}$$

subject to the periodicity constraints. The above equation can be further simplified given that since, in view of (3.55), $\lambda \sim O(\phi_0)$, the first term of (3.56) involving λ can be neglected when $\phi_0 \ll 1$. It should be noted, however, that in the "modified lubrication analysis" of the three-dimensional coating flows, the viscous force in the momentum balance equations in both angular and axial directions (*cf* equations (3.4) and (3.10)) only contains the leading order term, $\partial^2 v/\partial z^2$ and $\partial^2 w/\partial z^2$, with other terms, such as $\alpha^2\partial^2 v/\partial x^2$ and $\alpha^2\partial^2 w/\partial x^2$, having been neglected on the assumption that $\alpha^2 \ll 1$ and that all axial variations occur over a length scale $O(1)$ or larger. Clearly, such a simplification is no longer permissible if $k > 1/\alpha$ given that, in that case, $\alpha^2\partial^2 v/\partial x^2$ and $\alpha^2\partial^2 w/\partial x^2$ are of the same order as $\partial^2 v/\partial z^2$ and $\partial^2 w/\partial z^2$ respectively. Under such circumstances, the MLA fails to describe the flow field and our linear analysis needs to be modified.

Note that, according to equation (3.56), the perturbation in the film profile is quasi-steady if $\lambda = O(\phi_0) \ll 1$ and that it is driven by the slow time evolution of the perturbation in the particle concentration, thereby justifying the use of the quasi-steady state expression for the axial particle flow rate J_p given by equation (3.34).

Under these circumstances, on integrating equation (3.56) and applying the periodicity constraints, we find that

$$\int_{-\pi}^{\pi} \eta_0^3 G \sin\theta \mathrm{d}\theta = 0 \tag{3.57}$$

as a result of which, the expression for λ, i.e. equation (3.55), becomes

$$\lambda = \alpha k^2 \phi_0 \frac{\int_{\theta_1}^{\theta_2} \left\{ \frac{1}{2}\eta_0(\eta_0^*)^2 - \frac{1}{6}(\eta_0^*)^3 - \frac{1}{3}\eta_0^3 \right\} G \sin\theta \mathrm{d}\theta}{\int_{-\pi}^{\pi} \left(1 - \frac{\alpha}{2}\eta_0^*\right) \eta_0^* \mathrm{d}\theta} \tag{3.58}$$

where θ_1 and θ_2, respectively, refer to the angular coordinates of the two stagnation points of the puddle (*cf* Fig 3.1). According to equation (3.58), it is clear then that the size and shape of the puddle play a crucial role in determining the sign and magnitude of the growth constant λ.

On solving equation (3.56) numerically, we first obtain the function G and then, on substituting G into equation (3.55), determine $\lambda/\alpha\phi_0$ vs. the wavenumber k. Such a result is shown in Fig 3.7 for the typical case $\alpha = 0.1$ and $\beta = 1.8$. Clearly, the growth constant λ is seen to increase monotonically with k thereby implying that the most rapidly amplified disturbances are those having the shortest wavelengths. This result is not surprising given that such disturbances, if left unhindered, are particularly efficient in rearranging the particles into regular lumps separated by thin regions of particle free liquid. In order to arrive at a more realistic prediction for the wavelength of the most rapidly amplified disturbance, it is therefore necessary to extend our analysis and include the effects of surface tension which, as is usually the case, would be expected to dampen the disturbances with $k \to \infty$.

To this end, we return to the expression for the pressure within the film[4] but include the surface tension contribution. In the thin film approximation, the leading order term of this pressure in dimensionless form is shown previously in equation (1.88), i.e.

$$p = \alpha(z - \eta)\sin\theta - \alpha\gamma\left(\eta + \frac{\partial^2\eta}{\partial\theta^2} + \frac{\partial^2\eta}{\partial x^2}\right)$$

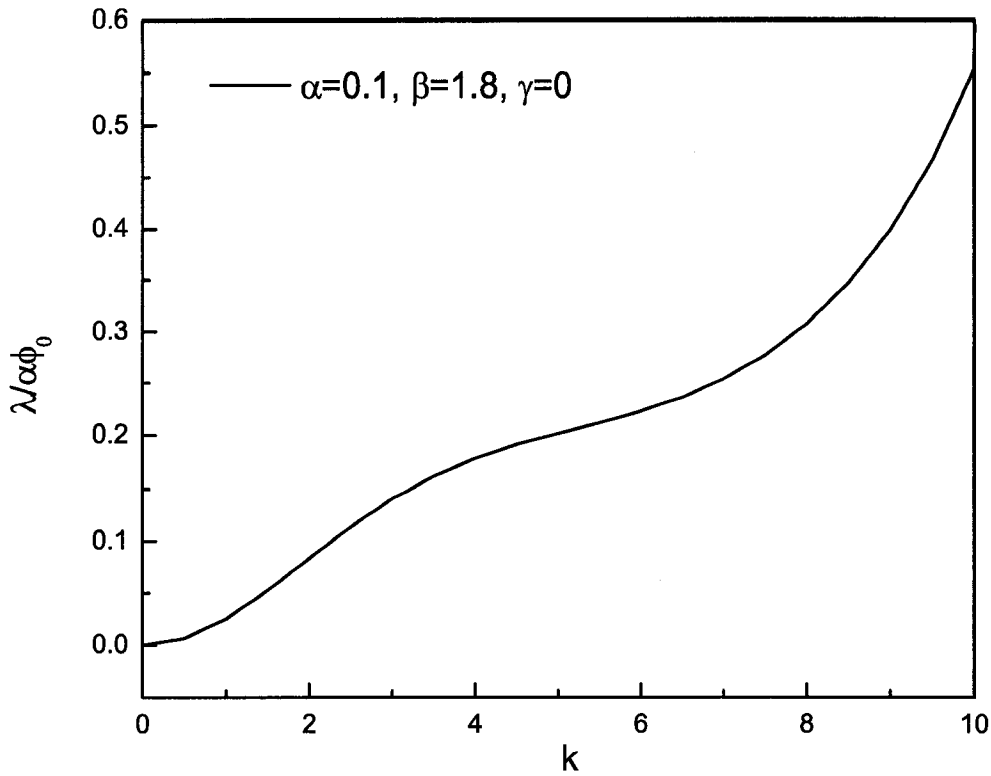

Figure 3.7: A plot of the growth constant λ for $\alpha = 0.1$ and $\beta = 1.8$ vs. the wave number k when $\gamma = 0$.

Therefore, according to the "modified lubrication analysis", the corresponding expressions for the angular and axial velocities outside the puddle are, respectively (*cf* equations (3.35) and (3.40)),

$$v = 1 - \frac{1}{\bar{\mu}}\left(\eta z - \frac{z^2}{2}\right)\left\{(1-\alpha\eta)\cos\theta - \alpha\frac{\partial\eta}{\partial\theta}\sin\theta - \alpha\gamma\left(\frac{\partial\eta}{\partial\theta} + \frac{\partial^3\eta}{\partial\theta\partial x^2} + \frac{\partial^3\eta}{\partial\theta^3}\right)\right\} \tag{3.59}$$

and

$$w = \frac{\alpha}{\bar{\mu}}\left(\eta z - \frac{z^2}{2}\right)\left\{\frac{\partial\eta}{\partial x}\sin\theta + \gamma\left(\frac{\partial\eta}{\partial x} + \frac{\partial\eta^3}{\partial\theta^2\partial x} + \frac{\partial^3\eta}{\partial x^3}\right)\right\} \tag{3.60}$$

Moreover, the axial particle flow rate J_p in equation (3.34) and the mass conservation equation (3.44) for the suspension now become

$$J_p = \phi\frac{\alpha}{\bar{\mu}}\int_{-\pi}^{\pi}\left\{\frac{1}{2}\eta(\eta^*)^2 - \frac{1}{6}(\eta^*)^3\right\}\left\{\frac{\partial\eta}{\partial x}\sin\theta + \gamma\left(\frac{\partial\eta}{\partial x} + \frac{\partial^3\eta}{\partial\theta^2\partial x} + \frac{\partial^3\eta}{\partial x^3}\right)\right\}\mathrm{d}\theta \tag{3.61}$$

and

$$(1-\alpha\eta)\frac{\partial\eta}{\partial t}+\frac{\partial q}{\partial\theta}+\frac{\partial W}{\partial x}=0 \tag{3.62}$$

where

$$q=\eta-\frac{1}{3\bar{\mu}}\left\{\eta^3+(\bar{\mu}-1)(\eta-\eta^*)^3\right\}\left\{(1-\alpha\eta)\cos\theta-\alpha\frac{\partial\eta}{\partial\theta}\sin\theta\right\}$$
$$+\alpha\gamma\frac{1}{3\bar{\mu}}\left\{\eta^3+(\bar{\mu}-1)(\eta-\eta^*)^3\right\}\left(\frac{\partial\eta}{\partial\theta}+\frac{\partial^3\eta}{\partial\theta\partial x^2}+\frac{\partial^3\eta}{\partial\theta^3}\right) \tag{3.63}$$

and

$$W=\frac{\alpha}{3}\left\{\left[\frac{\eta^3}{\bar{\mu}}\frac{\partial\eta}{\partial x}\sin\theta+\gamma\frac{\eta^3}{\bar{\mu}}\left(\frac{\partial\eta}{\partial x}+\frac{\partial^3\eta}{\partial\theta^2\partial x}+\frac{\partial^3\eta}{\partial x^3}\right)\right]\left[1+(\bar{\mu}-1)\left(1-\frac{\eta^*}{\eta}\right)^3\right]\right\} \tag{3.64}$$

Hence, in place of equations (3.55) and (3.56), we have

$$\lambda=\alpha k^2\phi_0\frac{\int_{-\pi}^{\pi}\left\{\frac{1}{2}\eta_0(\eta_0^*)^2-\frac{1}{6}(\eta_0^*)^3\right\}\left\{G\sin\theta+\gamma\left(G-k^2G+\frac{\mathrm{d}^2G}{\mathrm{d}\theta^2}\right)\right\}\mathrm{d}\theta}{\int_{-\pi}^{\pi}\left(1-\frac{\alpha}{2}\eta_0^*\right)\eta_0^*\mathrm{d}\theta} \tag{3.65}$$

and

$$\frac{\mathrm{d}(f_0G)}{\mathrm{d}\theta}+\frac{\alpha}{3}\frac{\mathrm{d}}{\mathrm{d}\theta}\left[\eta_0^3\sin\theta\frac{\mathrm{d}G}{\mathrm{d}\theta}\right]+\frac{5}{2}\frac{\mathrm{d}\eta_0}{\mathrm{d}\theta}-\frac{5}{2}\frac{\mathrm{d}}{\mathrm{d}\theta}\left[(\eta_0-q_0)\left(1-\frac{\eta_0^*}{\eta_0}\right)^3\right]=$$
$$\frac{\alpha\gamma}{3}\left\{k^2\eta_0^3\left[G\left(1+\frac{\sin\theta}{\gamma}\right)-k^2G+\frac{\mathrm{d}^2G}{\mathrm{d}\theta^2}\right]-\frac{\mathrm{d}}{\mathrm{d}\theta}\left[\eta_0^3\left(\frac{\mathrm{d}G}{\mathrm{d}\theta}-k^2\frac{\mathrm{d}G}{\mathrm{d}\theta}+\frac{\mathrm{d}^3G}{\mathrm{d}\theta^3}\right)\right]\right\} \tag{3.66}$$

where

$$q_0=\eta_0-\frac{\eta_0^3}{3}\left\{(1-\alpha\eta_0)\cos\theta-\alpha\frac{\mathrm{d}\eta_0}{\mathrm{d}\theta}\sin\theta-\alpha\gamma\left(\frac{\mathrm{d}\eta_0}{\mathrm{d}\theta}+\frac{\mathrm{d}^3\eta_0}{\mathrm{d}\theta^3}\right)\right\} \tag{3.67}$$

and

$$f_0=\frac{3q_0}{\eta_0}-2+\frac{\alpha}{3}\eta_0^3\cos\theta$$

Again, for the same reason as that in the previous case with $\gamma=0$, equations (3.65) and (3.66) are no longer valid when $k>1/\alpha$. Moreover, as was done earlier for the case $\gamma=0$, *cf* equations (3.57) and (3.58), we integrate equation (3.66) to obtain

$$\int_{-\pi}^{\pi}\eta_0^3\left\{G\sin\theta+\gamma\left(G-k^2G+\frac{\mathrm{d}^2G}{\mathrm{d}\theta^2}\right)\right\}\mathrm{d}\theta=0 \tag{3.68}$$

on account of which equation (3.65) becomes

$$\lambda = \alpha k^2 \phi_0 \frac{\int_{\theta_1}^{\theta_2} \left\{ \frac{1}{2}\eta_0(\eta_0^*)^2 - \frac{1}{6}(\eta_0^*)^3 - \frac{1}{3}\eta_0^3 \right\} \left\{ G\sin\theta + \gamma \left(G - k^2 G + \frac{\mathrm{d}^2 G}{\mathrm{d}\theta^2} \right) \right\} \mathrm{d}\theta}{\int_{-\pi}^{\pi} \left(1 - \frac{\alpha}{2}\eta_0^* \right) \eta_0^* \mathrm{d}\theta} \tag{3.69}$$

As was the case with equation (3.58), the expression given above again illustrates the crucial importance played by the size and shape of the puddle in determining λ.

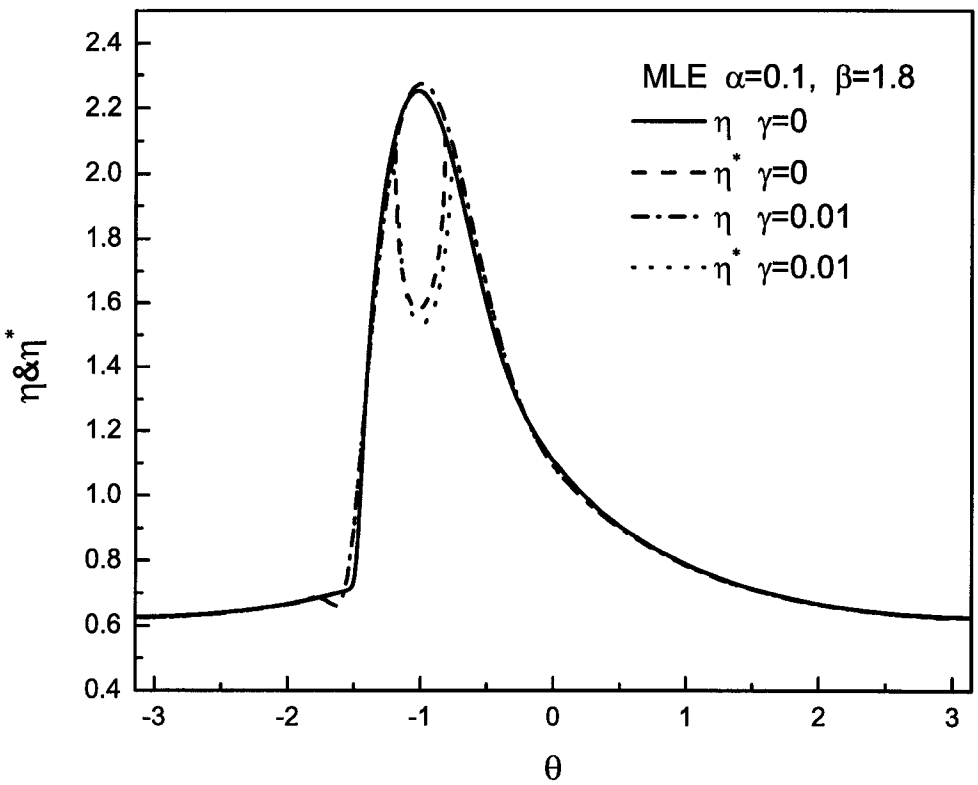

Figure 3.8: The film profile η and the corresponding profile η^* given by the modified lubrication equation with $\gamma = 0.01$ and $\gamma = 0$ for $\alpha = 0.1$ and $\beta = 1.8$.

To obtain the base film profiles η_0 and the corresponding profile of η_0^*, we now have to solve equation (3.67) rather than (3.52). However, we find that the inclusion of surface tension has little effect on the shape of the axially uniform profiles of η as well as those of η^* provided that $\gamma \ll 1$ (*cf* Fig 3.8). Hence, in solving equation (3.66) numerically for G, we retained the values of η_0 and η_0^* given by the MLE with $\gamma = 0$,

i.e. equation (3.52) instead of equation (3.67). Then, after obtaining the function G, we computed, by means of equation (3.65) or (3.69), the growth constant λ as function of the wave number k for different values of γ. Such a family of profiles is shown in Fig 3.9 for the typical case $\alpha = 0.1$, $\beta = 1.8$. Clearly, a most rapidly

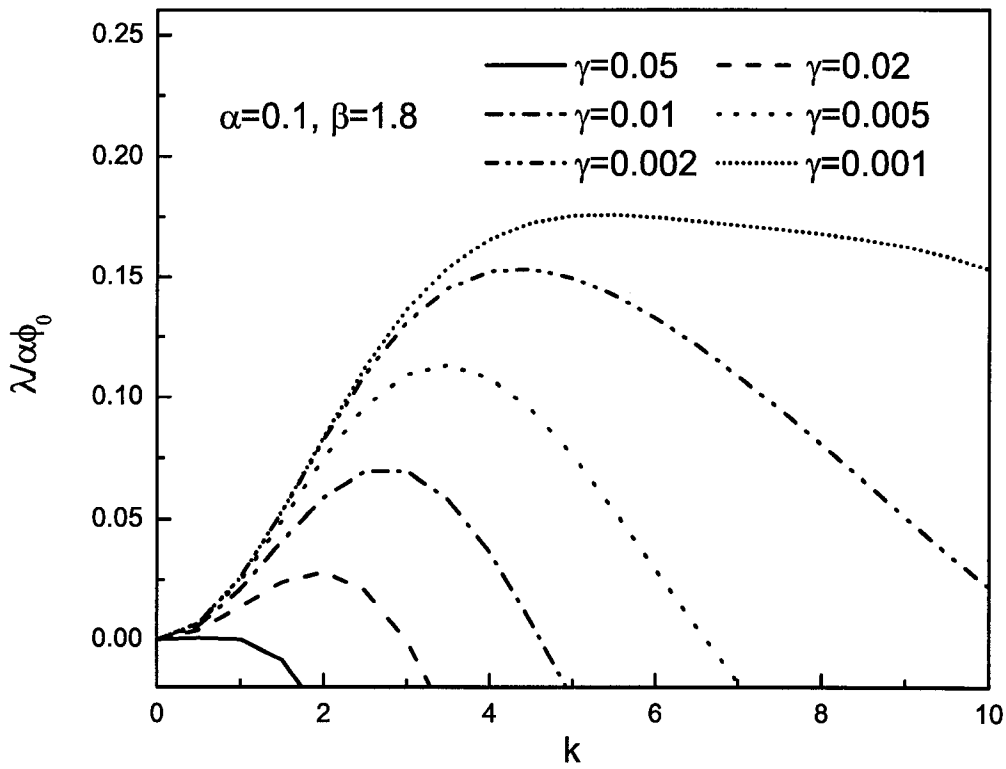

Figure 3.9: The growth constant λ has a maximum when $\gamma > 0$ with the wave number of the most rapidly amplified disturbance increasing with a decrease in the dimensionless surface tension parameter γ.

growing disturbance now exists having a wavenumber $k = k_c$, the value of which is sensitive to the magnitude of the dimensionless surface tension parameter γ. Moreover, for the typical case of Fig 3.9, the dimensionless wavelength, $2\pi/k_c$, is seen to increase with increasing γ, consistent with the experimental observations shown in the Table 3.1. In order to observe further the effects of varying the surface tension parameter γ on the axial instability of this suspension for $k = 0$, we calculated the integral in the numerator of the right-hand side of equations (3.65) or (3.69) for $\alpha = 0.1$, $\beta = 1.8$ and for different values of γ. As shown in Fig 3.10, even though

the sign of the integral is positive within the range $\gamma \ll 1$, the magnitude of the integral decreases with increasing γ. Therefore, these calculations suggest that this type of instability is dampened by surface tension effects (as expected) and will even disappear if the value of γ is large enough, but the latter case is beyond the scope of our analysis which, being restricted to $\gamma \ll 1$, would require modification.

Table 3.1: A list of the various parameters for some of the experiments

#	R	$2\hat{a}$	ϕ	α	F	β	L/R	Re	γ	$h_m/2\hat{a}$	τ	l/R
	cm	μm	%					10^{-5}	10^{-3}		10^3	
2	1.27	463	1	0.09	0.16	1.8	22.8	7.9	17	1.4	3.48	2.7
29	1.27	463	5	0.09	0.15	1.7	22.8	6.1	17	1.5	0.66	2.6
60	5	463	1	0.09	0.16	1.8	6	500	1.1	6	1.80	0.7
63	5	463	5	0.09	0.16	1.8	6	400	1.1	6	0.54	0.7
75	0.635	60	1	0.09	0.16	1.8	45.6	1.40	69	6	3.24	3.6
80	0.635	60	5	0.09	0.16	1.8	45.6	0.95	69	6	0.90	3.2
52	0.635	463	1	0.23	0.39	1.7	45.6	35	69	1.9	3.12	4.7
77	0.635	60	1	0.22	0.39	1.8	45.6	47	69	14.8	3.42	3.6

Here, the experiments in ref[12] were performed by using a mixture of Triton X-100, $ZnCl_2$ and water[1, 2] with a viscosity of 4000 cP and a density of 1.172 g/cm^3 at T=23^{o}C. Seven dimensionless parameters were identified as influencing the observed phenomena, specifically: $Re \equiv \Omega\rho h_0^2/\mu$, $\alpha \equiv \sqrt{\Omega\mu/\rho g R}$, F, $\gamma \equiv \sigma/\rho g R^2$, L/R, $h_m/2\hat{a}$ and ϕ, where Re is the Reynolds number, Ω is the angular velocity of the cylinder, h_0 is the mean thickness of the film, ρ is the density of the suspension, μ is the effective viscosity of the suspension, α is a measure of the ratio of the viscous to the gravitational forces, R is the inner radius of the cylinder, g is the gravity constant, F is the fill-fraction of the suspension, γ is dimensionless surface tension parameter, σ is the surface tension at the air-liquid interface, L is the length of the cylinder, $\eta_m = h_m/\alpha R$ is the minimum dimensionless thickness with h_m being the minimum film thickness, $a = \hat{a}/\alpha R$ is the dimensionless particle radius with $\hat{a}$ being the dimensional particle radius, ϕ is the particle concentration, $\beta \equiv F/\alpha$, $\tau \equiv \Omega t$ is the dimensionless time required for the particles to reach the finial stage with t being the dimensional time, and l/R is the dimensionless wavelength with l being the average space between two neighboring bands.

Now, let us compare the calculated and measured spaces between the bands, shown in Table 3.2 for $\alpha = 0.1$ and $\beta = 1.8$. For example, for $\gamma = 0.017$ ($R = 1.27$ cm), the computed wavelength of the most rapidly amplified disturbance is approxi-

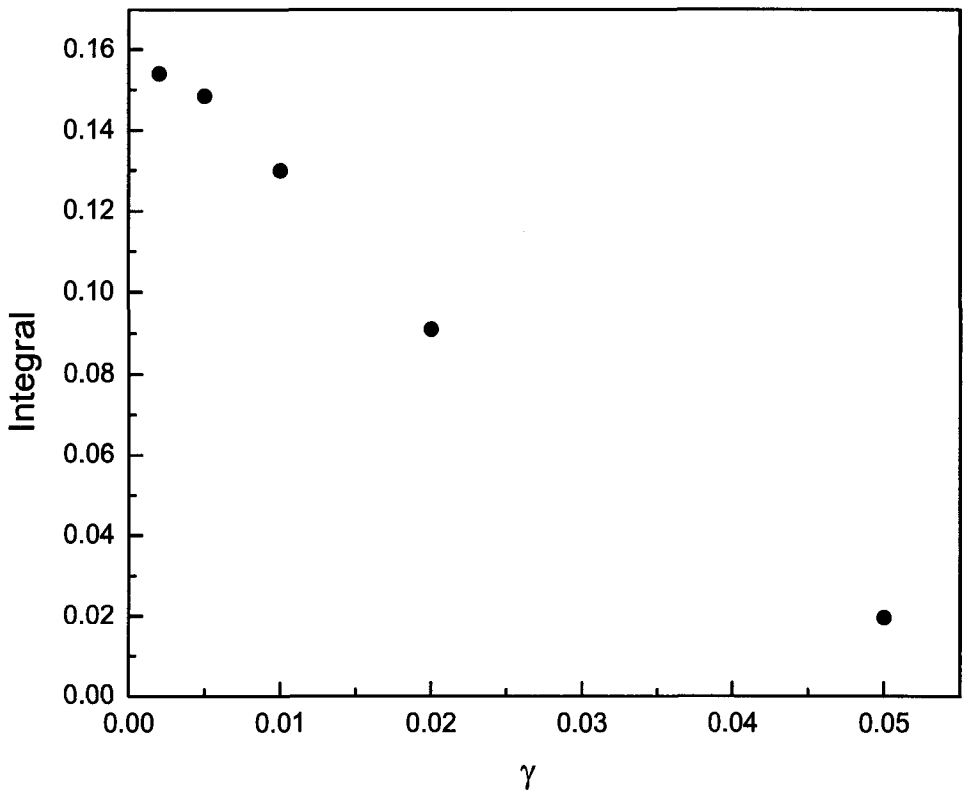

Figure 3.10: The value of integral in the numerator of the right-hand of equations (3.65) for $k = 0$ plotted vs. γ for $\alpha = 0.1$ and $\beta = 1.8$.

mately $3R$ which is close to the value $2.7R$, found experimentally (*cf* Table 3.1 #2). However, the comparison between theory and experiment is less satisfactory when $\gamma = 0.0011$ ($R = 5$ cm) in that the predicted critical wavelength is approximately R, vs. the value $0.72R$ in Table 3.1(#60), and is even worse for $\gamma = 0.069$ ($R = 0.635$ cm) with the analysis predicting neutral stability (and, therefore, no axial particle segregation) for any finite wavelength vs. the observed wavelength $3.6R$ found in the experiments (Table 3.1 #75). The slight difference between the values of the fill fraction F in the experiments and that used in the calculations has a negligible effect on the corresponding difference between the two sets of the wavelengths, given that $\beta = 1.8$ is the same in both.

Clearly, although the increase, with increasing γ, of the theoretically computed wavelengths is consistent with the experimental observations, significant quantita-

Table 3.2: Comparison of the wavelengths for $\alpha = 0.1$, $\beta = 1.8$, and various values of γ

$R(cm)$	γ	l/R	$2\pi/k_c$ (MLA)	$2\pi/k_c$ (BPTA)
1.27	0.017	2.7	3	3
5	0.0011	0.7	1	0.6
0.635	0.069	3.6	*	13

Here, l/R is the dimensionless wavelength from the experimental measurements (*cf* Table 3.1) with l being the average space between two neighboring bands; $2\pi/k_c$ is the dimensionless wavelength predicted by the stability analysis with k_c being the critical wave number. * The MLA predicts neutral stability (and, therefore, no axial particle segregation) for $\gamma = 0.069$.

tive difference obviously exist between the two sets for the larger($R = 5$ cm) and especially for the small ($R = 0.635$ cm) cylinders. One possible reason for this discrepancy is that, as shown in the Appendix A, the modified lubrication analysis (MLA), on which the present analysis is based, underestimates the extent of the "puddle" which, as was pointed out earlier in connection with equations (3.58) and (3.69), plays a crucial role in determining the growth rate and therefore the wavelength of the most rapidly amplified disturbance. In order to test this possibility, we therefore repeated the computations using as a starting point the analysis by Benjamin *et al*[4], referred to as the BPTA, which, as will be shown later in the Appendix A, accurately describes the shape of the "puddle". The governing equations for the steady states, as obtained from the BPTA and from the MLA, are very similar, and so are the linearized equations for the disturbances, although, in the case of the BPTA, they are much more complicated than those presented in the previous section. Hence, the details pertaining to the stability calculations using the BPTA are presented in the Appendix A.

As can be seen in Table 3.2, the predicted wavelengths on the basis of BPTA, is in excellent agreement with those found experimentally not only for the intermediate cylinder ($R = 1.27$ cm) but for the large ($R = 5$ cm) as well. This agreement,

for the case of the large cylinder, may be partly fortuitous, however, given that the computed value of the critical wavenumber $k_c \sim 10.5$, is practically identical to $1/\alpha$ rather than being much smaller as required by the analysis presented in the previous section (i.e. the discussion following equation (3.56)). Also, the experimental observations are subject to some uncertainty due to the influence of end effects given that the aspect of ratio of the large cylinder was only 6 (*cf* Table 3.1). On the other hand, although, for the small cylinder ($R = 0.635$ cm), the BPTA predicted instability (and, therefore, axial particle segregation) at a well defined critical wavelength, rather than neutral stability (and, therefore, no axial particle segregation) as was the case with the MLA, the value of the predicted wavelength is still three times higher than that found experimentally. One possible source of error in the analysis refers to the fact that, as was already mentioned following equation (3.69), the base state profiles for η_0 and η_0^* were computed by neglecting the surface tension terms in equation (3.67), as well as in the corresponding equation of the BPTA. As was shown earlier, this is permissible when γ is $O(10^{-2})$ or smaller, but, when γ becomes as large as 0.07, as is the case with the small cylinder ($R = 0.635$ cm), the simplification referred to above becomes questionable, especially considering the sensitivity as seen in Fig 3.9, of the stability calculations to the value of γ. In addition, however, it should be kept in mind that ours is a small disturbance linear theory whereas the experiments refer of course, to the final spacing of the particle bands which are created via a complicated non-linear evolution of the initial infinitesimally small amplitude disturbance. This point is particularly relevant in the case of the small cylinder ($R = 0.635$ cm) given that two or three additional bands can form in the space between two initial neighboring bands (*cf* Fig 3.11) during the experiments thereby accounting for a certain degree of quantitative disagreement between theory and experiment. Such a difference between the initial and final number of bands was not found in the experiments using the other two cylinders. Thus, considering

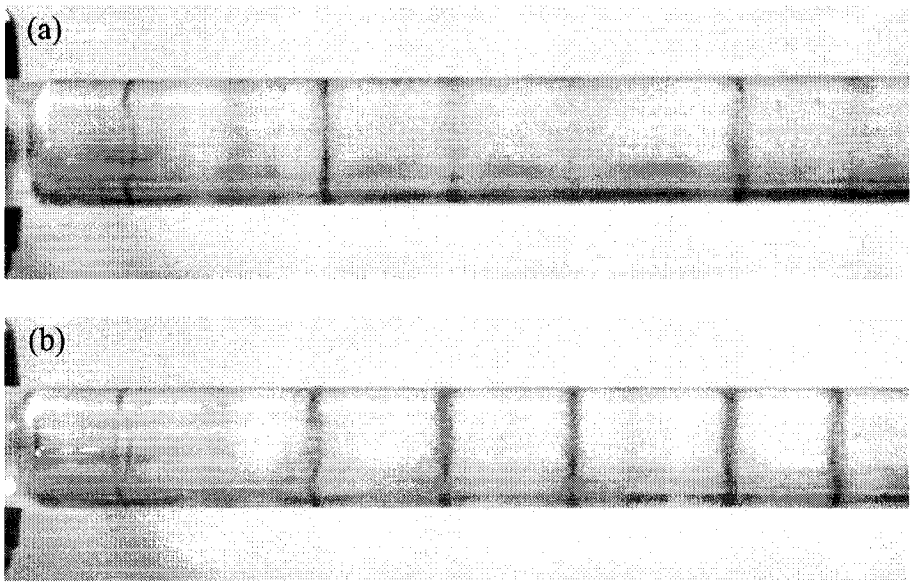

Figure 3.11: A set of photographs showing the bands which form along the small cylinder with $R = 0.635$ cm at different times (t) after the start of the experiments (a) $t \sim 4$ hours; (b) $t \sim 5$ hours.

the numerous simplifications of the analysis and the lack of precision in the experimental observations on the spacing of the particle bands, the agreement between theory and experiment, is as good as one might have expected. Clear, though, this point requires further attention.

3.6 Discussion

As was already shown in ref[4] and chapter 1, on the basis of, respectively, the "standard" and "modified" lubrication analysis, rimming flows of pure fluids, within a rotating horizontal cylinder are stable to axial disturbances when inertia effects are negligible provided that the film contains a region of recirculating flow, the so-called "puddle". This stability is retained if the pure fluid is replaced by a suspension containing neutrally buoyant particles provided the particle concentration within any cross-section is uniform and the suspension is viewed as an effective Newtonian fluid. But if the particles segregate radially such that their concentration is

reduced within the "puddle", a linear stability analysis, that models the suspension as an effective continuum fluid with a concentration dependent viscosity, shows that such a particle arrangement is unstable to axial disturbances in the particle concentration, with the surface tension effects, which are often thought to be of minor importance in rimming flows, being responsible for selecting the wavelength of the most rapidly amplified disturbance. The predictions of this stability analysis at least are qualitatively, and often even quantitatively, consistent with all the experimental observations. For example, in agreement with the experimental results summarized in the Table 3.1, the analysis predicts that, for the dilute suspensions with fixed F and α, the wavelength of the particle bands which are formed should be independent of the particle concentration ϕ but should decrease with an increase in the cylinder radius R. Also, the particle size does not enter into the picture given that the stability analysis treats the suspension as a continuum. Again this is consistent with the experimental observations, according to which the banding pattern that is established is insensitive to the ratio of the particle diameter to the film thickness. In fact, it appears that the particle size is of importance only during the first phase of the segregation process, in which the particles segregate radially, in that large particles leave the puddle more readily than small ones. Thus, small particles form bands just as the big ones do, but more slowly.

We wish to stress, however, that although our analysis appears to have left little doubt regarding the mechanism responsible for the band formation along the axis of the cylinder, it has not addressed the issue of why, to begin with, the particles leave the puddle and thereby trigger the radial segregation which subsequently induces the segregation along the cylinder axis. An explanation for this phenomenon is in need of further study.

Appendix A

Stability analysis based on the BPTA

A.1 Introduction

The purpose of this part of the thesis is to investigate the stability of a dilute suspension with complete radial segregation by means of the extended lubrication analysis developed by Benjamin, Pritchard and Tavener[4], henceforth to be referred as the BPTA, which contains all the $O(\alpha)$ correction terms to the standard lubrication equation, as well as the capillary pressure in the thin film approximation.

Before embarking on this analysis, however, we shall compare the BPTA with the "modified lubrication analysis" (MLA) introduced in chapter 1. In the two-dimensional case, according to ref[4], the BPTA leads to an expression for the angular velocity,

$$v = 1 - \alpha z - \left(\eta z - \frac{1}{2}z^2\right)\{\cos\theta - \alpha\eta' \sin\theta - \alpha\gamma(\eta' + \eta''')\} + \alpha\left(\frac{1}{3}z^3 - \eta z^2 + \frac{3}{2}\eta^2 z\right)\cos\theta \tag{A.1}$$

Note that the notation here is the same as that used in the MLA case. The dimensionless flow rate within the film per unit axial distance is hence given by

$$q = \int_0^\eta v\mathrm{d}z = \eta - \frac{1}{3}\eta^3\cos\theta + \alpha\left\{\frac{1}{2}\eta^4\cos\theta - \frac{1}{2}\eta^2 + \frac{1}{3}\eta^3\eta'\sin\theta + \frac{\gamma}{3}\eta^3(\eta' + \eta''')\right\} \tag{A.2}$$

where η is required to be periodic in 2π and to satisfy the exact liquid volume conservation condition

$$\beta \equiv \frac{F}{\alpha} = \frac{1}{\pi}\int_{-\pi}^{\pi}\left(1-\frac{\alpha}{2}\eta\right)\eta \mathrm{d}\theta \tag{A.3}$$

As was the case with the "modified lubrication equation"(MLE), equation (A.2), to be referred to as the BPTE, has also continuous periodic solutions $\eta(\theta)$ for given F (below some critical value, as shown below) over the whole range of β, even when $\gamma = 0$, i.e. in the absence of the capillary pressure term.

When $\gamma = 0$, entirely analogous results to those presented in chapter 1, are obtained starting from equation (A.2) in lieu of the MLE. Specifically, the appropriate expressions corresponding to eqs.(1.27-1.29) (*cf* chapter 1) are now:

$$q = a_0 - \frac{1}{3}a_0^3 + \frac{\alpha}{2}a_0^2(a_0^2-1), \tag{A.4}$$

$$\frac{\mathrm{d}q}{\mathrm{d}a_0} = 0 = 1 - a_0^2 + \alpha a_0(2a_0^2-1), \tag{A.5}$$

$$1 - a_0^2 + \alpha a_0\left(\frac{7}{3}a_0^2 - 1\right) = 0 \tag{A.6}$$

respectively, according to which equation (A.2) is found to have a continuous, periodic solution for all α only if $F \leq 0.29$, which is less than $F \leq 0.36$ found on the basis of the MLE (the detailed procedure for obtaining 0.29 is the exactly same as that for the MLE shown in chapter 1). As shown in Fig A.1, for $F = 0.29$ and for two representative values of $\beta \equiv F/\alpha$, there is good agreement between the film profiles, as obtained from (A.2) and (A.3) with $\gamma = 0$ and those computed by solving numerically the full two-dimensional Stokes equations using the FIDAP software (Fluent, Inc.). [Note that, as was already revealed, in order to dampen the numerical instabilities in the computation with the FIDAP software, the capillary coefficient γ had to be set to a finite but small value, equal to 10^{-2} in this case.] In addition, the corresponding value of β^* is also a function of α, shown in Fig A.2, and when $\beta = \beta^*$, both symmetric and asymmetric solutions of equation (A.2) subject

to (A.3) coexist, which are shown in Fig A.3 for $F = 0.2$. [The corresponding figures as obtained from the MLA are Figs 1.5-1.6 in chapter 1.]

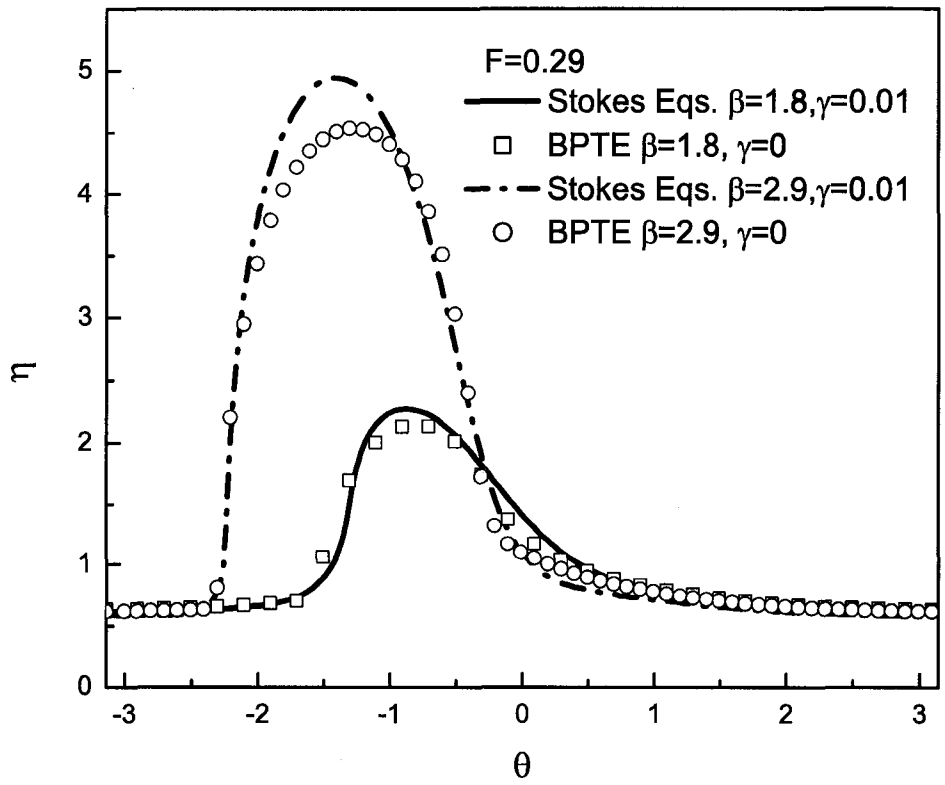

Figure A.1: The solutions obtained from the two-dimensional Stokes equations and the BPTE equation (A.2) with $\gamma = 0$ agree with each other for $\beta = 2.0$ and $\beta = 3.0$ when the fill fraction F is 0.29.

On the basis of the BPTA, we can also derive the expression for the streamline ψ at $z = \eta^*$, where η^* refers to the lower boundary of the recirculating flow region,

$$\psi = \int_0^{\eta^*} v\mathrm{d}z = \eta^* - \frac{\alpha}{2}(\eta^*)^2 + \alpha\left\{\frac{1}{12}(\eta^*)^4 - \frac{1}{3}\eta(\eta^*)^3 + \frac{3}{4}\eta^2(\eta^*)^2\right\}\cos\theta + \left\{\frac{1}{2}\eta(\eta^*)^2 - \frac{1}{6}(\eta^*)^3\right\}\frac{3\left(q - \eta + \frac{\alpha}{2}\eta^2 - \frac{\alpha}{2}\eta^4\cos\theta\right)}{\eta^3} = q \qquad \text{(A.7)}$$

which can be solved for η^* given that η and q are already known.

As shown in Fig A.4, for $F = 0.2$ and $\beta = 2.0$, the recirculating flow region predicted by the BPTE with $\gamma = 0$ is somewhat smaller than that given by solving the full Stokes equations (with γ set equal to $O(10^{-2})$) using the FIDAP software

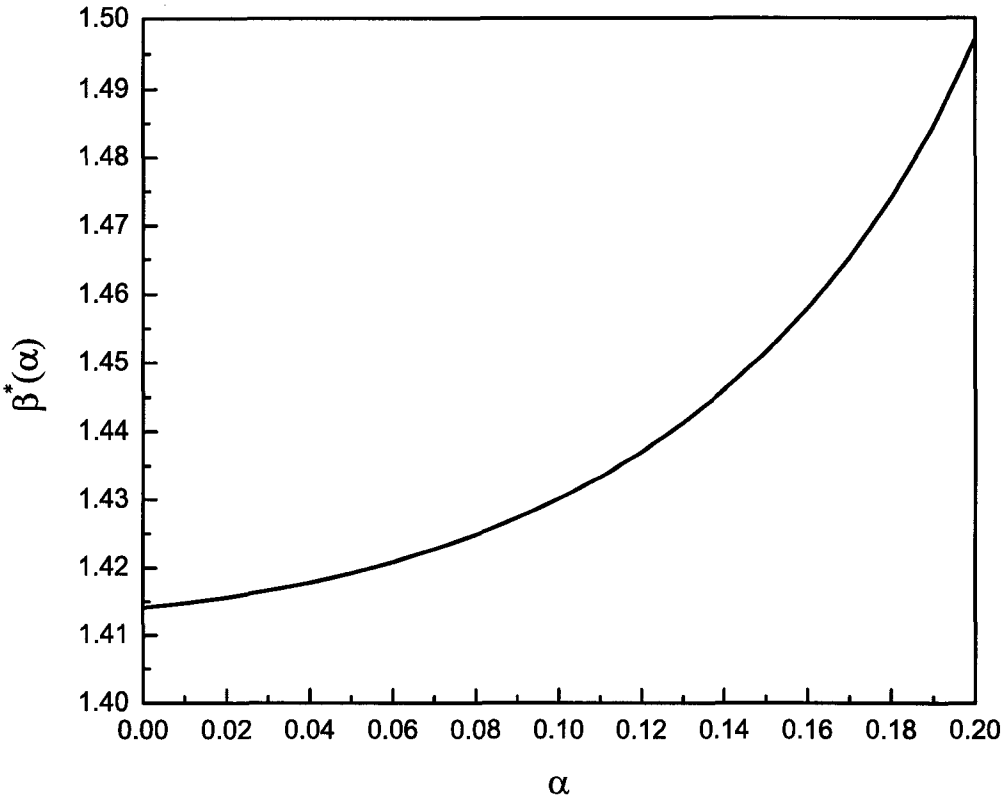

Figure A.2: The parameter $\beta^*(\alpha)$ given by the BPTE equation (A.2) with $\gamma = 0$ is increasing monotonically with α.

(Fluent, Inc.). We also show, in Fig A.4, a comparison, again for $\gamma = 0$, between the values of η and η^* given by the BPTE and those computed from the solution of MLE, and find that, even though the film profiles η are quite close to each other, this is not the case with the η^* profiles. In fact, the size of the recirculating flow region, as predicted from the solution of BPTE is much larger than that given by the MLE, and close to that given by solving the full Stokes equations.

In order to ascertain whether this difference is due to the difference in the values of the capillary parameter γ, we also solved the full BPTE, equation (A.2) subject to (A.3), for $\gamma = 10^{-2}$, and then, using equation (A.7), obtained the profiles for η and η^* respectively, shown in Fig A.5. A comparison with the corresponding profiles found earlier with $\gamma = 0$, shows that, exactly as was the case with the MLE, the

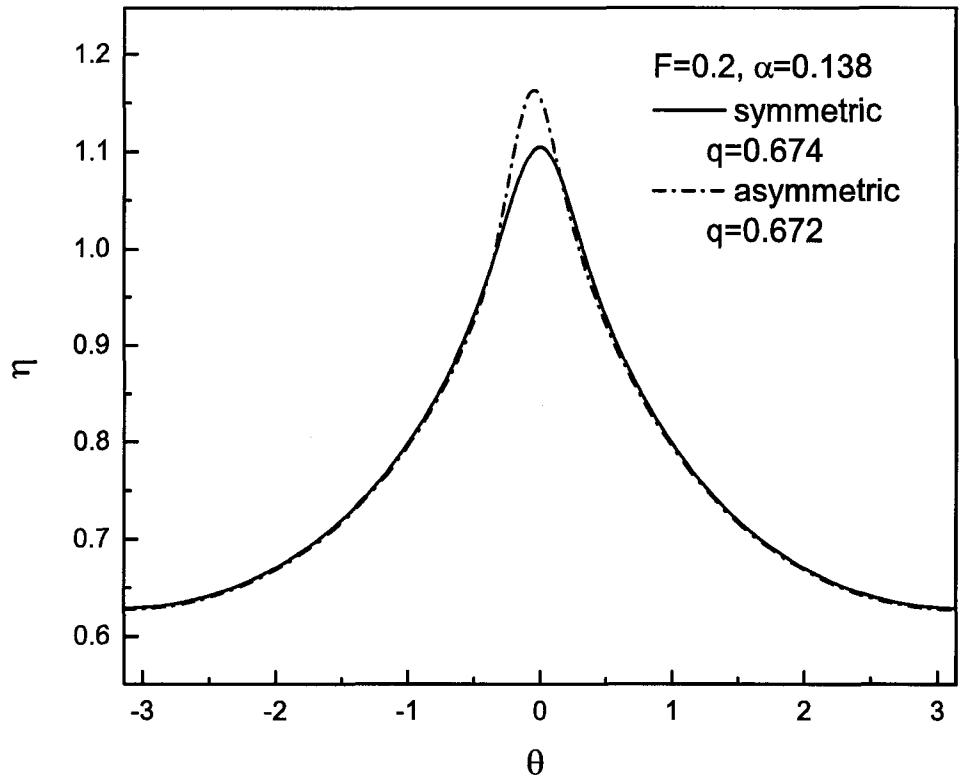

Figure A.3: The asymmetric and symmetric solutions of the BPTE equation (A.2) with $\gamma = 0$ for $F = 0.20$ and $\alpha = 1.38$.

difference is negligible, that is, the small surface tension terms in equation (A.2) have little effect on the surface profile as well as the boundary of the recirculating flow region when $\gamma \ll 1$.

By repeating the analysis in the MLA case (*cf* chapter 3), it is a straightforward matter to extend the BPTA to rimming flows with an axially varying viscosity. In Fig A.6-A.7, we show that the corresponding three-dimensional free surface shape obtained on the basis of the BPTA also agree with those determined by solving numerically the three-dimensional Stokes equations. Moreover, on the basis of the BPTA for the steady rimming flows of a pure liquid with an axially varying viscosity, we also find, in conformity with the results given by the MLA, that, within the range of a monotonically increasing liquid viscosity $\bar{\mu}$, the axial flow rate in the circumferential flow region, J^c, is positive at steady state (i.e. towards the high

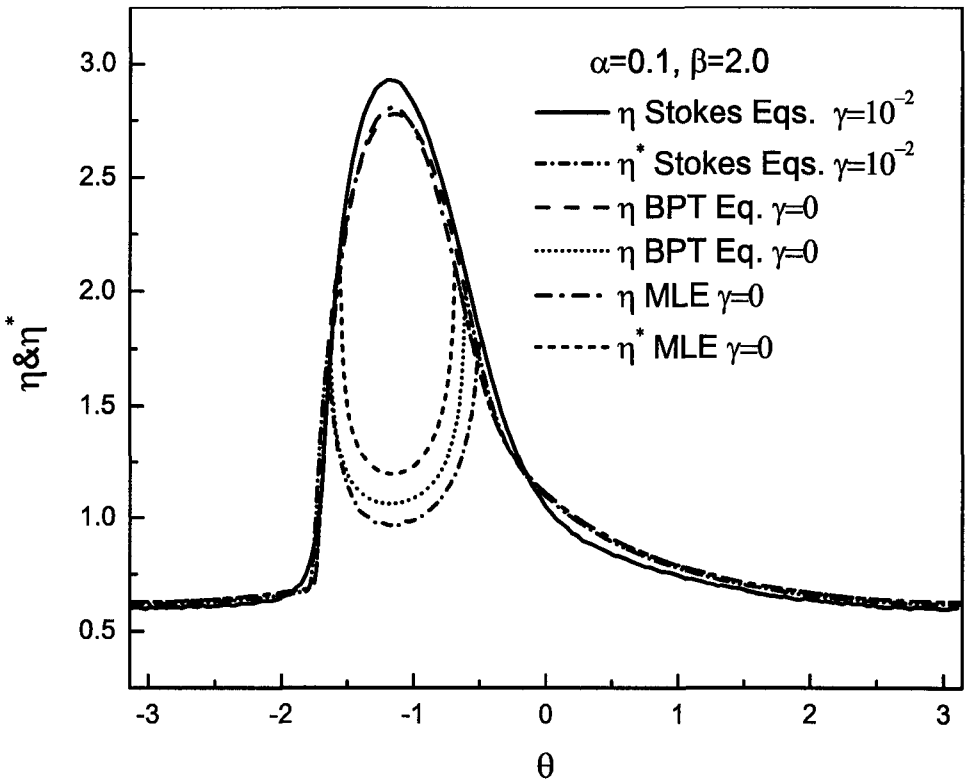

Figure A.4: The film profile η and that of the lower boundary of the recirculating flow region η^* for $\alpha = 0.1$ and $\beta = 2$. Comparison between η as well as η^* as obtained by solving the full two-dimensional Stokes equations with $\gamma = 10^{-2}$ and those given by the BPTE as well as MLE with $\gamma = 0$.

viscosity) and therefore, that the axial flow rate in the recirculating flow region, J^r, is equal but opposite in sign. Therefore, it is easy to derive the same expression for the axial particle flow rate J_p (i.e. equation (3.30)), and thereby provide the same explanation for the band formation in the rotating cylinder as given in chapter 3. Now, as we already see, the region of the recirculating flow has important implications for the band formation in suspensions. Since we have already shown that the prediction of η^* by the BPTA is better than that by the MLA, it is necessary for us to repeat the linear stability analysis on the basis of the BPTA. In what follows, we first derive the BPTE for complete radial segregation, and then linearize the relative equations to carry out the stability analysis.

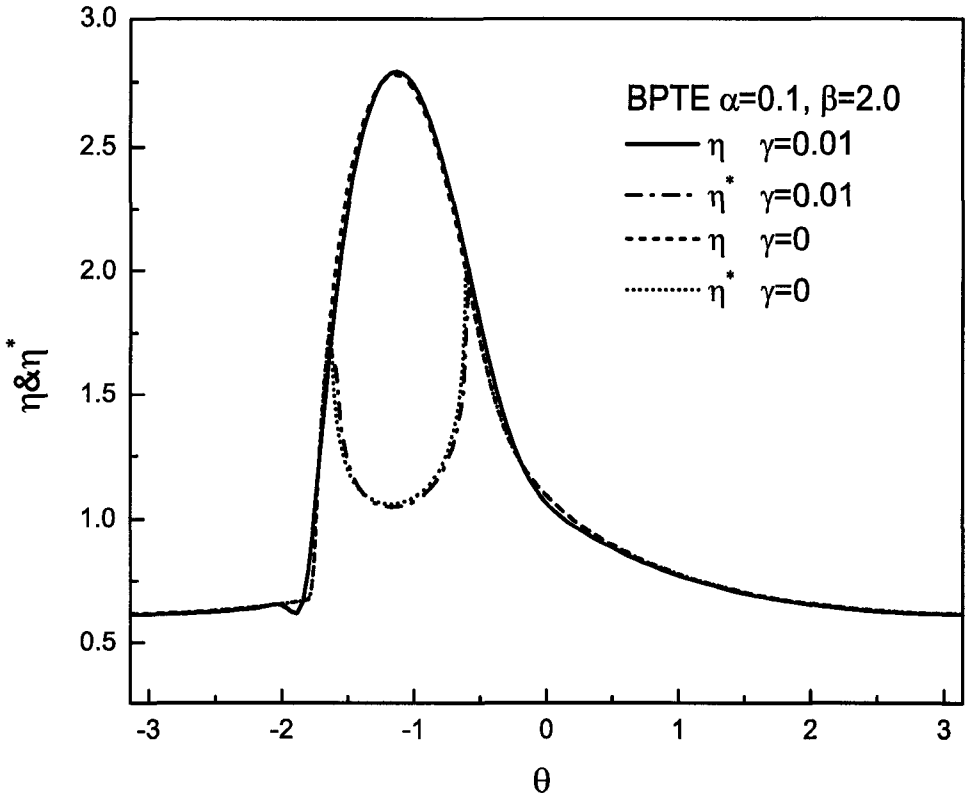

Figure A.5: The film profile η and that of the lower boundary of the recirculating flow region η^* for $\alpha = 0.1$ and $\beta = 2$. Comparison between η as well as η^* for $\gamma = 10^{-2}$ and $\gamma = 0$ given by the BPTE.

A.2 BPTA for complete radial segregation

Choosing the same notation as that for the MLA case (*cf* chapter 3), we start from the basic angular momentum equations in the circumferential and recirculating flow regions without the surface tension terms, i.e.

$$\frac{\partial^2 v}{\partial z^2} - \alpha \frac{\partial v}{\partial z} = \frac{1}{\bar{\mu}} \{1 + \alpha(z - \eta)\} \cos\theta - \frac{\alpha}{\bar{\mu}} \frac{\partial \eta}{\partial \theta} \sin\theta \tag{A.8}$$

and

$$\frac{\partial^2 v^*}{\partial z^2} - \alpha \frac{\partial v^*}{\partial z} = \{1 + \alpha(z - \eta)\} \cos\theta - \alpha \frac{\partial \eta}{\partial \theta} \sin\theta \tag{A.9}$$

respectively. The boundary conditions are as follows:

$$v = 1 \quad \text{at} \quad z = 0$$

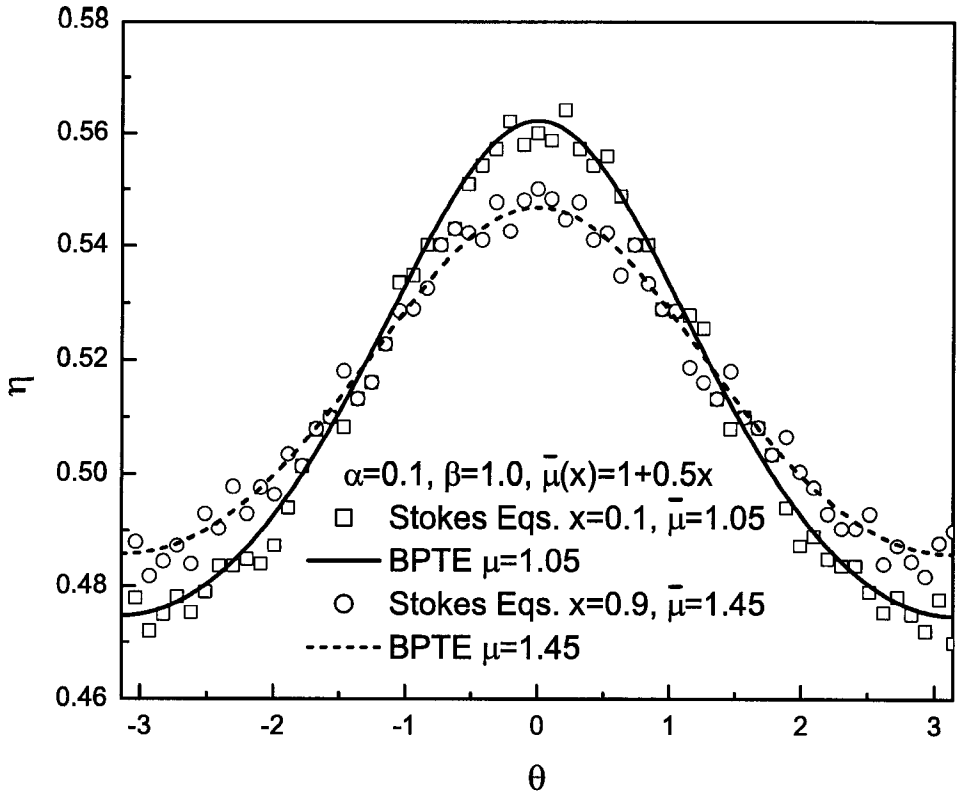

Figure A.6: The film profiles at different locations ($x = 0.1$ and $x = 0.9$) along the cylinder. Comparison between the numerical solutions of the three-dimensional Stokes equations with $\gamma = 10^{-2}$ and those of the BPT lubrication model with $\gamma = 0$ for the case of an axially varying viscosity of the form $\bar{\mu}(x) = 1 + 0.5x$, $0 \leq x \leq 1$: symmetric profiles for an axial uniform fill fraction $F = 0.1$ and $\alpha = 0.1$.

$$\frac{\partial v^*}{\partial z} + \alpha v^* = 0 \quad \text{at} \quad z = \eta$$

$$v = v^* \quad \text{at} \quad z = \eta^*$$

$$\bar{\mu}\frac{\partial v}{\partial z} = \frac{\partial v^*}{\partial z} \quad \text{at} \quad z = \eta^*$$

Let $v = v^0 + \alpha v^1$ and $v^* = v^{0^*} + \alpha v^{1^*}$, then equations for v^0 and v^{0^*} become

$$\frac{\partial^2 v^0}{\partial z^2} = \frac{1}{\bar{\mu}}\cos\theta \tag{A.10}$$

and

$$\frac{\partial^2 v^{0^*}}{\partial z^2} = \cos\theta \tag{A.11}$$

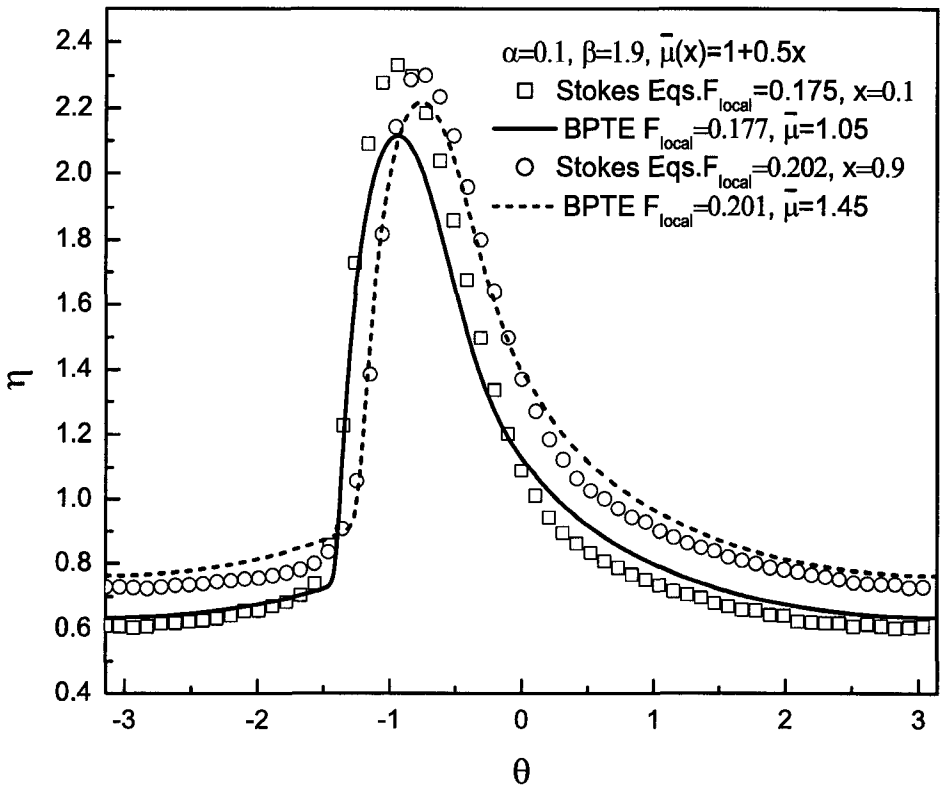

Figure A.7: The film profiles at different locations ($x = 0.1$ and $x = 0.9$) along the cylinder. Comparison between the numerical solutions of the three-dimensional Stokes equations with $\gamma = 10^{-2}$ and those of the BPT lubrication model with $\gamma = 0$ for the case of an axially varying viscosity of the form $\bar{\mu}(x) = 1 + 0.5x$, $0 \leq x \leq 1$: asymmetric profiles for an average fill fraction $F = 0.19$ and $\alpha = 0.1$.

respectively. The corresponding boundary conditions are

$$\begin{aligned} v^0 &= 1 \quad \text{at} \quad z = 0 \\ \frac{\partial v^{0^*}}{\partial z} &= 0 \quad \text{at} \quad z = \eta \\ v^0 &= v^{0^*} \quad \text{at} \quad z = \eta^* \\ \bar{\mu}\frac{\partial v^0}{\partial z} &= \frac{\partial v^{0^*}}{\partial z} \quad \text{at} \quad z = \eta^* \end{aligned}$$

The solutions to equations (A.10) and (A.11) with the above boundary conditions are

$$v^0 = 1 - \frac{1}{\bar{\mu}}\left\{z\eta - \frac{1}{2}z^2\right\}\cos\theta \tag{A.12}$$

and

$$v^{0^*} = 1 - \left\{z\eta - \frac{1}{2}z^2\right\}\cos\theta + \left(\frac{1}{\bar{\mu}} - 1\right)\left\{\frac{1}{2}\eta^{*^2} - \eta^*\eta\right\}\cos\theta \tag{A.13}$$

On the other hand, the equations for v^1 and v^{1^*} are

$$\frac{\partial^2 v^1}{\partial z^2} = \frac{2}{\bar{\mu}}(z-\eta)\cos\theta - \frac{1}{\bar{\mu}}\frac{\partial \eta}{\partial \theta}\sin\theta \tag{A.14}$$

and

$$\frac{\partial^2 v^{1^*}}{\partial z^2} = 2(z-\eta)\cos\theta - \frac{\partial \eta}{\partial \theta}\sin\theta \tag{A.15}$$

and the corresponding boundary conditions are

$$\begin{aligned} v^1 &= 0 \quad \text{at} \quad z = 0 \\ \frac{\partial v^{1^*}}{\partial z} &= -v^{0^*} \quad \text{at} \quad z = \eta \\ v^1 &= v^{1^*} \quad \text{at} \quad z = \eta^* \\ \bar{\mu}\frac{\partial v^1}{\partial z} &= \frac{\partial v^{1^*}}{\partial z} \quad \text{at} \quad z = \eta^* \end{aligned}$$

The solutions to equations (A.14) and (A.15) with the above boundary conditions are

$$v^1 = \frac{1}{\bar{\mu}}\left\{\left(\frac{1}{3}z^3 - \eta z^2\right)\cos\theta - \frac{1}{2}\frac{\partial \eta}{\partial \theta}z^2\sin\theta + Cz\right\} \tag{A.16}$$

and

$$v^{1^*} = \left(\frac{1}{3}z^3 - \eta z^2\right)\cos\theta - \frac{1}{2}\frac{\partial \eta}{\partial \theta}z^2\sin\theta + Cz + D \tag{A.17}$$

where

$$C = -1 + \frac{3}{2}\eta^2\cos\theta + \frac{\partial \eta}{\partial \theta}\eta\sin\theta - \left(\frac{1}{\bar{\mu}} - 1\right)\left\{\frac{1}{2}\eta^{*^2} - \eta\eta^*\right\}\cos\theta$$

and

$$D = \left(\frac{1}{\bar{\mu}} - 1\right)\left\{C\eta^* + \left(\frac{1}{3}\eta^{*^3} - \eta\eta^{*^2}\right)\cos\theta - \frac{1}{2}\frac{\partial \eta}{\partial \theta}\eta^{*^2}\sin\theta\right\}$$

Now we compute the flow rate q. Letting $q = q^0 + \alpha q^1$, we find that

$$q^0 = \int_0^{\eta^*} v^0 \mathrm{d}z = \eta^* - \frac{1}{\bar{\mu}}\left(\frac{1}{2}\eta\eta^{*^2} - \frac{1}{6}\eta^{*^3}\right)\cos\theta \tag{A.18}$$

and

$$\int_{\eta^*}^{\eta} v^{0^*} \mathrm{d}z = 0 = (\eta - \eta^*) + \left(1 - \frac{1}{\bar{\mu}}\right)\left(\eta\eta^* - \frac{1}{2}\eta^{*^2}\right)(\eta - \eta^*)\cos\theta + \left\{\frac{1}{2}\eta\eta^{*^2} - \frac{1}{6}\eta^{*^3} - \frac{1}{3}\eta^3\right\}\cos\theta \qquad \text{(A.19)}$$

Combining the above equations, we reach,

$$q^0 = \eta - \frac{1}{3\bar{\mu}}\left\{\eta^3 + (\bar{\mu} - 1)(\eta - \eta^*)^3\right\}\cos\theta \qquad \text{(A.20)}$$

Furthermore,

$$q^1 = \int_0^{\eta^*} v^1 \mathrm{d}z = \frac{1}{\bar{\mu}}\left\{\left(\frac{1}{12}\eta^{*^4} - \frac{1}{3}\eta^{*^3}\eta\right)\cos\theta - \frac{1}{6}\eta^{*^3}\frac{\partial\eta}{\partial\theta}\sin\theta + \frac{1}{2}C\eta^{*^2}\right\} \qquad \text{(A.21)}$$

and

$$0 = \int_{\eta^*}^{\eta} v^{1^*} \mathrm{d}z = -\left\{\left(\frac{1}{12}\eta^{*^4} - \frac{1}{3}\eta^{*^3}\eta\right)\cos\theta - \frac{1}{6}\eta^{*^3}\frac{\partial\eta}{\partial\theta}\sin\theta + \frac{1}{2}C\eta^{*^2}\right\} + D(\eta - \eta^*) + \left\{-\frac{1}{4}\eta^4\cos\theta - \frac{1}{6}\eta^3\frac{\partial\eta}{\partial\theta}\sin\theta + \frac{1}{2}C\eta^2\right\} \qquad \text{(A.22)}$$

Again, combining the above equations, we obtain,

$$q^1 = \frac{1}{2}\eta^4\cos\theta - \frac{1}{2}\eta^2 + \frac{1}{3}\eta^3\frac{\partial\eta}{\partial\theta}\sin\theta + D(\eta - \eta^*) - \left(\frac{1}{\bar{\mu}} - 1\right)\left\{\frac{1}{2}\eta^{*^2} - \eta\eta^*\right\}\frac{\eta^2}{2}\cos\theta + \left(\frac{1}{\bar{\mu}} - 1\right)\left\{\left(\frac{1}{12}\eta^{*^4} - \frac{1}{3}\eta^{*^3}\eta\right)\cos\theta - \frac{1}{6}\eta^{*^3}\frac{\partial\eta}{\partial\theta}\sin\theta + \frac{1}{2}C\eta^{*^2}\right\} \qquad \text{(A.23)}$$

Therefore, we obtain

$$q = q^0 + \alpha q^1 = \eta - \frac{1}{3\bar{\mu}}\eta^3\cos\theta + \alpha\left\{\frac{1}{2}\eta^4\cos\theta - \frac{1}{2}\eta^2 + \frac{1}{3}\eta^3\frac{\partial\eta}{\partial\theta}\sin\theta\right\} + \frac{1}{3}\left(\frac{1}{\bar{\mu}} - 1\right)(\eta - \eta^*)^3\cos\theta + \alpha D(\eta - \eta^*) - \alpha\left(\frac{1}{\bar{\mu}} - 1\right)\left\{\frac{1}{2}\eta^{*^2} - \eta\eta^*\right\}\frac{\eta^2}{2}\cos\theta + \alpha\left(\frac{1}{\bar{\mu}} - 1\right)\left\{\left(\frac{1}{12}\eta^{*^4} - \frac{1}{3}\eta^{*^3}\eta\right)\cos\theta - \frac{1}{6}\eta^{*^3}\frac{\partial\eta}{\partial\theta}\sin\theta + \frac{1}{2}C\eta^{*^2}\right\} \qquad \text{(A.24)}$$

Note that, it is easy to show that the modification of the axial velocity component, w, due to the complete segregation is exactly same as the MLA case, i.e. equations (3.40) and (3.41).

A.3 Stability analysis

We first linearize equation (A.24) by letting $\bar{\mu} = \bar{\mu}_0 + \frac{5}{2}\zeta$, $\eta = \eta_0(\theta) + \xi$, $\eta^* = \eta_0^* + \xi^*$ and $q = q_0 + \delta$ where the subscript 0 refers to the initial axially uniform state. Then, in the dilute limit, i.e. $\bar{\mu}_0 \sim 1$, we obtain,

$$\delta = f_0\xi + \frac{\alpha}{3}\eta_0^3\frac{\partial\xi}{\partial\theta}\sin\theta + \frac{5}{2}B\zeta \tag{A.25}$$

where

$$\begin{aligned} B = {} & \frac{\eta_0^3}{3}\cos\theta - \frac{1}{3}(\eta_0 - \eta_0^*)^3\cos\theta + \alpha\left(\frac{1}{2}\eta_0^{*2} - \eta_0\eta_0^*\right)\frac{\eta_0^2}{2}\cos\theta \\ & -\alpha\left\{\left(\frac{1}{12}\eta_0^{*4} - \frac{1}{3}\eta_0^{*3}\eta_0\right)\cos\theta - \frac{1}{6}\eta_0^{*3}\frac{\mathrm{d}\eta_0}{\mathrm{d}\theta}\sin\theta + \frac{1}{2}C_0\eta_0^{*2}\right\} \\ & -\alpha\left\{C_0\eta_0^* + \left(\frac{1}{3}\eta_0^{*3} - \eta_0\eta_0^{*2}\right)\cos\theta - \frac{1}{2}\frac{\mathrm{d}\eta_0}{\mathrm{d}\theta}\eta_0^{*2}\sin\theta\right\}(\eta_0 - \eta_0^*) \\ q_0 = {} & \eta_0 - \frac{1}{3}\eta_0^3\cos\theta + \alpha\left\{-\frac{1}{2}\eta_0^2 + \frac{1}{2}\eta_0^4\cos\theta + \frac{1}{3}\eta_0^3\frac{\mathrm{d}\eta_0}{\mathrm{d}\theta}\sin\theta\right\} \\ f_0 = {} & \frac{3q_0}{\eta_0} - 2 + \frac{1}{2}\alpha\eta_0^3\cos\theta + \frac{1}{2}\alpha\eta_0 \end{aligned} \tag{A.26}$$

and

$$C_0 = -1 + \frac{3}{2}\eta_0^2\cos\theta + \frac{\mathrm{d}\eta_0}{\mathrm{d}\theta}\eta_0\sin\theta$$

It is easy to see that the general expressions of mass conservation equations of particles and suspension, i.e. equations (3.43) and (3.44), are the same irrespective of whether the MLA or the BPTA are used. Therefore, equations for the growth constant and function are as follows:

$$\lambda = \alpha k^2\phi_0\frac{\int_{-\pi}^{\pi}\left\{\frac{1}{2}\eta_0(\eta_0^*)^2 - \frac{1}{6}(\eta_0^*)^3\right\}G\sin\theta\mathrm{d}\theta}{\int_{-\pi}^{\pi}\left(1 - \frac{\alpha}{2}\eta_0^*\right)\eta_0^*\mathrm{d}\theta} \tag{A.27}$$

and

$$\frac{\mathrm{d}(f_0G)}{\mathrm{d}\theta} + \frac{\alpha}{3}\frac{\mathrm{d}}{\mathrm{d}\theta}\left[\eta_0^3\sin\theta\frac{\mathrm{d}G}{\mathrm{d}\theta}\right] - \frac{\alpha}{3}k^2\eta_0^3\sin\theta G = -\frac{5}{2}\frac{\mathrm{d}B}{\mathrm{d}\theta} \tag{A.28}$$

provided that $\phi_0 \sim 0.01$. After solving equation (A.28) for the function G, we substitute G into equation (A.28) to obtain the growth constant λ. As shown in

Fig A.8, λ is monotonically increasing with the increase of wave number k, which is similar as that given by the MLA in Fig 3.7. Note that, for this typical case ($\alpha = 0.1$, $\beta = 1.8$), the region occupied by the recirculating flow predicted by the BPTA is about 6% of the total volume of the suspension, which is twice as much as that given by the MLA.

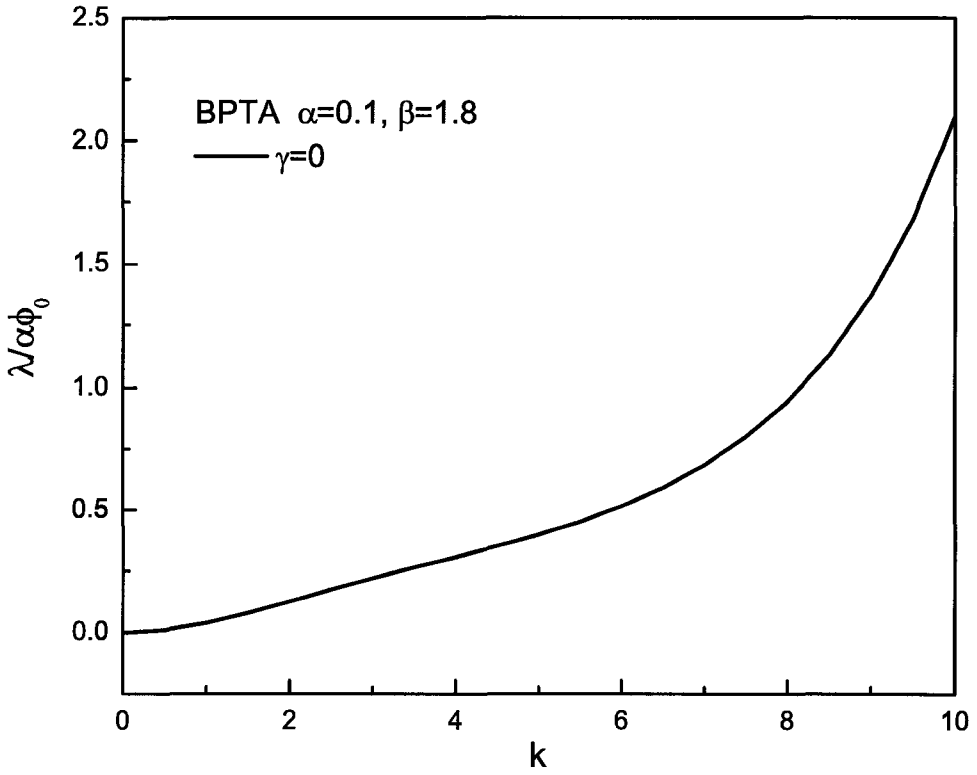

Figure A.8: A plot of the growth constant λ given by the BPT model for $\alpha = 0.1$ and $\beta = 1.8$ vs. the wave number k when $\gamma = 0$.

When we consider the surface tension effects, the corresponding expressions for q_0 and δ become

$$q_0 = \eta_0 - \frac{1}{3}\eta_0^3 \cos\theta + \alpha\left\{-\frac{1}{2}\eta_0^2 + \frac{1}{2}\eta_0^4\cos\theta + \frac{1}{3}\eta_0^3\frac{\mathrm{d}\eta_0}{\mathrm{d}\theta}\sin\theta + \frac{1}{3}\gamma\eta_0^3\left(\frac{\mathrm{d}\eta}{\mathrm{d}\theta} + \frac{\mathrm{d}^3\eta}{\mathrm{d}\theta^3}\right)\right\} \tag{A.29}$$

and

$$\delta = f_0\xi + \frac{\alpha}{3}\eta_0^3\frac{\partial\xi}{\partial\theta}\sin\theta + \frac{\alpha}{3}\gamma\eta_0^3\left(\frac{\partial\xi}{\partial\theta} + \frac{\partial^3\xi}{\partial\theta\partial x^2} + \frac{\partial^3\xi}{\partial\theta^3}\right) + \frac{5}{2}B\zeta \tag{A.30}$$

where

$$B = \frac{\eta_0^3}{3}\cos\theta - \frac{1}{3}(\eta_0 - \eta_0^*)^3\cos\theta + \alpha\left(\frac{1}{2}\eta_0^{*2} - \eta_0\eta_0^*\right)\frac{\eta_0^2}{2}\cos\theta$$
$$-\alpha\left\{\left(\frac{1}{12}\eta_0^{*4} - \frac{1}{3}\eta_0^{*3}\eta_0\right)\cos\theta - \frac{1}{6}\eta_0^{*3}\frac{\mathrm{d}\eta_0}{\mathrm{d}\theta}\sin\theta - \frac{\gamma}{6}\eta_0^{*3}\left(\frac{\mathrm{d}\eta_0}{\mathrm{d}\theta} + \frac{\mathrm{d}^3\eta_0}{\mathrm{d}\theta^3}\right) + \frac{1}{2}C_0\eta_0^{*2}\right\}$$
$$-\alpha\left\{C_0\eta_0^* + \left(\frac{1}{3}\eta_0^{*3} - \eta_0\eta_0^{*2}\right)\cos\theta - \frac{1}{2}\frac{\mathrm{d}\eta_0}{\mathrm{d}\theta}\eta_0^{*2}\sin\theta - \frac{\gamma}{2}\left(\frac{\mathrm{d}\eta_0}{\mathrm{d}\theta} + \frac{\mathrm{d}^3\eta_0}{\mathrm{d}\theta^3}\right)\eta_0^{*2}\right\}(\eta_0 - \eta_0^*)$$

$$f_0 = \frac{3q_0}{\eta_0} - 2 + \frac{1}{2}\alpha\eta_0^3\cos\theta + \frac{1}{2}\alpha\eta_0$$

and

$$C_0 = -1 + \frac{3}{2}\eta_0^2\cos\theta + \frac{\mathrm{d}\eta_0}{\mathrm{d}\theta}\eta_0\sin\theta + \gamma\left(\frac{\mathrm{d}\eta_0}{\mathrm{d}\theta} + \frac{\mathrm{d}^3\eta_0}{\mathrm{d}\theta^3}\right)\eta_0$$

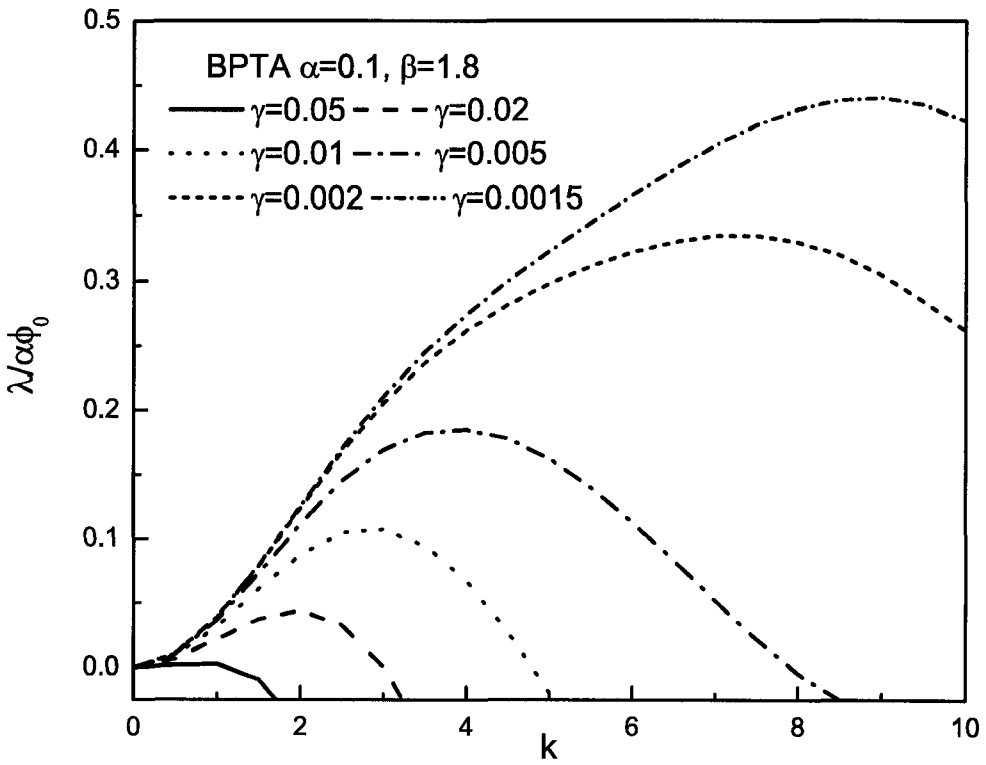

Figure A.9: The growth constant λ has a maximum when $\gamma > 0$, with the value of the wave number of the most rapidly amplified disturbance increasing with a decrease in the value of dimensionless surface tension parameter γ.

Following the same procedure for the MLA, we obtain equations for the growth

constant and the function as follows:

$$\lambda = \alpha k^2 \phi_0 \frac{\int_{-\pi}^{\pi} \left\{ \frac{1}{2}\eta_0(\eta_0^*)^2 - \frac{1}{6}(\eta_0^*)^3 \right\} \left\{ G\sin\theta + \gamma \left(G - k^2 G + \frac{\mathrm{d}^2 G}{\mathrm{d}\theta^2} \right) \right\} \mathrm{d}\theta}{\int_{-\pi}^{\pi} \left(1 - \frac{\alpha}{2}\eta_0^* \right) \eta_0^* \mathrm{d}\theta} \tag{A.31}$$

and

$$\frac{\mathrm{d}(f_0 G)}{\mathrm{d}\theta} + \frac{\alpha}{3}\frac{\mathrm{d}}{\mathrm{d}\theta}\left[\eta_0^3 \sin\theta \frac{\mathrm{d}G}{\mathrm{d}\theta} \right] + \frac{5}{2}\frac{\mathrm{d}B}{\mathrm{d}\theta} - \frac{\alpha}{3}k^2 \eta_0^3 G\sin\theta =$$
$$\frac{\alpha}{3}\gamma k^2 \eta_0^3 \left(G - k^2 G + \frac{\mathrm{d}^2 G}{\mathrm{d}\theta^2} \right) - \frac{\alpha}{3}\gamma \frac{\mathrm{d}}{\mathrm{d}\theta}\left\{ \eta_0^3 \left(\frac{\mathrm{d}G}{\mathrm{d}\theta} - k^2 \frac{\mathrm{d}G}{\mathrm{d}\theta} + \frac{\mathrm{d}^3 G}{\mathrm{d}\theta^3} \right) \right\} \tag{A.32}$$

Again, we obtain the value of λ by numerical calculation. The curves of λ vs. k for different value of γ are plotted in Fig A.9. The trend of those curves here are similar as that in Fig 3.9, but the locations of the maximums of every curves (i.e. $k = k_c$) are different from those given by the MLA, especially for the case with the larger value γ. For example, when $\gamma = 0.067$, $k_c = 0.5$, but $k_c = 0$, shown in Fig A.10. Under this situation, only the stability analysis based on the BPTE can predict the finite wavelength.

In summary, the stability analysis based on the BPTA provides results that are similar to that on the MLA. Even though the wavelength predicted by the BPTA is closer to the experimental results than by the MLA, the mechanism of particle segregation in the rotating cylinder, which is revealed in chapter 3, is independent of whether the MLA or the BPTA is used.

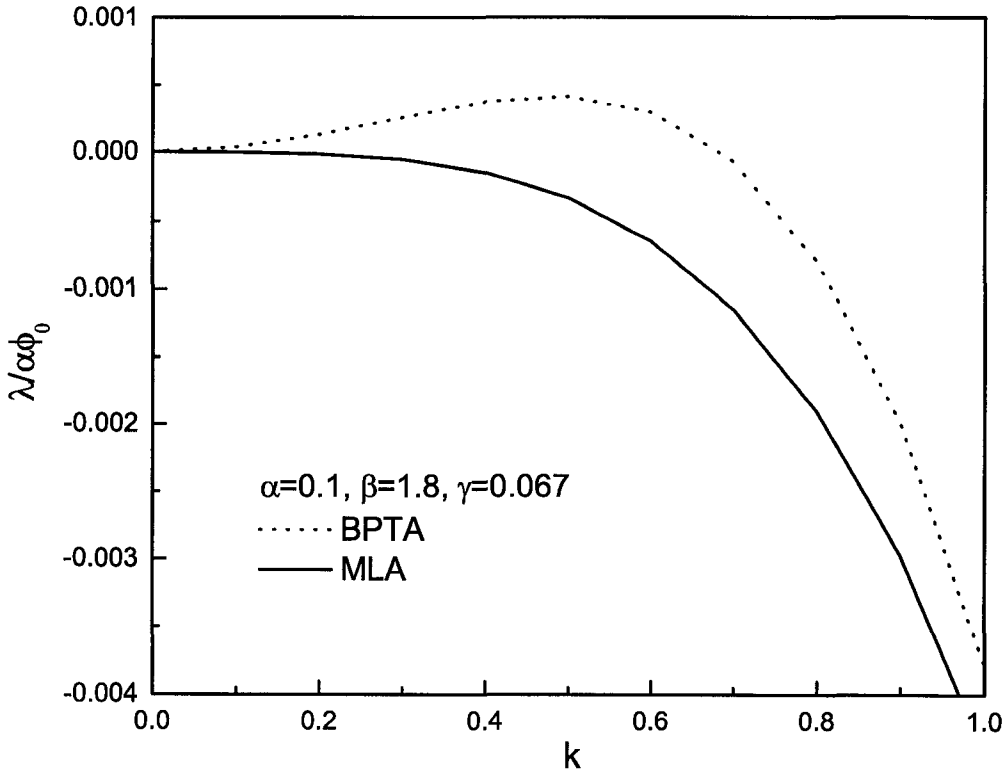

Figure A.10: Comparison of the growth constant λ given by the BPTA and the MLA when $\gamma = 0.067$.

Appendix B

Finite-difference formulation and method of solution

We describe the numerical scheme for solving Eq. (3.66) in chapter 3 (i.e. Eq. (34) in Ref[17]) via a finite-difference method.

$$\frac{\mathrm{d}(f_0 G)}{\mathrm{d}\theta} + \frac{\alpha}{3}\frac{\mathrm{d}}{\mathrm{d}\theta}\left[\eta_0^3 \sin\theta \frac{\mathrm{d}G}{\mathrm{d}\theta}\right] + \frac{5}{2}\frac{\mathrm{d}\eta_0}{\mathrm{d}\theta} - \frac{5}{2}\frac{\mathrm{d}}{\mathrm{d}\theta}\left[(\eta_0 - q_0)\left(1 - \frac{\eta_0^*}{\eta_0}\right)^3\right] - \frac{\alpha}{3}k^2\eta_0^3 G\sin\theta$$
$$= \frac{\alpha}{3}\gamma k^2 \eta_0^3 \left(G - k^2 G + \frac{\mathrm{d}^2 G}{\mathrm{d}\theta^2}\right) - \frac{\alpha}{3}\gamma\frac{\mathrm{d}}{\mathrm{d}\theta}\left\{\eta_0^3\left(\frac{\mathrm{d}G}{\mathrm{d}\theta} - k^2\frac{\mathrm{d}G}{\mathrm{d}\theta} + \frac{\mathrm{d}^3 G}{\mathrm{d}\theta^3}\right)\right\} \qquad \text{(B.1)}$$

where

$$q_0 = \eta_0 - \frac{\eta_0^3}{3}\left\{(1 - \alpha\eta_0)\cos(\theta) - \alpha\frac{\mathrm{d}\eta_0}{\mathrm{d}\theta}\sin(\theta) - \alpha\gamma\left(\frac{\mathrm{d}\eta_0}{\mathrm{d}\theta} + \frac{\mathrm{d}^3\eta_0}{\mathrm{d}\theta^3}\right)\right\} \qquad \text{(B.2)}$$

and

$$f_0 = \frac{3q_0}{\eta_0} - 2 + \frac{\alpha}{3}\eta_0^3\cos\theta$$

First, we rearrange Eq. (B.1) and thereby obtain

$$C_0 G + C_1\frac{\mathrm{d}G}{\mathrm{d}\theta} + C_2\frac{\mathrm{d}^2 G}{\mathrm{d}\theta^2} + C_3\frac{\mathrm{d}^3 G}{\mathrm{d}\theta^3} + C_4\frac{\mathrm{d}^4 G}{\mathrm{d}\theta^4} = P \qquad \text{(B.3)}$$

where

$$C_0 = \frac{\mathrm{d}f_0}{\mathrm{d}\theta} - \frac{\alpha}{3}k^2\eta_0^3\sin\theta - \frac{\alpha}{3}\gamma k^2(1-k^2)\eta_0^3$$
$$C_1 = f_0 + \alpha\eta_0^2\frac{\mathrm{d}\eta_0}{\mathrm{d}\theta}\sin\theta + \frac{\alpha}{3}\eta_0^3\cos\theta + \alpha\gamma(1-k^2)\eta_0^2\frac{\mathrm{d}\eta_0}{\mathrm{d}\theta}$$
$$C_2 = \frac{\alpha}{3}\eta_0^3\sin\theta - \frac{\alpha}{3}\gamma k^2\eta_0^3 + \frac{\alpha}{3}\gamma(1-k^2)\eta_0^3$$

$$C_3 = \alpha\gamma\eta_0^2\frac{\mathrm{d}\eta_0}{\mathrm{d}\theta}$$

$$C_4 = \frac{\alpha}{3}\gamma\eta_0^3$$

and

$$P = -\frac{5}{2}\frac{\mathrm{d}\eta_0}{\mathrm{d}\theta} + \frac{5}{2}\frac{\mathrm{d}}{\mathrm{d}\theta}\left[(\eta_0 - q_0)\left(1 - \frac{\eta_0^*}{\eta_0}\right)^3\right]$$

Next, we discretize the solution domain $[-\pi, \pi]$ into N evenly spaced intervals separated by the points $\theta_i = -\pi + (i-1)\Delta\theta$, where $\Delta\theta = 2\pi/N = h$ and $i = 1, \ldots, N+1$, and approximate Eq. (B.3) using the second-order central finite-difference formula, i.e.

$$\left.\frac{\mathrm{d}G}{\mathrm{d}\theta}\right|_i = \frac{G_{i+1} - G_{i-1}}{2h}$$

$$\left.\frac{\mathrm{d}^2G}{\mathrm{d}\theta^2}\right|_i = \frac{G_{i+1} - 2G_i + G_{i-1}}{h^2}$$

$$\left.\frac{\mathrm{d}^3G}{\mathrm{d}\theta^3}\right|_i = \frac{G_{i+2} - 2G_{i+1} + 2G_{i-1} - G_{i-2}}{2h^3}$$

and

$$\left.\frac{\mathrm{d}^4G}{\mathrm{d}\theta^4}\right|_i = \frac{G_{i+2} - 4G_{i+1} + 6G_i - 4G_{i-1} + G_{i-2}}{h^4}$$

Therefore, at the ith point, the finite-difference form of Eq. (B.3) is

$$A_0^i G_{i-2} + A_1^i G_{i-1} + A_2^i G_i + A_3^i G_{i+1} + A_4^i G_{i+2} = P_i \tag{B.4}$$

where

$$A_0^i = -\frac{C_3^i}{2h^3} + \frac{C_4^i}{h^4}$$

$$A_1^i = -\frac{C_1^i}{2h} + \frac{C_2^i}{h^2} + \frac{2C_3^i}{2h^3} - \frac{4C_4^i}{h^4}$$

$$A_2^i = C_0^i - \frac{2C_2^i}{h^2} + \frac{6C_4^i}{h^4}$$

$$A_3^i = \frac{C_1}{2h} + \frac{C_2}{h^2} - \frac{2C_3}{2h^3} - \frac{4C_4^i}{h^4}$$

$$A_4^i = \frac{C_3^i}{2h^3} + \frac{C_4^i}{h^4}$$

and

$$P_i = -\frac{5}{2}\frac{\left\{\eta_0 - (\eta_0 - q)\left(1 - \frac{\eta_0^*}{\eta_0}\right)^3\right\}\Big|_{i+1} - \left\{\eta_0 - (\eta_0 - q)\left(1 - \frac{\eta_0^*}{\eta_0}\right)^3\right\}\Big|_{i-1}}{2h}$$

Note that all the values of A_n^i and P_i where $n = 0, \ldots, 4$ and $i = 1, \ldots N+1$ are known given that η_0 can be obtained by solving numerically Eq. (B.2) with $\gamma = 0$. The corresponding periodic boundary conditions require that $G_1 = G_{N+1}$, $G_2 = G_{N+2}$ ($G_0 = G_N$), and $G_3 = G_{N+3}$ ($G_{-1} = G_{N-1}$). In view of Eq. (B.1), the periodic boundary conditions also lead to

$$\begin{aligned}\int_{-\pi}^{\pi} \eta_0^3 \left\{G\sin\theta + \gamma\left(G - k^2 G + \frac{\mathrm{d}^2 G}{\mathrm{d}\theta^2}\right)\right\}\mathrm{d}\theta = 0 \\ = \int_{-\pi}^{\pi} \left\{\eta_0^3\left[\sin\theta + \gamma(1-k^2)\right] + \gamma\frac{\mathrm{d}^2\eta_0^3}{\mathrm{d}\theta^2}\right\} G\mathrm{d}\theta \end{aligned} \tag{B.5}$$

which provides an alternative boundary condition, i.e.

$$\sum_1^{N+1} A_w^i G_i = 0 \qquad \text{where} \qquad A_w^i = \left[\sin\theta_i + \gamma(1-k^2)\right]\eta_0^3|_i + \gamma\frac{\eta_0^3|_{i+1} - 2\eta_0^3|_i + \eta_0^3|_{i-1}}{h^2} \tag{B.6}$$

Here, we chose $N = 20000$ and constructed the $(N+1) \times (N+1)$ matrix M incorporating (B.6), i.e.

$$M = \begin{bmatrix} A_2^1 & A_3^1 & A_4^1 & 0 & \cdots & 0 & A_0^1 & A_1^1 & 0 \\ A_1^2 & A_2^2 & A_3^2 & A_4^2 & 0 & \cdots & 0 & A_0^2 & 0 \\ A_0^3 & A_1^3 & A_2^3 & A_3^3 & A_4^3 & 0 & \cdots & 0 & 0 \\ \cdots & \cdots & \cdots & \cdots & \cdots & \cdots & \cdots & \cdots & \cdots \\ 0 & \cdots & 0 & 0 & A_0^{N-1} & A_1^{N-1} & A_2^{N-1} & A_3^{N-1} & A_4^{N-1} \\ 0 & A_4^N & 0 & \cdots & 0 & A_0^N & A_1^N & A_2^N & A_3^N \\ A_w^1 & A_w^2 & A_w^3 & A_w^4 & \cdots & A_w^{N-2} & A_w^{N-1} & A_w^N & A_w^{N+1} \end{bmatrix}$$

in terms of which the linear algebraic system Eq. (B.4) becomes $MG = P$, where $G = (G_1, G_2, \ldots, G_N, G_{N+1})^T$ and $P = (P_1, P_2, \ldots, P_N, 0)^T$. Since such a linear system has no singularity if $\gamma > 0$ and also the matrix M is a sparse one, we chose a direct method (i.e. Gaussian elimination) in the Matlab package to solve $MG = P$ and thereby obtained G. However, this is not the case when $\gamma = 0$ given

the existence of a singularity at $\theta = 0$. Under this condition, we can obtain G asymptotically at $\gamma = 0$ by solving the full Eq. (B.1) but letting $\gamma \to 0$.

Recall that the base flow here is given by Eq. (B.2) with $\gamma = 0$ even though the eigen equation (B.1) is derived based on the full Eq. (B.2). The reason why we made this approximation is that, when $\gamma \ll 1$, the free surface profile η_0 given by Eq. (B.2) with $\gamma = 0$ was found to be essentially the same as that given by the full Eq. (B.2).

We solved Eq. (B.2) with $\gamma = 0$ using a shooting method as described in Ref[3]. Obviously, we could not use such a method to solve the full Eq. (B.2). In this case, Eq. (B.2) together with the kinematic condition, i.e.

$$(1 - \alpha\eta)\frac{\partial \eta}{\partial t} + \frac{\partial q}{\partial \theta} = 0$$

was solved using an iteration scheme in which we first chose an initial value of η (i.e η at $t = 0$), then obtained η at $t = \Delta t$ and so on until $t \to \infty$ when the solution achieved steady state.

Appendix C

Particle segregation in a partially filled rotating cone/sphere

Abstract

Particle segregation in rimming flows of suspensions containing neutrally buoyant particles within a partially filled rotating cylinder has been observed experimentally [M. Tirumkudulu, A. Mileo and A. Acrivos, Phys. Fluids **12**, 1615 (2000)] and then explained quantitatively on the basis of a linear stability analysis [B. Jin and A. Acrivos, Phys. Fluids **16**, 641 (2004)]. Here, we performed similar experiments but in a different geometry, viz. a cone (or a sphere) partially filled with the same suspension and rotated horizontally about their axis of symmetry. As expected, an initially uniform suspension was found to segregate, under certain conditions, owing to the existence of a steady axial flow which is created by this new geometry. In addition, the particles formed a single band near the narrower end of the cone and two bands on both sides of the center cross section in the case of the sphere. It is shown that this location of the band(s) seen experimentally can be predicted theoretically by solving numerically a general model equation for rimming flows within any axisymmetric horizontally rotating container and then taking into account the observed radial particle segregation similar to that found in the case of the cylinder [B. Jin and A. Acrivos, Phys. Fluids **16**, 641 (2004)].

Recently, a quantitative explanation[17] was given for the curious particle banding phenomenon which is observed when an initially uniform suspension of neutrally buoyant particles in a viscous Newtonian fluid is sheared in a partially filled, horizontal rotating cylinder [1]. According to Ref. [17], the whole process for the creation of such band structures is as follows: when rimming flows of suspensions contain a region of recirculating flow (puddle), the particles have been observed to segregate radially by migrating out of the puddle into the unidirectional circumferential flow region (cf. Fig. C.1(a) for a sketch of these two flow regions). Consequently, the particle concentration within the puddle is thereby lowered while that in the circumferential flow region is enhanced. By means of a linear stability analysis, such a particle cross-sectional distribution was shown to be unstable to axial disturbances in the particle concentration, which induce corresponding axial variations in the effective viscosity of the suspension, with the surface tension being responsible for selecting the wavelength of the most rapidly amplified disturbance.

The mechanism which leads to the amplification of the initial axial disturbances was identified by solving numerically a model equation for rimming flows with an imposed axially varying viscosity [18]. It was found that, in the presence of a puddle, the three-dimensional axial flow induced by the axially varying viscosity was directed, on average, along two opposite directions, specifically, towards the high viscosity region across the circumferential flow and towards the low viscosity region across the puddle. Thus, it was concluded that, even when the corresponding volumetric flow rates of the pure fluid exactly balanced each other, in the presence of the radial particle segregation described above, a net particle migration towards the region of high viscosity was expected to set in thereby further amplifying the original particle concentration (and therefore viscosity) disturbances.

Of course, in the case of the rotating cylinder, the axial flow referred to above will vanish if the viscosity of the fluid is kept constant everywhere. But since it is also

obvious that, even when the viscosity is kept uniform, a steady axial flow can still be generated by changing the geometry of the container, e.g. using a cone (or a sphere) rather than a cylinder, one would expect on the basis of the earlier study[17] that, in such a geometry, an initially uniform suspension should also segregate axially into one or more bands if the flow contained a puddle.

To test this hypothesis, experiments were performed in a horizontal cone as well as in a sphere. The cone, shown schematically in Fig. C.1(b), was 100 mm long and had inner radii at its two ends equal to 13 mm and 26 mm respectively, while the radius of the sphere was 36.3 mm. Both the cone and the sphere were made of glass which is completely wetted by the liquid Triton mixture used earlier [1]. In experiments with such a particle-free liquid, the front of the recirculating region (puddle) in the cone (cf. Fig. C.1(b)) and that in the sphere (cf. Fig. C.1(c)) always remained stationary after a short transient period thereby indicating that the corresponding flows were stable. But, when the pure liquid was replaced with a uniformly mixed suspension of neurally buoyant spherical PMMA particles of mean diameter 463 μm dispersed in the same Triton mixture, it was found that, as long as the flow contained a puddle, particle segregation always occurred (cf. Fig. C.2(a) and (b) for the cone and sphere cases, respectively) by a process similar to that observed in the case of the cylinder. Specifically, in all cases, the particles first segregated radially by migrating out of the puddle into the unidirectional circumferential flow region (a relatively short time step), and then segregated axially to form bands (a longer time interval). [In fact, these two intervals were found to overlap in the presence of a deep puddle.] However, the time required for the particle band formation in the cone and the sphere was much shorter than that in the cylinder. For example, in a dilute suspension with particle volume fraction $\phi = 10^{-2}$, essentially complete particle segregation was attained within one hour in the former case, in contrast to the case of the cylinder where, under similar conditions, the experiments had to be

run for at least several hours before any band structure could be discerned. [Note that, here, we focused on experiments with suspensions having low concentrations ($\phi = 10^{-2}$) and fill fractions ($F \leq 0.3$). Also, the corresponding Reynolds numbers for the fluid were always less than 10^{-2} which allowed us to neglect inertia effects.] Moreover, here, the band(s) were located near the region where the size of the puddle was the smallest, rather than at random locations as was the case for the cylinder where only the spacing between the neighboring bands was determined by the surface tension.

Although, as was said earlier, the observed formation of particle bands in the case of a cone and a sphere is hardly surprising in view of the earlier analysis[17], it is still necessary to account for the observation that these bands were found to form near those regions where the puddle was smallest, for it is not obvious why bands could not form at some other location, e.g. where the puddle is largest. To be sure, although one might have anticipated this result by analogy to the earlier observation[1] of particle migration to regions of highest viscosity where the size of the puddle is smallest[18], it is far from clear that this analogy is appropriate given that, in these earlier experiments[1], the reduction in the puddle resulted from the increased viscosity[18] which, as shown in the subsequent analysis[17], provided the primary driving force for the subsequent particle segregation.

To settle this issue we consider, therefore, a steady-state rimming flow within an axisymmetric container, the inner surface of which is formed by rotating, about the x-axis, a curve $r = R(x)$ with $\mathrm{d}R/\mathrm{d}x$ being everywhere $O(1)$ or less, and define

$$\alpha \equiv \sqrt{\frac{\Omega\nu}{gR(x)}} \tag{C.1}$$

where Ω is the angular speed of the rotation, ν is the kinematic viscosity of the fluid and g is the gravitational acceleration. Note that, α is here a function of x instead of being a constant as in Ref. [18]. Then, on supposing that the film is

everywhere thin, the expression for the dimensionless pressure in the thin film, with surface tension effects being negligible, has the same form as Eq. (6) in Ref. [3], i.e. $p = \alpha(z - \eta)\sin\theta$, where $p = \frac{\tilde{p}-\tilde{p}_0}{\rho g R}$, $z = \frac{R-r}{\alpha R}$ and $\eta = \frac{h}{\alpha R}$ with $\tilde{p}$ being the dimensional pressure and $\tilde{p}_0$ the pressure of the empty space, ρ is the density of the fluid, r and θ are, respectively, the radial and the angular coordinates and h is the film thickness (cf. Fig. C.1(a)). Therefore, by repeating the modified lubrication analysis presented in Refs. [3, 18], we can easily show that the dimensionless flow rate within the film at any axial location x, is given by

$$q(x) \equiv \int_0^\eta v dz = \eta - \frac{\eta^3}{3}\left\{(1-\alpha\eta)\cos\theta - \alpha\frac{\partial\eta}{\partial\theta}\sin\theta\right\}, \tag{C.2}$$

where v is the corresponding dimensionless angular velocity, subject to

$$F = \frac{1}{L}\int_{-L/2}^{L/2} F_{\text{local}}(x)\mathrm{d}x \qquad \text{with} \qquad F_{\text{local}}(x) = \frac{\alpha}{\pi}\int_{-\pi}^{\pi}\left(1 - \frac{\alpha}{2}\eta\right)\eta\mathrm{d}\theta, \tag{C.3}$$

where F is the average fill fraction, L is the length of the device (neglecting end effects), and F_{local} is the *a priori* unknown fill fraction per unit length at every cross section of the container.

Now, by repeating the analysis for the flow in the axial direction presented in Ref. [18], we find, after some straightforward manipulations, that the expression for the dimensionless axial velocity w becomes,

$$w = \left\{\alpha R\frac{\partial\eta}{\partial x} - \left(1 - \frac{\alpha}{2}\eta\right)\frac{\mathrm{d}R}{\mathrm{d}x}\right\}\left(\eta z - \frac{1}{2}z^2\right)\sin\theta \tag{C.4}$$

and therefore, the expression for the dimensionless axial flow rate is

$$J \equiv \int_{-\pi}^{\pi}\mathrm{d}\theta\int_0^\eta w\mathrm{d}z = \frac{\alpha}{3}R\int_{-\pi}^{\pi}\eta^3\frac{\partial\eta}{\partial x}\sin\theta\mathrm{d}\theta - \frac{\mathrm{d}R}{\mathrm{d}x}\int_{-\pi}^{\pi}\left(\frac{1}{3} - \frac{\alpha}{6}\eta\right)\eta^3\sin\theta\mathrm{d}\theta, \tag{C.5}$$

which must vanish at steady state, i.e.

$$\frac{\mathrm{d}}{\mathrm{d}x}\int_{-\pi}^{\pi}\eta^4\sin\theta\mathrm{d}\theta = \frac{12}{\alpha R}\frac{\mathrm{d}R}{\mathrm{d}x}\int_{-\pi}^{\pi}\left(\frac{1}{3} - \frac{\alpha}{6}\eta\right)\eta^3\sin\theta\mathrm{d}\theta. \tag{C.6}$$

Evidently, since w vanishes if $\mathrm{d}R/\mathrm{d}x = 0$ everywhere, the steady axial flow is induced here by the three-dimensional geometry of the container.

Let us suppose, for the sake of simplicity, that $R(x)$ is periodic with period equal to L. In order to solve Eq. (C.2) subject to (C.3) and thereby determine the three-dimensional free surface shape, we have to first approximate the condition given by Eq. (C.6) by means of

$$A(x+\delta) = A(x) + \frac{12\delta}{\alpha R}\frac{\mathrm{d}R}{\mathrm{d}x}B(x) \qquad \text{with} \qquad A(x) \equiv \int_{-\pi}^{\pi} \eta(\theta,x)^4 \sin\theta \mathrm{d}\theta,$$
$$\text{and} \quad B(x) \equiv \int_{-\pi}^{\pi} \left(\frac{1}{3} - \frac{\alpha}{6}\eta(\theta,x)\right)\eta(\theta,x)^3 \sin\theta \mathrm{d}\theta \quad \text{(C.7)}$$

where δ is a number chosen small enough to guarantee that the approximation given above will converge into the original Eq. (C.6). We can then repeat the numerical procedure described in Ref. [18] to deal with both symmetric and asymmetric profiles. For the former case, in which the film profiles $\eta(\theta, x)$ are everywhere symmetric about $\theta = 0$, $A(x)$ as well as $B(x)$ in Eq. (C.7) vanish at every cross section so that, according to Eq. (28) and the relevant discussion in Ref. [18], the local fill fractions $F_{\mathrm{local}}(x)$ should remain at their initial and presumable known values. Therefore, we can solve Eq. (C.2) subject to (C.3) for any x and thereby obtain the steady-state symmetric profile $\eta(\theta, x)$. On the other hand, if the film profile is asymmetric about $\theta = 0$, we can solve Eq. (C.2) for a given q at $x = 0$, and obtain $A(\delta)$ by calculating the sum of the two terms involving $A(0)$ and $B(0)$ on the right-hand side of Eq. (C.7). By repeating this procedure, it is straightforward then to obtain $\eta(\theta, x)$ at any cross section and thereby determine the profiles of $F_{\mathrm{local}}(x)$ and also the relation between the chosen value of $q(0)$ and the *a priori* specified value of F. Clearly, according to the present analysis, a steady flow cannot exist if $\eta(\theta, x)$ is symmetric about $\theta = 0$ over a certain range of x and asymmetric otherwise.

In what follows, we shall focus on the case in which a recirculating flow region is present near the bottom of the container for all x, because no particle segregation has

ever been observed in the absence of a puddle. Without loss of generality, we choose, as a typical container, the cone $R(x) = R_0(1+0.25x/R_0)$, with $0 \leq x/R_0 \leq 0.5$, and use our model to calculate the three-dimensional free surface shape for $F = 0.19$ and $\alpha(0) = 0.1$. The corresponding film profiles $\eta(\theta, x)$ at $x = 0$ and $x/R_0 = 0.5$ are plotted in Fig. C.3. As expected, the size of the puddle was found to increase with increasing $R(x)$. Now, let us calculate the total axial volumetric flow rate through the circumferential flow region,

$$J^c \equiv \int_{-\pi}^{\pi}\int_0^{\eta^*} w\mathrm{d}\theta\mathrm{d}z = \int_{-\pi}^{\pi}\left\{\alpha R\frac{\partial\eta}{\partial x} - \left(1-\frac{\alpha}{2}\eta\right)\frac{\mathrm{d}R}{\mathrm{d}x}\right\}\left(\frac{1}{2}\eta\eta^{*2} - \frac{1}{6}\eta^{*3}\right)\sin\theta\mathrm{d}\theta \tag{C.8}$$

where η^* is the lower boundary of the recirculating flow region (cf. Ref. [18]), and that through the puddle, J^r, which must equal $-J^c$ at steady state. [Here we chose the local linear interpolation formula used earlier [18] to compute $\partial\eta/\partial x$.] We find the crucial result that, within the range of monotonically increasing $R(x)$ along x, J^c is *negative* at steady state and therefore, J^r is equal but opposite in sign. For example, in the case of the cone mentioned above, J^c was found to equal -3.7×10^{-2} at $x/R_0 = 0.25$ while the corresponding value of J given by Eq. (C.5), which should have been zero, was computed to be -2.7×10^{-5}. Therefore, we can conclude that, due to the presence of the three-dimensional geometry of the container, the net axial flow rate of a pure liquid, having constant viscosity, integrated across the circumferential region is towards the region of *smaller* $R(x)$, whereas that across the puddle is towards the region of larger $R(x)$.

Now consider a dilute suspension containing neutrally buoyant particles in the presence of such a flow field in which the particles have the essentially same velocity as the surrounding fluid. Following the corresponding analysis in the case of the cylinder [17], we find that there exists a net particle flow rate J_p (cf. Ref.[17]),

$$J_p = (\phi^c - \phi^r)J^c \tag{C.9}$$

which, given that $J^c < 0$, is towards the region of smaller $R(x)$ if the particle concentration in the circumferential region (ϕ^c) is higher than that in the puddle (ϕ^r). Due to this net particle flow, the particles would be expected to segregate into a particle band in the region of smallest $R(x)$. This prediction is in complete agreement with the experimental observations, i.e. that particles were found to segregate into a single band near the small end of the cone (cf. Fig. C.2(a)), while two bands were found to form on both sides of the center cross section of the sphere separated by a distance essentially equal to the width of the puddle (cf. Fig. C.2(b)). Moreover, since the particle segregation reported here results from the existence of a steady three-dimensional flow due to the geometry of the cone or that of the sphere, rather than to an instability resulting from concentration fluctuations (as in the case of the cylinder), it is not surprising that the particle band(s) described above required a much shorter time to form and, also, that the location of the band(s) here is deterministic rather than random as was the case for the cylinder [17].

The results presented here support the basic features of the earlier analysis[17] which would have been seriously compromised if J_c had been found positive rather than negative for, in this case, the predicted location of the particle bands would have been near the region of *maximum* puddle size in contradiction with the experiments. In addition, the present results, as well as those in the earlier references [17, 1], provide further evidence in support of the argument that, as a rule, neutrally buoyant particles in a suspension have a tendency to leave regions of recirculating flow, even under creeping flow conditions, and thereby to trigger the formation of the particle bands seen here as well as earlier [1]. The reason for this radial segregation, however, is still unknown and requires further study.

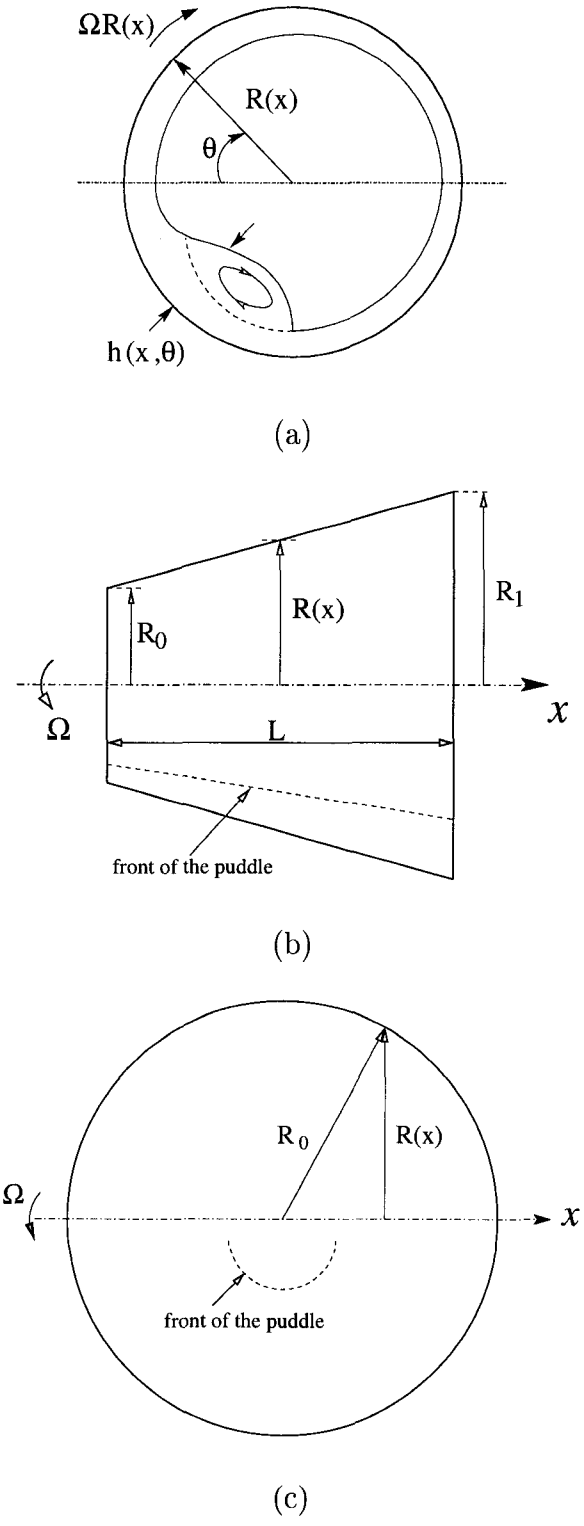

Figure C.1: (a) A sketch of the liquid film profile in the cross section of the cylinder as well as that in the cone (or in the sphere). (b) A sketch of the cone with $R_0 = 13$ mm, $R_1 = 26$ mm and $L = 100$ mm plus the front of the puddle; (c) a sketch of the sphere with $R_0 = 36.3$ mm plus the front of the puddle.

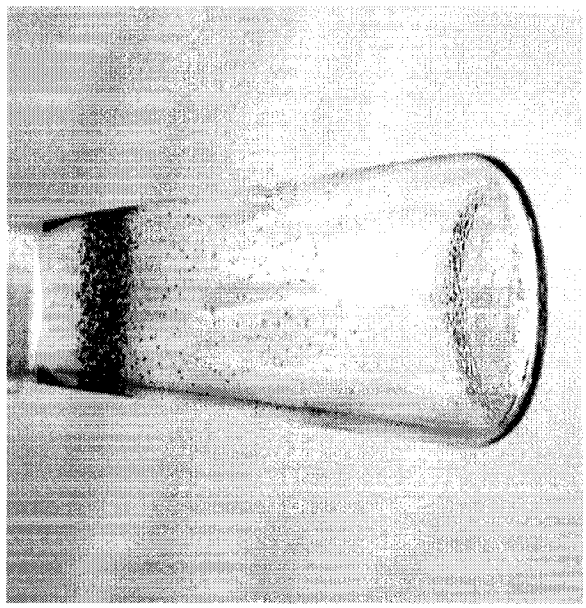

(a)

(b)

Figure C.2: (a) A single band is observed near the small end of the cone for $\Omega =$ 3.8 rpm, $F = 0.20$ and $\phi = 0.01$. (b) Two bands are observed on both sides of the center cross section of the sphere for $\Omega = 9.2$ rpm, $F = 0.20$ and $\phi = 0.01$.

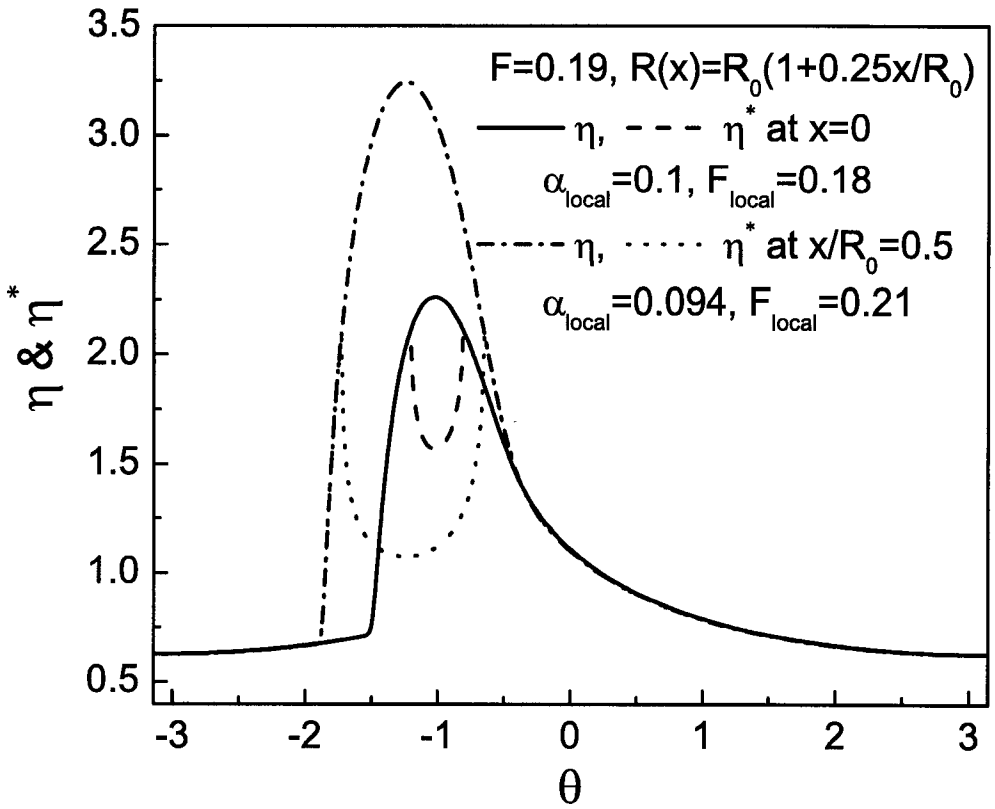

Figure C.3: The dimensionless film profiles as well as the lower boundary of the puddle at different locations ($x/R_0 = 0$ and 0.5) along the cone $R(x) = R_0(1 + 0.25x/R_0)$ ($0 \leq x/R_0 \leq 0.5$) as determined from the numerical solution of Eq. (C.6) for $\alpha(0) = 0.1$ and $F = 0.19$.

Appendix D

Viscous flows in a partially filled horizontal Couette device

D.1 Base flows of a highly viscous liquid in a partially filled horizontal Couette device

Here, we consider the flow of a highly viscous liquid having constant density and viscosity in a partially filled horizontal Couette device, shown in Fig D.1(a), consisting of two concentric cylinders with the outer cylinder fixed and the inner cylinder free to rotate. On assuming that such a flow is axially uniform, and that inertial effects are negligible (e.g. that the Reynolds number $Re \ll 1$), the corresponding governing equations are the two-dimensional Stokes equations, i.e.

$$\mu\left\{\frac{\partial^2\tilde{u}}{\partial r^2}+\frac{1}{r}\frac{\partial\tilde{u}}{\partial r}+\frac{1}{r^2}\left(\frac{\partial^2\tilde{u}}{\partial\theta^2}-\tilde{u}-2\frac{\partial\tilde{v}}{\partial\theta}\right)\right\}=\rho g\sin\theta+\frac{\partial\tilde{p}}{\partial r}, \tag{D.1}$$

and

$$\mu\left\{\frac{\partial^2\tilde{v}}{\partial r^2}+\frac{1}{r}\frac{\partial\tilde{v}}{\partial r}+\frac{1}{r^2}\left(\frac{\partial^2\tilde{v}}{\partial\theta^2}-\tilde{v}+2\frac{\partial\tilde{u}}{\partial\theta}\right)\right\}=\rho g\cos\theta+\frac{1}{r}\frac{\partial\tilde{p}}{\partial\theta}, \tag{D.2}$$

plus the continuity equation,

$$\frac{\partial\tilde{u}}{\partial r}+\frac{1}{r}\tilde{u}+\frac{1}{r}\frac{\partial\tilde{v}}{\partial\theta}=0, \tag{D.3}$$

where $\tilde{u}$, $\tilde{v}$ represent the dimensional velocity components respective to cylindrical coordinates r, θ (cf Fig D.1(b)), $\tilde{p}$ is the dimensional pressure, g is the gravitational acceleration, ρ and μ are the density and the viscosity of the liquid respectively.

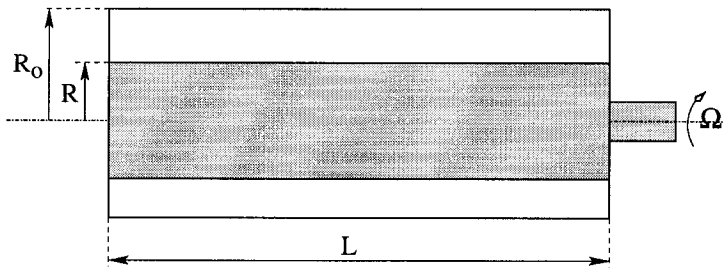

(a)

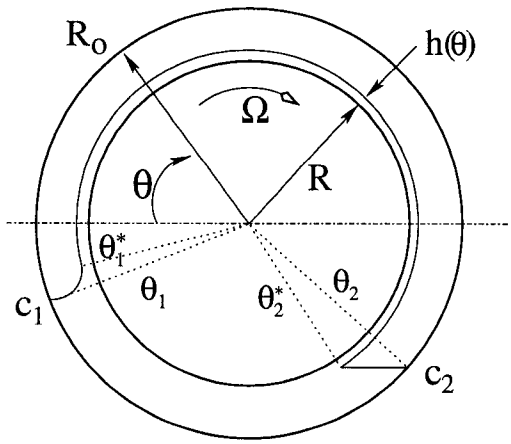

(b)

Figure D.1: A sketch of the horizontal Couette device (a) side view; (b) cross sectional view.

Before non-dimensionlizing all the variables, we introduce two important dimensionless parameters,

$$\alpha \equiv \sqrt{\frac{\Omega\mu}{\rho g R}} \tag{D.4}$$

and

$$\epsilon \equiv \frac{R_o - R}{R} \tag{D.5}$$

where Ω is the angular speed of the rotating inner cylinder, and R_o and R are the radii of the outer and inner cylinders respectively.

Next, the radial space $(r - R)$ is scaled with ϵR as

$$z \equiv \frac{r - R}{\epsilon R} \tag{D.6}$$

and the scaled dependent variables are

$$(u, v) = (\tilde{u}, \tilde{v})/\Omega R, \qquad \text{and} \qquad p = \tilde{p}/\rho g R.$$

Therefore, in terms of the new variables, Eq. (D.3) becomes

$$\frac{\partial u}{\partial z} + \frac{\epsilon}{1+\epsilon z}\left(u + \frac{\partial v}{\partial \theta}\right) = 0 \tag{D.7}$$

and also the dynamical Eqs. (D.1) and (D.2) become

$$\frac{\partial^2 u}{\partial z^2} + \frac{\epsilon}{1+\epsilon z}\frac{\partial u}{\partial z} + \frac{\epsilon^2}{(1+\epsilon z)^2}\left(\frac{\partial^2 u}{\partial \theta^2} - u - 2\frac{\partial v}{\partial \theta}\right) = \frac{\epsilon^2}{\alpha^2}\left\{\sin\theta + \frac{1}{\epsilon}\frac{\partial p}{\partial z}\right\} \tag{D.8}$$

and

$$\frac{\partial^2 v}{\partial z^2} + \frac{\epsilon}{1+\epsilon z}\frac{\partial v}{\partial z} + \frac{\epsilon^2}{(1+\epsilon z)^2}\left(\frac{\partial^2 v}{\partial \theta^2} - v + 2\frac{\partial u}{\partial \theta}\right) = \frac{\epsilon^2}{\alpha^2}\left\{\cos\theta + \frac{1}{1+\epsilon z}\frac{\partial p}{\partial \theta}\right\} \tag{D.9}$$

For the sake of simplicity, we focus on the Couette device with a small gap $\epsilon \ll 1$ plus $\alpha < O(\epsilon)$. Therefore, according to Eq. (D.7), we find that $u = O(\epsilon)$ given that $v = O(1)$. In addition, Eq. (D.8) shows that

$$\frac{\partial p}{\partial z} = -\epsilon \sin\theta + O(\epsilon^2(\alpha^2/\epsilon^2)) \tag{D.10}$$

which leads to

$$p = -\epsilon z \sin\theta + C(\theta) + O(\epsilon^2(\alpha^2/\epsilon^2)) \tag{D.11}$$

with C being an unknown function of θ. Consequently, to a first approximation, Eq. (D.9) reduces to

$$\frac{\partial^2 v}{\partial z^2} = \frac{\epsilon^2}{\alpha^2}\left\{\cos\theta + \frac{\mathrm{d}C}{\mathrm{d}\theta}\right\} \tag{D.12}$$

To solve the above equation, we divide the typical flow domain, shown in Fig D.1(b), into two regions, i.e. the thin film region and the bulk region, since the necessary boundary conditions there are different.

In the thin film region, the normal stress vanishes on the free surface $z = \eta(\theta)$(where $\eta(\theta) \equiv h(\theta)/\epsilon R$ with $h(\theta)$ being the dimensional film thickness) provided that surface tension effects are negligible. In the thin film approximation, this

implies, from Eq. (D.11), that $C = \epsilon\eta\sin\theta$, so that the pressure within the thin film, say p_f, is

$$p_f = \epsilon(\eta - z)\sin\theta \tag{D.13}$$

Moreover, the boundary conditions for the angular velocity in this region are: no-slip at the wall (i.e. $v_f = 0$ at $z = 0$) and zero shear stress on the free surface (i.e. $\partial v_f/\partial z = 0$ at $z = \eta(\theta)$). Therefore, the solution to Eq. (D.12) gives the expression for the angular velocity in the thin film (v_f),

$$v_f = 1 - \frac{\epsilon^2}{\alpha^2}\left(\eta z - \frac{1}{2}z^2\right)\left\{(1+\epsilon\eta)\cos\theta + \epsilon\frac{\mathrm{d}\eta}{\mathrm{d}\theta}\sin\theta\right\} \tag{D.14}$$

which, on integration across the thin film, leads to

$$q_f \equiv \int_0^\eta v\mathrm{d}z = \eta - \frac{\epsilon^2}{3\alpha^2}\eta^3\left\{(1+\epsilon\eta)\cos\theta + \epsilon\frac{\mathrm{d}\eta}{\mathrm{d}\theta}\sin\theta\right\} \tag{D.15}$$

where q_f is the dimensionless flow rate in the thin film.

On the other hand, by solving Eq. (D.12) with the no-slip boundary conditions at the solid walls (i.e. $v_b = 1$ at $z = 0$ and $v_b = 0$ at $z = 1$), we obtain for the angular velocity in the bulk region (say v_b)

$$v_b = 1 - (1+B)z + Bz^2 \tag{D.16}$$

with

$$B \equiv \frac{\epsilon^2}{2\alpha^2}\left(\cos\theta + \frac{\mathrm{d}C}{\mathrm{d}\theta}\right) \tag{D.17}$$

Therefore, the corresponding flow rate across the annulus is

$$q_b \equiv \int_0^1 v_b\mathrm{d}z = \frac{1}{2} - \frac{B}{6} \tag{D.18}$$

At steady state,

$$q_b = q_f,$$

both of which are independent of θ.

In view of Eqs. (D.11) and (D.17), the pressure gradient along the θ-direction in the bulk region becomes

$$\frac{\partial p_b}{\partial \theta} = \frac{2\alpha^2}{\epsilon^2} B - (1 + \epsilon z)\cos\theta \tag{D.19}$$

On integrating the above expression with respect to θ from θ_2 to θ_1 along $z = 1$, we have, at steady state, that

$$B = \frac{\epsilon^2}{2\alpha^2} \frac{\sin\theta_1 - \sin\theta_2}{\theta_1 - \theta_2}(1 + \epsilon) \tag{D.20}$$

given that the local pressures at two contact points c_1 and c_2 (cf. Fig D.1(b)) are the same. Moreover, the liquid conservation condition, in the narrow gap approximation, requires that

$$F = \frac{1}{2\pi}\left\{\theta_1 - \theta_2 + \int_{\theta_1}^{\pi}\left[\eta + \frac{\epsilon}{2}(\eta^2 - \eta)\right] \mathrm{d}\theta + \int_{-\pi}^{\theta_2}\left[\eta + \frac{\epsilon}{2}(\eta^2 - \eta)\right] \mathrm{d}\theta\right\} \tag{D.21}$$

provided that $\theta_1^* \approx \theta_1$ and $\theta_2^* \approx \theta_2$ (cf. Fig D.1(b)), where θ_1^* denotes the angular coordinate of the stagnation point at the free surface while θ_2^* is the angular coordinate of the cusp.

At steady state, as long as q_f(or q_b) has been chosen, θ_1 as well as θ_2 can be determined by solving Eq. (D.20) together with (D.21) given that F, α and ϵ are already known and that B can be evaluated from Eq. (D.18). [Note that, as long as $\epsilon \ll 1$, η in (D.21) can be obtained by solving Eq. (D.15) by successive approximations.] As expected, the value of θ_1 is found to decrease with decreasing α and that the size of the bulk region increases. In the case $\alpha \to 0$, the film is thin enough to allow us to assume that the net flow rate q vanishes giving $B = 3$ in Eq. (D.18). [Previous work [19, 20] related to this problem used such a assumption for the flow with liquids of low viscosity.] In addition, when $v_b = 0$, Eq. (D.16) has two roots, i.e. $z = 1/B$ and $z = 1$, which implies that a recirculating flow is present in the bulk region if the first root is less than the second one (i.e. $B > 1$). When these

two roots are equal, the recirculating flow vanishes and the corresponding flow rate q_b equals $1/3$.

If a recirculating flow exists (i.e. if $0 \leq q < 1/3$ or $1 < B < 3$), it is confined between $z = z^*$ and $z = 1$, where z^* is the smaller of the two roots of

$$q_b = z^* - \frac{1}{2}(1+B)z^{*^2} + \frac{1}{3}Bz^{*^3} \tag{D.22}$$

with the other root being at $z = 1$ (c.f. Eq. (D.18)).

D.2 A model of partially filled Couette flows with an axially varying viscosity

Consider next a steady-state flow in the partially filled Couette device described above but with an imposed axially varying viscosity. Here, we still use the same definition of α in (D.4) so that the dimensionless dynamical equations in the radial and angular directions will remain exactly the same as those in the two-dimensional case. Therefore, on letting $\epsilon \ll 1$, it is a straightforward matter to show that the corresponding expressions for the pressure and for the flow rate in the thin film as well as in the bulk region remain of the same form as those in Sec. 1. For the sake of simplicity, we suppose that $\mu(x)$ is periodic in x, the axial distance divided by R, i.e. $\mu(x) = \mu(x + nL)$ with n being an integer and L taken to be $O(1)$. The corresponding expression for the fill fraction F, the *a priori* specified variable, is

$$F = \frac{1}{L}\int_{-L/2}^{L/2} F_{local}(x)\mathrm{d}x \tag{D.23}$$

with F_{local} being the *a priori* unknown fill fraction at every cross section of the Couette device. The dynamical equation in the axial direction is

$$\mu\left\{\frac{\partial^2\tilde{w}}{\partial r^2} + \frac{1}{r}\frac{\partial\tilde{w}}{\partial r} + \frac{1}{r^2}\left(\frac{\partial^2\tilde{w}}{\partial\theta^2} - \tilde{w}\right)\right\} + \frac{\partial^2\tilde{w}}{\partial\tilde{x}^2} = \frac{\partial\tilde{p}}{\partial\tilde{x}}, \tag{D.24}$$

where $\tilde{w}$ is the dimensional axial velocity and $\tilde{x}$ is the dimensional distance in the axial direction. After non-dimensionlization, this equation becomes

$$\frac{\partial^2 w}{\partial z^2} + \frac{\epsilon}{1+\epsilon z}\frac{\partial w}{\partial z} + \frac{\epsilon^2}{(1+\epsilon z)^2}\left(\frac{\partial^2 w}{\partial \theta^2} - w\right) + \epsilon^2 \frac{\partial^2 w}{\partial x^2} = \frac{\epsilon^2}{\alpha^2}\frac{\partial p}{\partial x} \tag{D.25}$$

which reduces to

$$\frac{\partial^2 w}{\partial z^2} = \frac{\epsilon^2}{\alpha^2}\frac{\partial p}{\partial x} \tag{D.26}$$

with $w \equiv \tilde{w}/\Omega R$ and $x = \tilde{x}/R$ provided that $\epsilon \ll 1$.

In the thin film region, the boundary conditions for the axial velocity (say w_f) are: no-slip at the wall (i.e. $w_f = 0$ at $z = 0$) and zero shear stress on the surface (i.e. $\partial w_f/\partial z = 0$ at $z = \eta$). Moreover, on account of Eq. (D.13) with η being a function of θ as well as of x, we obtain for w_f,

$$w_f = \epsilon \frac{\epsilon^2}{\alpha^2}\frac{\partial \eta}{\partial x}\left\{\frac{z^2}{2} - \eta z\right\}\sin\theta \tag{D.27}$$

hence, the axial flow rate across the thin film is

$$J_f \equiv \int_0^{\eta} \mathrm{d}z \left(\int_{\theta_1}^{\pi} w_f \mathrm{d}\theta + \int_{-\pi}^{\theta_2} w_f \mathrm{d}\theta\right) = -\frac{\epsilon}{3}\frac{\epsilon^2}{\alpha^2}\left(\int_{\theta_1}^{\pi} \eta^3 \frac{\partial \eta}{\partial x}\sin\theta \mathrm{d}\theta + \int_{-\pi}^{\theta_2} \eta^3 \frac{\partial \eta}{\partial x}\sin\theta \mathrm{d}\theta\right) \tag{D.28}$$

the magnitude of which is at most $O(\epsilon)$ given that $\alpha < O(\epsilon)$.

In the bulk region, the corresponding pressure, according to Eq. (D.19), becomes

$$p_b = \frac{2\alpha^2}{\epsilon^2} B(\theta - \theta_1) - (1+\epsilon z)(\sin\theta - \sin\theta_1) \tag{D.29}$$

with $p_b = 0$ at $\theta = \theta_1$ where θ_1 now, as in the case with α, is now a function of x. Therefore, from Eq. (D.26) and after applying the boundary conditions for the axial velocity in the bulk region (say w_b) (i.e. $w_b = 0$ at $z = 0$ and $z = 1$), we can obtain its expression

$$w_b = \left[\left(\frac{\mathrm{d}B}{\mathrm{d}x} + \frac{1}{\mu}\frac{\mathrm{d}\mu}{\mathrm{d}x}\right)(\theta - \theta_1) - B\frac{\mathrm{d}\theta_1}{\mathrm{d}x}\right](z^2 - z) + \frac{\epsilon^2}{2\alpha^2}\frac{\mathrm{d}\theta_1}{\mathrm{d}x}\left[(z^2 - z) + \frac{\epsilon}{3}(z^3 - z)\right]\cos\theta_1 \tag{D.30}$$

and that of the corresponding axial flow rate

$$J_b = \int_{\theta_2}^{\theta_1} \mathrm{d}\theta \int_0^1 w_b \mathrm{d}z$$
$$= \frac{\theta_1 - \theta_2}{12}\left\{\left(\frac{1}{\mu}\frac{\mathrm{d}\mu}{\mathrm{d}x}B + \frac{\mathrm{d}B}{\mathrm{d}x}\right)(\theta_1 - \theta_2) - \frac{\mathrm{d}\theta_1}{\mathrm{d}x}\left[\left(1+\frac{\epsilon}{2}\right)\frac{\epsilon^2}{\alpha^2}\cos\theta_1 - 2B\right]\right\} \quad \text{(D.31)}$$

At steady state,

$$J_f + J_b = 0$$

which leads to

$$\frac{\mathrm{d}\theta_1}{\mathrm{d}x} = \frac{\frac{12J_f}{\theta_1-\theta_2} + (\theta_1-\theta_2)\left(\frac{1}{\mu}\frac{\mathrm{d}\mu}{\mathrm{d}x}B + \frac{\mathrm{d}B}{\mathrm{d}x}\right)}{\left(1+\frac{\epsilon}{2}\right)\frac{\epsilon^2}{\alpha^2}\cos\theta_1 - 2B} \quad \text{(D.32)}$$

Substituting the above expression into Eq. (D.30), we obtain

$$w_b = \left(\frac{\mathrm{d}B}{\mathrm{d}x} + \frac{1}{\mu}\frac{\mathrm{d}\mu}{\mathrm{d}x}B\right)\left[\theta - \frac{1}{2}(\theta_1+\theta_2)\right](z^2 - z) + \frac{6J_f}{\theta_1-\theta_2}(z^2-z)$$
$$+\frac{\left(\frac{z^3}{3} - \frac{z^2}{2} + \frac{z}{6}\right)\epsilon\cos\theta_1}{\left(1+\frac{\epsilon}{2}\right)\cos\theta_1 - \frac{2\alpha^2}{\epsilon^2}B}\left\{\frac{6J_f}{\theta_1-\theta_2} + \frac{1}{2}\left(\frac{\mathrm{d}B}{\mathrm{d}x} + \frac{1}{\mu}\frac{\mathrm{d}\mu}{\mathrm{d}x}B\right)(\theta_1-\theta_2)\right\} \quad \text{(D.33)}$$

Then, the axial flow rate through the recirculating flow region is

$$J^r = \int_{\theta_2}^{\theta_1} \mathrm{d}\theta \int_{z^*}^1 w_b \mathrm{d}z = -J_f(1 + 2z^{*3} - 3z^{*2})$$
$$-\frac{1}{12}\frac{\epsilon z^{*2}(z^*-1)^2\cos\theta_1}{\left(1+\frac{\epsilon}{2}\right)\cos\theta_1 - \frac{2\alpha^2}{\epsilon^2}B}\left\{6J_f + \left(\frac{1}{\mu}\frac{\mathrm{d}\mu}{\mathrm{d}x}B + \frac{\mathrm{d}B}{\mathrm{d}x}\right)\frac{(\theta_1-\theta_2)^2}{2}\right\} \quad \text{(D.34)}$$

It is interesting to note that, according to the above equation, the magnitude of J^r is $O(\epsilon)$, i.e.

$$J^r = -J_f(1 + 2z^{*3} - 3z^{*2}) - \frac{\epsilon}{24}\frac{(\theta_1-\theta_2)^2\cos\theta_1}{\cos\theta_1 - \frac{2\alpha^2}{\epsilon^2}B}z^{*2}(z^*-1)^2 + O(\epsilon^2)$$

This is because, as can be seen from Eq. (D.33), the contribution to J^r from the $O(1)$ term in the expression for w_b vanishes identically.

To evaluate J^r, we assumed that $q = q_0\alpha/\epsilon$ where q_0 is a constant independent of x, and found numerically that, at steady state, J^r is negative with J_f, as expected, being negative in the direction of increasing viscosity. For example, when $\alpha = 0.2$,

$\epsilon = 0.4$ and $\mu = 1 + 0.5x$, we obtained $J^r \approx -0.005$ and $J_f \approx -0.001$ at $x = 0.5$ with a given $F_{local} = 0.5$ and a given $q_0 = 0.55$. This implies that the three-dimensional axial flow induced by the axially varying viscosity was directed, on average, along two opposite directions, specifically, towards the low viscosity region across the recirculating flow area and towards the high viscosity region across the rest of the area, which is similar to the case of rimming flows with an axially varying viscosity[18].

Bibliography

[1] M. Tirumkudulu, A. Tripathi & A. Acrivos "Particle segregation in monodisperse sheared suspensions," *Phys. Fluids* **11**, 507 (1999).

[2] M.Tirumkudulu, A.Mileo & A.Acrivos, "Particle segregation in monodisperse sheared suspensions in a partially filled rotating horizontal cylinder," *Phys. Fluids* **12**, 1615 (2000).

[3] M.Tirumkudulu & A.Acrivos, "Coating flows within a rotating horizontal cylinder: lubrication analysis, numerical computations and experimental measurements," *Phys. Fluids* **13**, 14 (2001).

[4] T.B. Benjamin, W.G. Pritchard & S.J. Tavener, "Steady and unsteady flow of a highly viscous fluid inside of a rotating horizontal cylinder," preprint (1993).

[5] H.K. Moffatt, "Behaviour of a viscous film on the outer surface of a rotating cylinder," *J. de Mecanique* **16**, 651 (1977).

[6] R.E. Johnson, "Steady-state coating flows inside a rotating horizontal cylinder," *J. Fluid Mech.* **190**, 321 (1988).

[7] S.D.R. Wilson & J. Williams, "The flow of a liquid film on the inside of a rotating cylinder, and some related problems," *Phys. Fluid* **9**, 2184 (1997).

[8] S.B.G. O'Brien & E.G. Gath, "The location of a shock in rimming flow," *Phys. Fluid* **10**, 1040 (1998).

[9] J. Ashmore, A.E. Hosoi & H.A. Stone, "The effect of surface tension on rimming flows in a partially filled rotating cylinder, " *J. Fluid Mech* **479**, 65 (2003).

[10] E.J. Hinch & M.A. Kelmanson, "On the decay and drift of free-surface perturbations in viscous thin-film flow exterior to a rotating cylinder," *Proc. R. Soc. Lond. A* **459**, 1193 (2003).

[11] A.E. Hosoi & L. Mahadevan, "Axial instability of a free-surface front in a partially filled horizontal rotating cylinder," *Phys. Fluids* **11**, 97 (1999)

[12] M. Tirumkudulu, "Viscous resuspension and particle segregation in concentrated suspensions undergoing shear", PhD thesis, The City University of New York (2000).

[13] D. Leighton & A. Acrivos, "Measurement of shear-induced self diffusion in concentration suspension of spheres," *J. Fluid Mech.* **177**, 109 (1987).

[14] T.B. Benjamin & S.K. Pathak, "Cellular flows of a viscous liquid that partly fills a horizontal rotating cylinder," *J. Fluid Mech.* **183**, 399 (1987)

[15] F. Melo, "Localized states in a film-dragging experiment," *Phys. Rev. E* **48**, 2704 (1993).

[16] J.F. Brady & I.C. Carpen "Second normal stress jump instability in non-Newonian fluids," *J. Non-Newtonian Fluid Mech.* **102**, 219 (2002).

[17] B. Jin & A. Acrivos "Theory of particle segregation in coating flows of suspensions containing neutrally buoyant particles," *Phys. Fluids* **16**, 641 (2004).

[18] B. Jin & A. Acrivos "Rimming flows with an axially varying viscosity," *Phys. Fluids* **16**, 633 (2004).

[19] D.B.Brewster and A.H. Nissan "The hydrodynamics of flow between horizontal concentric cylinders-I," *Chem. Eng. Sci.* **7**, 215 (1958).

[20] I. Mutabazi, J.J. Hegseth, and C.D. Andereck "Pattern formation in the flow between two horizontal coaxial cylinders with a partially filled gap," *Phys. Rev. A.* **38**, 4752 (1988).